NOTICE

The quality of this microform is heavily dependent upon the quality of the original thesis submitted for microfilming. Every effort has been made to ensure the highest quality of reproduction possible.

If pages are missing, contact the university which granted the degree.

Some pages may have indistinct print especially if the original pages were typed with a poor typewriter ribbon or if the university sent us an inferior photocopy.

Previously copyrighted materials (journal articles, published tests, etc.) are not filmed.

Reproduction in full or in part of this microform is governed by the Canadian Copyright Act, R.S.C. 1970, c. C-30.

AVIS

La qualité de cette microforme dépend grandement de la qualité de la thèse soumise au microfilmage. Nous avons tout fait pour assurer une qualité supérieure de reproduction.

S'il manque des pages, veuillez communiquer avec l'université qui a conféré le grade.

La qualité d'impression de certaines pages peut laisser à désirer, surtout si les pages originales ont été dactylographiées à l'aide d'un ruban usé ou si l'université nous a fait parvenir une photocopie de qualité inférieure.

Les documents qui font déjà l'objet d'un droit d'auteur (articles de revue, tests publiés, etc.) ne sont pas microfilmés.

La reproduction, même partielle, de cette microforme est soumise à la Loi canadienne sur le droit d'auteur, SRC 1970, c. C-30.

Canada

FINITE ELEMENT ANALYSIS OF WIRE COATING

by

Roy E. Wagner

B.A.Sc. Chem. Eng.

A Thesis

Submitted to the School of Graduate Studies

in Partial Fulfilment of the Requirements for

the Degree of Master of Applied Science

in

Chemical Engineering

University of Ottawa

April 1987

ISBN 0-315-40752-2

UNIVERSITÉ D'OTTAWA
UNIVERSITY OF OTTAWA

MASTER OF APPLIED SCIENCE (1987) UNIVERSITY OF OTTAWA
(Chemical Engineering) Ottawa, Ontario

TITLE	Finite Element Analysis of Wire Coating
AUTHOR	Roy E. Wagner B.A.Sc. (University of Windsor, Windsor, Ontario)
SUPERVISOR	Dr. E. Mitsoulis (Chemical Engineering)
NUMBER of PAGES:	xvi, 162

Abstract

The wire-coating process has been analyzed numerically making use of particular die designs employed in high-speed industrial operations. Here, both the lubrication approximation theory (LAT) and a fully two-dimensional finite element method (FEM) have been applied to study the steady, incompressible, creeping polymeric melt flow under isothermal and nonisothermal conditions, respectively. The commercial coating resins considered were low-density polyethylene (LDPE) and plasticized polyvinyl-chloride (PPVC). Use of the LAT yielded important qualitative information, particularly on the pressure distribution and possible flow recirculation, while the FEM solved the coupled mass-, momentum-, and energy conservation equations to yield realistic predictions for the flow and temperature fields, pressure distribution, shear stresses and shear rates at both the die wall and the wire, and haul-off wire tension. For the first time the FEM is extended to a full nonisothermal analysis considering both the entrance channel before melt-wire impact and the distance beyond the die exit, where the coating melt free surface is determined through an iterative procedure. The effect of different operating conditions, die design parameters, melt properties, and product specifications on the overall coating performance is examined. From this, operating limits are found to prevent damaged coating surfaces resulting from melt fracture, flow recirculation, or excessive local heating of the melt due to viscous dissipation. The numerical results also showed good agreement with a set of experimental data for a particular LDPE resin employed in an industrial operation.

Acknowledgements

In presenting this thesis, I wish to acknowledge my appreciation to my research supervisor, Dr. Evan Mitsoulis of the Department of Chemical Engineering, for his constant guidance and valued assistance throughout the research, and for making this such a valuable learning experience. I would also like to express my gratitude to fellow graduate student Mr. F.L. Heng and Ms. E. Clerin of User Services (Computing Centre) for their help in putting this all together.

Contents

List of Figures

List of Tables

Nomenclature

a	constant in viscosity expression
A	area, m^2
b	exponent constant of temperature-dependent viscosity, K^{-1}
	constant in viscosity expression
Bi	Biot Number, dimensionless
c	constant in viscosity expression
C	mean circumference, m
C_p	specific heat, $J/g \cdot K$
D	diameter, m
D_R	Drawdown Ratio, dimensionless
E_r	activation energy at constant stress, J/mol
F	wire tension, N
	load vector
F_0	pay-off tension, N
g	gravitational force per unit mass N/kg
GS	gum space, m
h	cold coating thickness, m
h_m	hot melt coating thickness, m
h_T	heat transfer coefficient, $J/s \cdot m^2 \cdot K$
H	channel gap (net radial gap), m
I_2	second invariant, s^{-2}
k	thermal conductivity, $J/s \cdot m \cdot K$
K	ratio: outer to inner diameter, dimensionless
	stiffness matrix
l	length (annular region), m
L	length, m
m	consistency index, $Pa \cdot s^n$
m_o	apparent viscosity, $Pa \cdot s$
MW	molecular weight, $kg/kmol$
n	power-law index, dimensionless
	outward normal vector to a surface
N	die dimension for gum space expression, m
p,P	pressure, Pa

Pe	Peclet Number, dimensionless
q	heat flux, $J/m^2 \cdot s$
Q	volumetric flow rate, m^3/s
Q_d	rate of viscous dissipation, J/s
r	radial coordinate, m
R	radius, m
Re	Reynolds Number, dimensionless
R_g	molar gas constant, $J/mol \cdot K$
S	dimensionless shear stress
t	time, s
T	temperature, $°C$
u	radial velocity component, m/s
v	velocity, m/s
V_w	boundary velocity, m/s
w	axial velocity component, m/s
W	dimensionless velocity
z	axial coordinate, m
Z	gap dimension for gum space expression, m

Greek Symbols

α	taper angle, degrees
β	taper angle, degrees
$\dot{\gamma}$	rate-of-strain (shear rate), s^{-1}
Γ	surface traction, Pa
δ	taper angle, degrees
$\dot{\epsilon}$	velocity gradient, s^{-1}
η	apparent viscosity, $Pa \cdot s$
θ	azimuthal coordinate, degrees
κ	ratio: inner to outer diameter, dimensionless
λ	radius of zero stress, dimensionless
μ	Newtonian viscosity, $Pa \cdot s$
π_A	dimensionless annular parameter
π_F	dimensionless wire tension gradient
π_P	dimensionless pressure gradient
ρ	density, kg/m^3

ρ_a	melt density at ambient temperature, kg/m^3
ρ_m	melt density at mean melt temperature, kg/m^3
τ	extra stress, Pa
$\overline{\tau}$	mean shear stress, Pa
ϕ	angle of taper, degrees
ψ	stream function, m^3/s
ω	vorticity, s^{-1}

Overscripts

$\bar{}$	mean value
$\underline{\ }$	vector
$=$	tensor or matrix
$*$	dimensionless quantity
$\dot{}$	rate
T	transpose of a matrix

Subscripts

a	ambient
abs	absolute
c	coated wire
cr	critical
d	die, dissipation
i	inner
m	melt
max	maximum
min	minimum
n	n^{th} element
N	Newtonian
o	outer
opt	optimum
P	power-law
r	radial component
t	torpedo

w	wire
z	axial component
0	reference datum
θ	azimuthal component
∞	infinite distance

Mathematical Symbols

∂	differential operator
∇	vector differential operator
$\sum_i$	summation
$\|\ \|$	magnitude of tensor
$\frac{D}{Dt}$	substantial derivative

Chapter 1

INTRODUCTION

1.1 The Wire-Coating Process

The wire-coating process is a continuous extrusion process for primary insulation of conducting wires with molten polymer resins for both mechanical strength and protection. The earliest use of an extruder for coating purposes dates back to the 1840's (Tadmor and Gogos, 1979). Such a process was used for the first underwater cable, laid between Dover and Calais in 1851. Modern technological developments in the use of plastics in wire-coating are offshoots of earlier efforts of cable covering with rubber (Hovey, 1961). The requirement for insulated wires and cables has produced greater industrial demand, creating a need for both more effective and cost-efficient operation and design of the basic process. Current techniques assist engineers to determine design specifications and to predict performance prior to actual operation.

The process of wire-coating consists of passing a bare wire through an extrusion die to obtain a polymeric coating of a predetermined thickness. A sketch supplied by Griff (1968) in Figure 1.1 illustrates the basic components of a wire-coating production line.

A bare wire is initially unwound, passes through a straightener and is then preheated to prevent premature shrinkage of the hot plastic around the wire. Tadmor and Gogos (1979) reveal that the wire is heated close to the melt temperature to allow better adhesion of the polymer to the wire surface. The wire then passes in the back of a crosshead die and enters into the die to meet the homogeneous molten polymer, which is pressure-

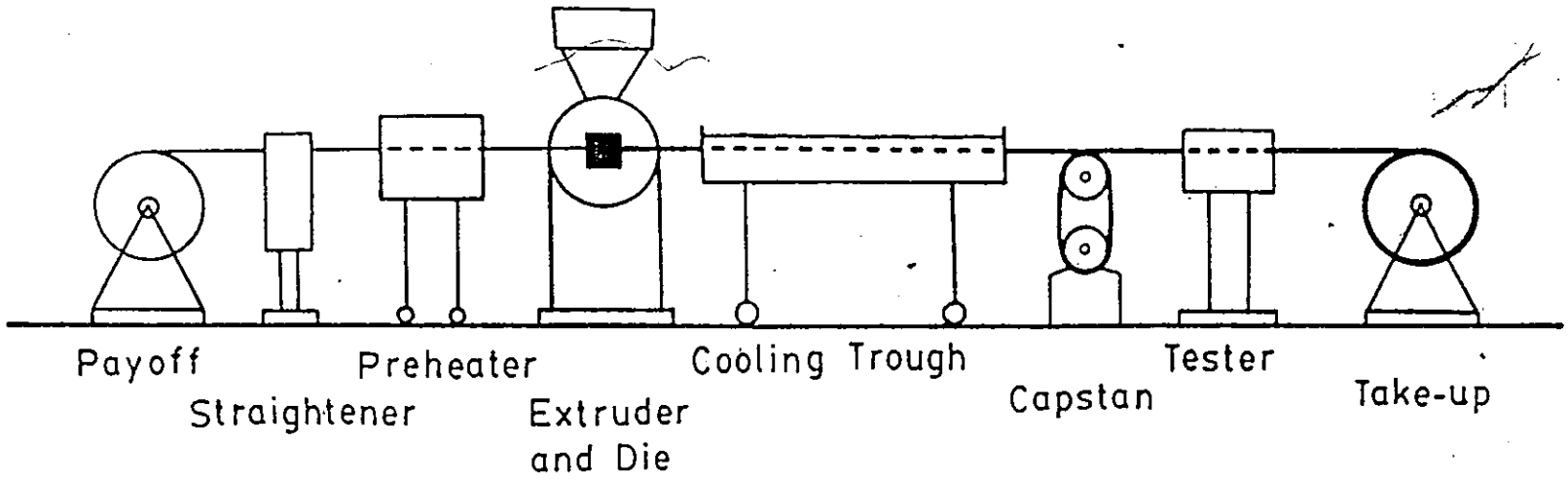

Figure 1.1: Schematic Diagram of the Wire-Coating Process (Griff, 1968).

fed from an extruder. The final product then passes through a cooling water trough, through a capstan (which pulls the wire), past a tester and is wound up on the take-up reel. The inability to feasibly recycle defective wire makes monitoring of the final product an important task. An actual wire-coating line in operation is shown in Figure 1.2. The wire (entering the die from the left) is shown leaving the die with its outer coat, and entering the cooling trough.

Griff (1968) has carried out a thorough survey of various production and equipment ranges pertaining to wire-coating operations. Wire sizes range from tiny wires of 0.2 mm in diameter to cables of 13 cm in diameter and more. Extruders used range from 2.5 to 25 cm in diameter, putting out from 5 to 450 kg/hr. Fenner (1970) reports that wire speeds range from 2 cm/s for large high-voltage electric cables, up to and exceeding 2000 cm/s for small telephone wires. Linear speed is usually the limit to output. Statistics from 1985 (Kline, 1986) indicate polyethylenes and polyvinyl chlorides comprised 55% of all coating polymers used in that year. In particular, low-density polyethylene (LDPE) and plasticized polyvinyl-chloride (PPVC) have in the past received most attention. In addition to LDPE and plasticized PVC, other resins such as high-density polyethylene (HDPE), Nylon and Polysulfone are also used. Since PVC is sensitive to thermal degradation, it is used under lower speeds at lower temperatures. It is frequently used as jacketing for other wires since it is self-extinguishing. Griff (1968) states typical melt temperatures as 185°C for PVC, 220°C for LDPE, 285°C for Nylon and 365°C for Polysulfone.

There are two types of dies used in the coating of wires: pressure dies and tubing dies. Figure 1.3 illustrates both of these configurations. Pressure dies utilize a pressure-fed polymer melt which contacts a high-speed wire inside the die while still under pressure. Passing from the back of a crosshead die, the wire enters into a guider tube (torpedo) prior to die entry and subsequent melt contact. In the entry region of this die the polymer melt flows in a convergent annulus which leads to the region where the melt meets the wire. The moving wire drags the melt and therefore both a pressure and drag type flow will now exist. Conversely, the tubing die operates by having the extruded melt form a coat around the moving wire outside the die, where it is drawn onto the wire by action of a vacuum. The vacuum is applied through a clearance between the conductor and the guider tube (usually in the order of 0.2 mm). Pressure dies are normally used for the

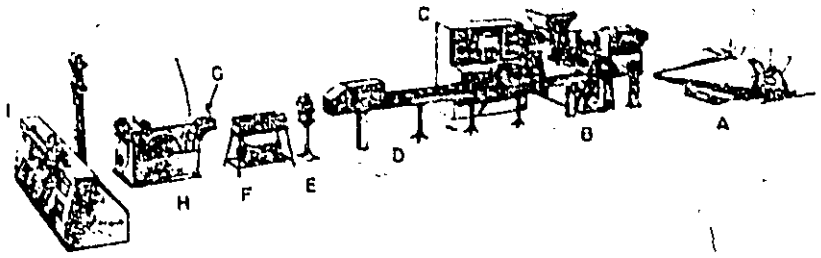

(A) dual flyer payoff; (B) extruder; (C) control panel; (D) multipass cooling trough; (E) diameter control gauge; (F) spark tester; (G) length counter; (H) positive-pull belt capstan; (I) winding equipment with automatic reel changing.

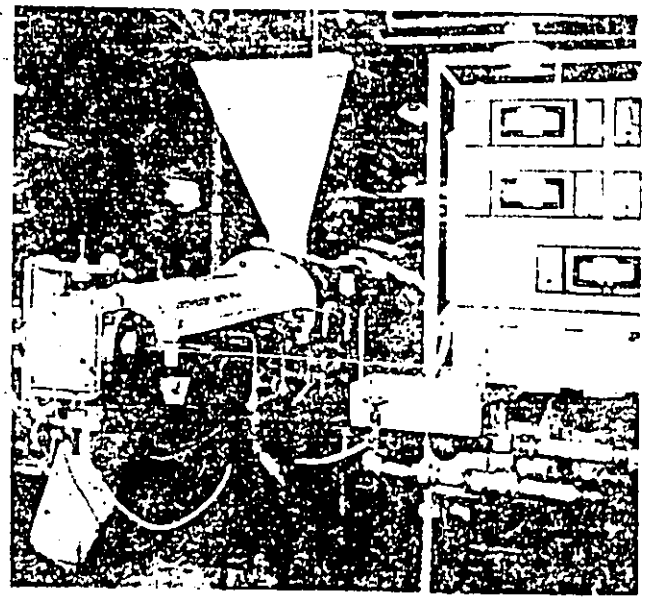

Figure 1.2: Operation of a Wire-Coating Line (Griff, 1968).

primary insulation of a conductor, whereas tubing dies find greater usage in insulating large cables, and when "jacketing" or "sheathing" of wires (or groups of wires) that have already been coated is required. In addition, tubing dies are preferable in the coating of very thin wires that may otherwise rupture when contacted with a highly viscous melt. Thin coatings can be applied without forcing the melt through an extremely small die opening, since the action of the vacuum results in small drawdown ratios. The drawdown ratio is the ratio of the cross-sectional area of the annular die gap to the cross-sectional area of the final wire product. Griff (1968) states that typical drawdown ratios range between 1 and 4 for major coating resins.

Most previous investigations have focused on design of pressure dies rather than tubing dies. The complex flow field that exists within a pressure-type die is of considerable interest to engineers since greater knowledge of it is necessary for improvements to die designs. Therefore, examination of this die type will be the focus of this work.

1.2 Literature Survey

A solid knowledge of the flow and heat transfer phenomena that occur inside a pressure-type die is required. A die must be designed to avoid excessive shear stresses at the wire which may lead to elongation or rupture of the wire or excessive shear stresses at the die wall resulting in an uneven and rough extrudate coating.

Variables which affect the wire-coating process through pressure-type dies are summarized by Rao (1979) as follows:

1. Die design variables, such as die diameter and angles, wire diameter and die land length.

2. The operating variables, such as total flow rate, wire speed and extrusion temperature.

3. The material variables or the rheological properties of the polymer melt, namely the viscosity and elasticity.

Previous research dealing with the wire-coating process focused more on material properties and general process techniques rather than analysis of phenomena encountered in the process.

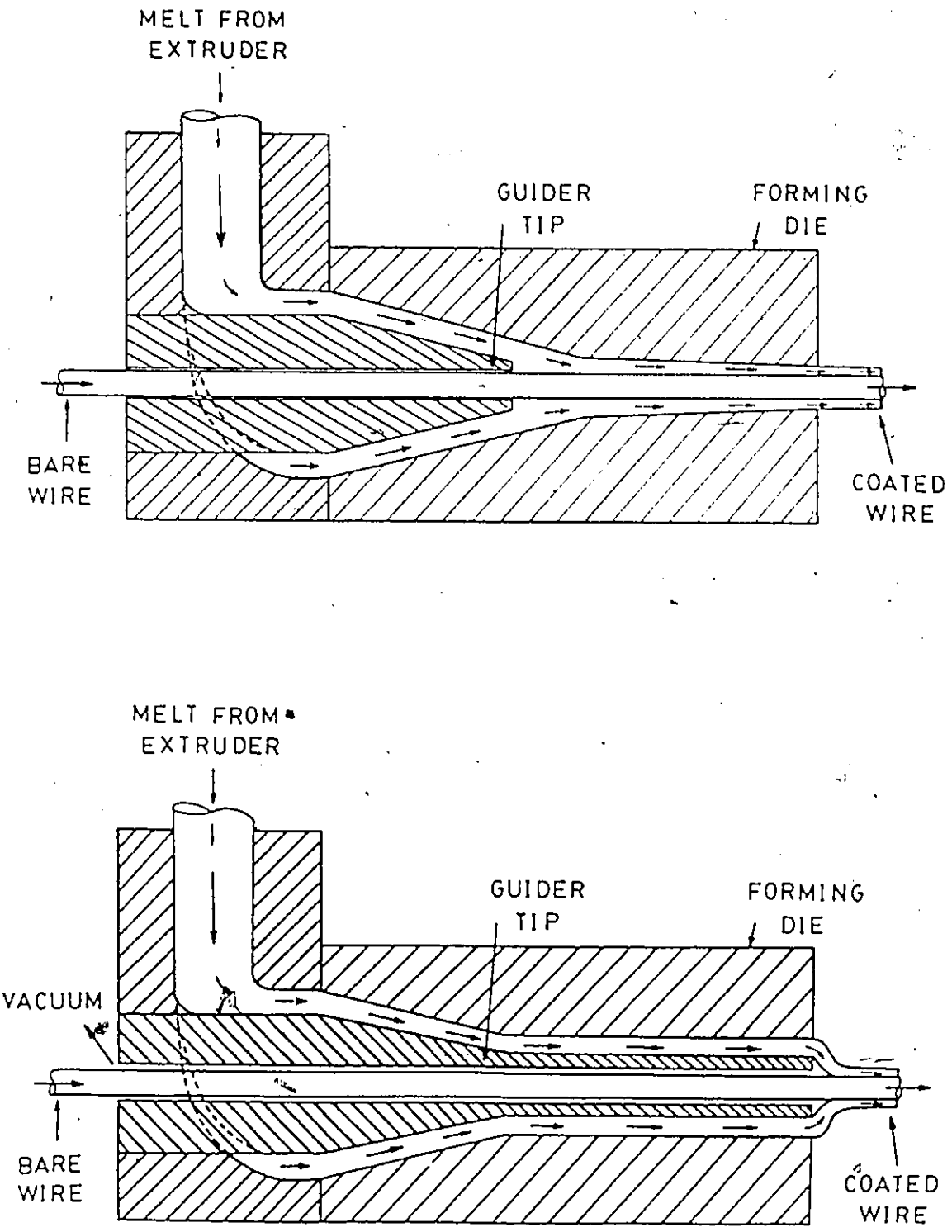

Figure 1.3: Types of Dies Employed in Wire-Coating:
(Top) Pressure-Type Die, (Bottom) Tubing-Type Die.

Early analyses of wire-coating die designs were made in an attempt to predict various desired field variables. An initial theoretical analysis was done by Carley (1959), in which the equations of motion, upon application of simplifying assumptions, were solved using the Lubrication Approximation Theory (LAT). The melt was assumed to be Newtonian and isothermal. McKelvey (1962) extended this analysis by taking into account the combined drag and pressure flow. Middleman (1977) , Tadmor and Gogos (1979), and Tiu (1986) undertake analytical treatments of coating dies. Tiu (1986) furthermore underlines the danger of superimposing pressure and drag flow components by suggesting that this is far from realistic for non-Newtonian fluids under standard conditions of wire-coating. Fenner (1970) uses the LAT and a series of dimensionless parameters for a detailed analysis.

The ultimate objective is to create a reliable predictive model with which design specifications can be found so that a given set of criteria is satisfied. Fenner and Williams (1967) present a die for coating of wires with an LDPE melt, and proceed to analyze the die assuming inelastic shear-thinning behavior under isothermal conditions. Various important variables such as required entry pressure, maximum wire tension and shear stresses are determined by utilizing the lubrication approximation as a basis of solution. This particular die is studied in detail further on.

Hammond (1960) examined existence of extrudate roughness with respect to different probable causes: poor extrusion mixing, insufficient feed material, low melt temperatures, and melt fracture. Griff (1968) also lists moisture, trapped air and polymer decomposition as other possibilities that may lead to surface roughness. Hammond (1960) cites the most common cause as melt fracture, which occurs when excessive shear stresses have developed within the melt. Hammond found experimentally that for a large final taper (i.e. small cone angle) the shear rate before melt fracture will be higher than for the case of a shorter taper with a larger convergent angle. However, longer die designs risk rupturing the wire due to excessive viscous drag of the fluid on the wire itself. This trade-off is an important consideration in the final design selection. Additional means of avoiding surface roughness might include operating at higher temperatures or lower speeds.

Die design criteria to achieve optimal performance and the effects of configurations and operating parameters on the performance have been

investigated by many authors, including Hammond (1960), Vaughan and Spohn (1960), Ferrari (1964), and Han and Rao (1978).

Shear rate data are essential to determine the relative probability of melt fracture occurence within the die. Haas and Skewis (1974) and Endo (1976) both report shear rates exceeding $10^5 s^{-1}$. Bagley and Storey (1963) initially derived an analytical means of determining velocities and shear rates for Newtonian fluids in cylindrical wire-coating dies under isothermal conditions. Many improvements have since been made on this model. Haas and Skewis (1974) presented a die design upon which experiments were performed. Proper design (e.g. adjustment of "gum space") of the die, it was claimed, could suppress melt fracture under conditions where it would be expected. This die receives further treatment later in this work.

At high wire speeds, it is expected that significant amounts of energy are dissipated within the flow due to the viscous nature of the melt. Therefore, the isothermal assumption made by previous authors may not be totally realistic. To account for viscous heating in the polymer melt, solution of the equation of energy is required. Winter (1975, 1977) presents a summary of work done in this area . He also shows graphically a means by which the temperature field and the increase in average temperature may be found via numerical solution of the equations of continuity, momentum, and energy for a power-law fluid. Although his work is done for straight dies with one-directional shear flow, it does illustrate principles at work inside the coating die. Basu (1981) examines nonisothermal flows in wire-coating co-extrusion dies, detailing the effects on pressure, stress and temperature distribution within each component of the flow. Stewart and McClelland (1983) perform an approximate analytical study of viscous dissipation for flow in a theoretical wire-coating die under adiabatic conditions, finding results significantly lower than those of Carley et al. (1979). Carley et al. (1979) performed a finite difference simulation to examine the flow through various wire-coating dies of different dimensions. A typical wire used in industrial operations at moderate to high speeds was assumed to be coated with either an LDPE or plasticized PVC resin, both regarded as non-Newtonian inelastic fluids under nonisothermal conditions. The conservation equations were solved to yield information on the flow field (e.g. profiles for the velocity, shear rate, viscosity and temperature). The effect of viscous dissipation in the temperature rise of the melt under typical processing conditions was shown for the two melts. The assumption of adiabatic boundaries was made and

compared to the isothermal boundary assumption. Although significant, this work had two important omissions. The assumption of negligible radial convection brings into question the accuracy of the temperature results. In addition, the domain under consideration includes only that portion of the die where the melt and wire meet. Therefore no analysis of the region located before this point has been made (entry to impact), nor has analysis been undertaken on the exit effects (e.g. development of free surface).

The first effort to analyze the whole flow field inside wire-coating dies without using the lubrication approximation was made by Caswell and Tanner (1978). Application of the Finite Element Method (FEM) was made for different die designs to generate important information, such as recirculatory regions within the flow field and the determination of the free coating surface at the die exit for both pressure and tubing dies. Their analysis also finds the pressure distribution throughout the die. This particular work considered isothermal flows of Newtonian and power-law fluids. Nonisothermal conditions were not studied. Caswell and Tanner (1978) presented an improved die design upon which numerical simulations have been performed and documented. Their die design will also be extensively studied in this work.

The literature contains very few experimental investigations of the wire-coating process. Experimental research is difficult due to the minute volume of melt within the region of interest and the small size of the dies used. Except for the overall pressure drop in the crosshead and the flow rate of the final product, all other quantities are extremely difficult to measure. Han and Rao (1978) conducted experiments on a selected die design but at speeds unrealistically low (around 1% of speeds used in actual production). Ettinger (1961) and Haas and Skewis (1974) presented experimental results for runs conducted, but they did not specify rheological properties of the melts used and operating temperatures. However, since the results given by Haas and Skewis (1974) represent the most complete set of experimental studies, their die design is also closely studied in this work, and comparisons are made between theory and experiment.

1.3 Objectives

The objective of this research is to study, using numerical analysis, the polymer melt flow inside pressure-type wire-coating extrusion dies. Two computer programs are employed: one based on the Lubrication Approximation Theory (LAT) and another on the Finite Element Method (FEM). Both are applied under isothermal operating conditions to compute important design data such as pressure distribution, shear stresses at the wire surface and die wall, haul-off wire tension and maximum wire tension. Nonisothermal conditions are handled primarily by FEM analysis. Furthermore, the FEM analysis will yield more information regarding the flow and temperature fields inside the die, along with other important variables of the process.

The effect of the geometric configuration of the die on these flow characteristics is studied by examining three different die designs found in the literature. Two separate polymer resins are used: LDPE and plasticized PVC. The different conditions likely required for proper coating operation are determined through numerical analysis. In addition, the effects of rheological behavior and boundary conditions on wire-coating operations are examined.

The numerical results are to be compared with experimental data on pressure for a particular die design and melt properties available in the literature.

1.4 Outline of Thesis

Chapter 2: The equations of conservation of mass, momentum and energy are introduced and simplified using the appropriate assumptions. The models in the constitutive equations for the description of flow of polymer melts are also presented, along with a set of boundary conditions. The LAT is discussed and applied to the wire-coating process.

Chapter 3: The relevant properties of the polymer melts used in this work are completely detailed, including viscosity curves, densities, thermal conductivities and specific heats. Further information on critical stresses and degradation temperatures is also presented.

Chapter 4: Results from runs performed on the die design given by Fenner (1970) are presented. Isothermal and nonisothermal conditions are examined assuming Newtonian and non-Newtonian behavior. Both LDPE and plasticized PVC are separately studied, as is the effect of decreased flow area (by increasing wire radius). Results are compared to other numerical findings.

Chapter 5: Results from runs performed on the die design given by Caswell and Tanner (1978) are presented. By the nature of this design, only a PVC melt is studied. Isothermal and nonisothermal conditions are examined for Newtonian and non-Newtonian models. Results are compared to other available findings.

Chapter 6: Results from runs performed on the die design given by Haas and Skewis (1974) are presented. Extensive research centred only on LDPE as the coating material. Isothermal and nonisothermal conditions are examined for Newtonian and non-Newtonian models. Results are compared to experimentally obtained data available in the literature.

Chapter 7: The results of this thesis are summarized for the various designs examined. Conclusions and recommendations for future work are presented.

Chapter 2

MATHEMATICAL MODELLING

This chapter introduces mathematical expressions to model the behavior of polymer melt flows in the wire-coating process, providing a basis for the overall numerical analysis.

The conservation equations are presented and simplified according to the assumptions made. The Lubrication Approximation Theory (LAT), a further simplified model, is then detailed for isothermal and nonisothermal conditions. Important dimensionless parameters used in the LAT analysis are introduced. A discussion of two-dimensional flow follows, and the assumed boundary conditions are presented. Finally, the methods of solution, i.e. LAT and the Finite Element Method (FEM), are outlined.

2.1 Conservation Equations

The flow of polymer melts inside wire-coating dies takes place at low Reynolds numbers (Re < 1) and the assumption of creeping flow is acceptable [1]. Due to axisymmetry, the mathematical analysis is carried out in terms of cylindrical coordinates (r,θ,z), where r is the radial direction, z is the axial direction and θ is the azimuthal direction. The conservation equations for

[1]For example, a wire of radius $R_w = 0.032$ cm and speeding at $V_w = 2000$ cm/s contacts an LDPE melt at 230°C having a density of 0.75 g/cm^3 and an average viscosity of $\mu = 1000$ poise (g/cm·s); the Reynolds number would be $Re = \frac{\rho V_w R_w}{\mu} = 0.048$.

mass, momentum and energy for steady-state flow may be expressed as follows:

Mass:

$$\frac{D\rho}{Dt} + \rho(\nabla \cdot \bar{v}) = 0 \tag{2.1}$$

Momentum:

$$\rho\frac{D\bar{v}}{Dt} = -\nabla p + (\nabla \cdot \bar{\bar{\tau}}) + \rho\bar{g} \tag{2.2}$$

Energy:

$$\rho C_p\frac{DT}{Dt} = -\nabla \cdot \bar{q} + p(\nabla \cdot \bar{v}) + [\bar{\bar{\tau}} : \nabla\bar{v}] \tag{2.3}$$

where ρ represents density, $\bar{v}$ velocity vector, p pressure, $\bar{\bar{\tau}}$ extra stress tensor, C_p specific heat, T temperature, $\bar{q}$ heat flux vector and $\bar{g}$ gravitational force per unit mass.

The following simplifying assumptions can now be made:

- *Incompressible fluid.*
- *Inertial effects are negligible in magnitude relative to viscous and pressure forces.*
- *Body forces (such as gravity) are negligible in magnitude relative to viscous and pressure forces.*
- *Rotational symmetry of the fluid.*
- *No slip at the wall.*

Basu (1981) notes that the steady-state assumption for short dies is the most severe restriction and Tadmor and Gogos (1979) agree that no process is truly steady-state. However, this assumption is not entirely unreasonable, and will remain in the present study. In addition, Chung (1986) questions the incompressibility assumption, suggesting that melt compressibility may become significant for certain coating fluids at high speeds, thus influencing die design parameters and final products. However, Endo (1976) does not consider this significant for typical polymer melts, supporting the incompressibility assumption by showing that density changes are very small for pressure drops in excess of 100 atm. The idealization of no-slip conditions is quite possibly erroneous to some degree at high speeds, and can be accounted for if the true state of slippage is known. However, no data has

thus far been produced for wire-coating materials to allow development of an accurate slippage expression and therefore relevant research previously done in this field has been conducted under the no-slip assumption.

Two additional assumptions may be made with respect to the equation of energy:

- *Constant thermal conductivity.*
- *Constant heat capacity.*

The assumption of constant ρ, C_p and k allows for further simplification of Eqs. (2.1) - (2.3) to give the following:

$$\nabla \cdot \bar{v} = 0 \tag{2.4}$$

$$-\nabla p + [\nabla \cdot \bar{\bar{\tau}}] = 0 \tag{2.5}$$

$$\rho C_p \bar{v} \cdot \nabla T = k\nabla^2 T + [\bar{\bar{\tau}} : \nabla \bar{v}] \tag{2.6}$$

where $\bar{q} = -k\nabla T$ with k being the thermal conductivity.

The preceding vectorial equations can be rewritten for axisymmetric geometries in cylindrical coordinates:

$$\frac{\partial v_r}{\partial r} + \frac{v_r}{r} + \frac{\partial v_z}{\partial z} = 0 \tag{2.7}$$

$$0 = -\frac{\partial p}{\partial r} + \frac{\partial \tau_{rr}}{\partial r} + \frac{\tau_{rr}}{r} + \frac{\partial \tau_{zr}}{\partial z} - \frac{\tau_{\theta\theta}}{r} \tag{2.8}$$

$$0 = -\frac{\partial p}{\partial z} + \frac{\partial \tau_{rz}}{\partial r} + \frac{\tau_{rz}}{r} + \frac{\partial \tau_{zz}}{\partial z} \tag{2.9}$$

$$\begin{aligned} \rho C_p \left(v_r \frac{\partial T}{\partial r} + v_z \frac{\partial T}{\partial z} \right) = & \\ k \left(\frac{1}{r}\frac{\partial T}{\partial r} + \frac{\partial^2 T}{\partial r^2} + \frac{\partial^2 T}{\partial z^2} \right) + \tau_{rr}\frac{\partial v_r}{\partial r} + \tau_{\theta\theta}\frac{v_r}{r} & \\ + \tau_{rz}\frac{\partial v_z}{\partial r} + \tau_{zr}\frac{\partial v_r}{\partial z} + \tau_{zz}\frac{\partial v_z}{\partial z} & \end{aligned} \tag{2.10}$$

It should be noted that due to the symmetry of the stress tensor, $\tau_{rz} = \tau_{zr}$.

2.2 Lubrication Approximation Theory

It is reasonable to assume that the flow in tapered pressure dies with small angles ($\phi < .10°$) will be nearly parallel so that $\frac{\partial}{\partial z} << \frac{\partial}{\partial r}$,$v_r << v_z$, $v_z = v_z(r,z)$ and p = p(z). This allows for further simplification of the previous equations to:

$$\frac{\partial v_r}{\partial r} + \frac{v_r}{r} + \frac{\partial v_z}{\partial z} = 0 \tag{2.11}$$

$$0 = -\frac{\partial p}{\partial z} + \frac{\partial \tau_{rz}}{\partial r} + \frac{\tau_{rz}}{r} \tag{2.12}$$

$$\rho C_p v_z \frac{\partial T}{\partial z} = k\left(\frac{1}{r}\frac{\partial T}{\partial r} + \frac{\partial^2 T}{\partial r^2}\right) + \tau_{rz}\frac{\partial v_z}{\partial r} \tag{2.13}$$

Problems for which Eqs.(2.11) and (2.12) are applicable are said to obey the Lubrication Approximation. The application of the Lubrication Approximation Theory (LAT) is done in detail in the books by Fenner (1970), Middleman (1977), Tadmor and Gogos (1979), and Pearson (1985). The continuity equation (Eq. 2.11) may be replaced by the integral form:

$$Q = 2\pi \int_{r_i(z)}^{r_o(z)} v_z(r,z) r dr \tag{2.14}$$

where Q is the volumetric flow rate and $r_i(z)$ and $r_o(z)$ are the inner and outer channel radii, respectively. For a given cold coating thickness h (at the ambient temperature), Q is computed from a mass balance on the melt which moves as a rigid coating on the wire surface outside the die:

$$Q = \pi V_w \left[(R_w + h)^2 - R_w^2\right] \frac{\rho_a}{\rho_m} \tag{2.15}$$

where ρ_a is the melt density at ambient temperature and ρ_m is the melt density at the mean melt temperature.

2.2.1 Isothermal Analysis

Assuming isothermal conditions at a mean die temperature, Eq. (2.13) is no longer required and the lubrication approximation equations for the cylindrical coordinate system shown in Figure 2.1 are Eq. (2.14) and:

$$\frac{dp}{dz} = \frac{1}{r}\frac{d}{dr}(r\tau_{rz}) \tag{2.16}$$

To solve the above equations, a constitutive equation that links stress to the velocity gradient is required. Furthermore, proper boundary conditions must also be imposed. No-slip boundary conditions are imposed on the moving wire and the stationary die wall in the die region between contact of the melt with the wire and die exit, i.e.

$$v_z = V_w \quad \text{at} \quad r = r_i(z) = R_w \tag{2.17}$$

$$v_z = 0 \quad \text{at} \quad r = r_o(z) \tag{2.18}$$

In the annular region before contact with the wire, Eq. (2.17) is replaced by a zero wall velocity.

For a generalized Newtonian fluid obeying a power-law, the following expression applies:

$$\tau_{rz} = m\left(\frac{dv_z}{dr}\right)^n \tag{2.19}$$

where m is the consistency index and n is the power-law index.

For a Newtonian fluid (n = 1, m = μ = constant), solutions may be obtained analytically for parallel- or tapered-channel dies. Han and Rao (1978) have developed analytical expressions for velocity profile and volumetric flow rate for the case of a straight annulus, whereas Fenner (1970) has presented results for the more general case including taper. This latter treatment is more comprehensive, and will be followed here as well for a power-law fluid.

Dimensionless parameters are introduced into this analysis. The dimensionless flow rate may be defined as:

$$\pi_Q = \frac{Q}{CHV_w} \tag{2.20}$$

where C is the mean circumference

$$C = \pi(r_i + r_o) \tag{2.21}$$

and H is the channel gap.

$$H = r_o - r_i \tag{2.22}$$

The dimensionless pressure gradient is expressed as

$$\pi_p = -\left(\frac{dp}{dz}\right)\frac{H}{\bar{\tau}} \tag{2.23}$$

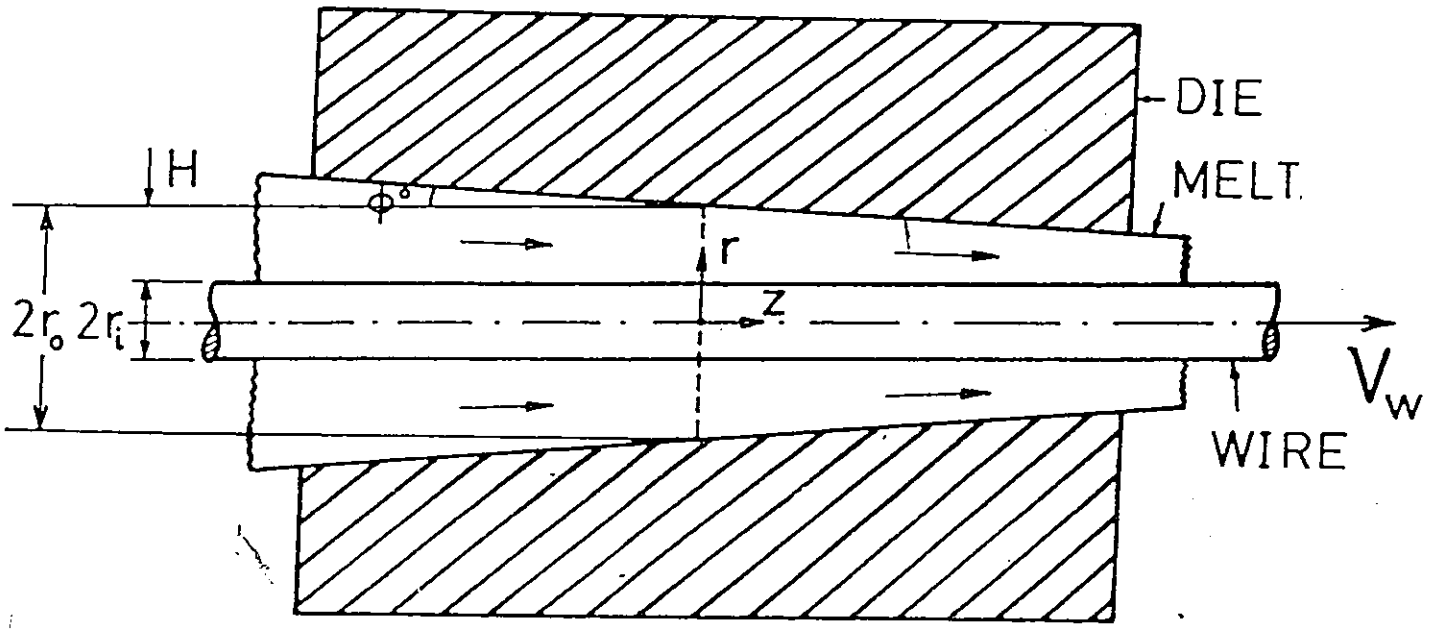

Figure 2.1: Notation for the Lubrication Flow Analysis in the Annular Gap between the Die Wall and the Moving Wire.

where $\bar{\tau}$ is the mean shear stress defined at the mean shear rate V_w/H:

$$\bar{\tau} = m\left(\frac{V_w}{H}\right)^n \tag{2.24}$$

A dimensionless wire shear stress S_w is defined by

$$S_w = \frac{\tau_w}{\bar{\tau}} \tag{2.25}$$

where τ_w is the shear stress at the wire. In addition, a dimensionless die wall shear stress, S_d, may be defined:

$$S_d = \frac{\tau_d}{\bar{\tau}} \tag{2.26}$$

where τ_d is the shear stress at the die wall. Furthermore, a wire tension gradient π_F is defined by

$$\pi_F = \frac{\left(\frac{dF}{dz}\right)}{C\bar{\tau}} \tag{2.27}$$

where dF/dz is the wire tension gradient given by

$$\frac{dF}{dz} = -2\pi r_i \tau_w \tag{2.28}$$

and F is the force exerted by the shearing melt on the wire. Other important dimensionless quantities include:
a diameter ratio:

$$\kappa = \frac{r_i}{r_o} \qquad \text{where} \quad 0 < \kappa < 1 \tag{2.29}$$

an inverse diameter ratio:

$$K = \frac{1}{\kappa} = \frac{r_o}{r_i} \qquad \text{where} \quad 1 < K < \infty \tag{2.30}$$

a dimensionless radius:

$$R = \frac{r}{r_i} \qquad \text{where} \quad 1 \leq R \leq K \tag{2.31}$$

a dimensionless stress:

$$S = \frac{\tau_{rz}}{r_i\left(\frac{dp}{dz}\right)} \tag{2.32}$$

and a dimensionless velocity:

$$W = \left(\frac{v_z(r,z)}{V_w} - 1\right) sgn\left(\frac{dp}{dz}\right) \left|\frac{\pi_p}{(K-1)^{n+1}}\right|^{-\frac{1}{n}} \tag{2.33}$$

The drawdown ratio D_R is defined as:

$$D_R = \frac{R_o^2 - R_w^2}{(R_w + h)^2 - R_w^2} \tag{2.34}$$

where R_o is the exit die radius and h the final coating thickness. A drawdown ratio of 1.0 indicates that the diameter of the coated wire is equal to the diameter of the die opening. If $D_R > 1$ the diameter of the coated wire is less than the diameter of the die opening. Note that the same D_R means the same h. Integrating Eq. (2.16) gives

$$\tau_{rz} = \left(\frac{dp}{dz}\right) \frac{[r^2 - (\lambda r_o)^2]}{2r} \tag{2.35}$$

where $\tau_{rz} = 0$ at $r = \lambda r_o$, the position of the zero stress surface as yet unknown. Using the dimensionless Eqs. (2.31) and (2.32), Eq. (2.35) may be written as:

$$S = \frac{1}{2} \cdot \frac{[R^2 - (\lambda K)^2]}{R} \tag{2.36}$$

Substituting the power-law Eq. (2.19) yields

$$\frac{dW}{dR} = |S|^{\frac{1}{n}} sgn[R^2 - (\lambda K)^2] \tag{2.37}$$

This is the governing ordinary differential equation in dimensionless form. The following dimensionless boundary conditions are also obtained:

$$\text{at} \quad R = 1, \quad W = 0 \tag{2.38}$$

$$\text{at} \quad R = K, \quad W = -sgn\left(\frac{dp}{dz}\right) \left|\frac{\pi_p}{(K-1)^{n+1}}\right|^{-\frac{1}{n}} \tag{2.39}$$

If λ is known, Eq. (2.37) is readily integrated from R = 1 to R = K by means of Simpson's rule. The dimensionless parameters are then obtained

as follows:

$$\pi_Q = 1 - \frac{2}{W(K)(K^2-1)} \int_1^K W(R) R dR \tag{2.40}$$

$$\pi_p = -sgn\left(\frac{dp}{dz}\right)(K-1)^{n+1}\,|W(K)|^{-n} \tag{2.41}$$

$$\pi_F = \frac{\pi_p[1-(\lambda K)^2]}{K^2-1} \tag{2.42}$$

$$S_d = \frac{\pi_p K[1-\lambda^2]}{2(K-1)} \tag{2.43}$$

For a Newtonian fluid (n = 1), we have the following equations:

$$(\lambda K)^2 = \frac{1}{\ln K}\left[\frac{(K^2-1)}{2} - \frac{2(K-1)^2}{\pi_p}\right] \tag{2.44}$$

$$\pi_Q = \frac{1}{2\ln K} - \frac{1}{K^2-1} + \frac{\pi_p}{8(K-1)^2}\left[K^2+1-\frac{K^2-1}{\ln K}\right] \tag{2.45}$$

$$\pi_F = \frac{2(K-1)}{(K+1)\ln K} + \pi_p\left[\frac{1}{K^2-1} - \frac{1}{2\ln K}\right] \tag{2.46}$$

$$S_d = -\frac{K-1}{K\ln K} + \pi_p\left[\frac{(K+1)}{4K\ln K} - \frac{K}{2(K-1)}\right] \tag{2.47}$$

The above equations are exact coming from the solution of Eq. (2.37) and the boundary conditions Eqs. (2.38) and (2.39). Eq. (2.44) is useful for defining suitable values of $(\lambda K)^2$ for use in the solution of the power-law case.

The general case of a power-law fluid does not have an exact solution and therefore a numerical solution is necessary. Fenner (1970) has generated characteristic curves for different values of K and n with π_Q appearing as a variable on each graph. Interpolation between these curves can be used to get the necessary information for calculations of overall die performance. For the analysis of the annular region before the melt contacts the wire a new dimensionless parameter is defined by

$$\pi_A = \frac{\pi_Q}{\pi_p} = \frac{Q\overline{\eta}}{CH^3\left(-\frac{dp}{dz}\right)} \tag{2.48}$$

where $\overline{\eta}$ is the mean viscosity defined at the mean shear rate V_w/H:

$$\overline{\eta} = \frac{\overline{\tau}}{\left(\frac{V_w}{H}\right)} \tag{2.49}$$

In general, π_A will be a function of n and K. Fenner (1970) shows that π_A is nearly independent of K and the exact solution for K = 1 ($\kappa = 1$) may therefore be used:

$$\pi_A = \frac{1}{2^{2n+1}} \left(\frac{2n}{2n+1}\right)^n \tag{2.50}$$

A more precise formula for the pressure drop of power-law fluids in annular tapered dies is given by Parnaby and Worth (1974). Overall, wire-coating results are little affected by the annular region calculations.

2.2.2 Overall Die Performance Analysis

Using Eqs. (2.15) and (2.20), the following expression for π_Q is found

$$\pi_Q = \frac{\rho_a}{\rho_m} \frac{h}{H} \frac{(2R_w + h)}{(2R_w + H)} \tag{2.51}$$

If the cold coating thickness h is known, a numerical value for π_Q can be found at any die section. This value may then be used to obtain the corresponding values of the other dimensionless parameters.

Overall die performance may be computed by integration over the axial length. Defining z = 0 at the entry to the annular region, the inlet pressure P (at z = 0) is given by:

$$P = -\int_0^L \left(\frac{dp}{dz}\right) dz \tag{2.52}$$

since p = 0 at the exit z = L. Therefore, overall:

$$P = \int_0^l \left(-\frac{dp}{dz}\right) dz + \int_l^L \left(-\frac{dp}{dz}\right) dz \tag{2.53}$$

where l is the axial length of the annular region and L the overall axial length of the die.

Introducing Eq. (2.48) and using the definition of π_p (Eq. 2.23) the following is obtained:

$$P = \frac{Q}{\pi_A}\int_0^l \frac{\overline{\eta}}{CH^3}dz + \int_l^L \frac{\pi_p \overline{\tau}}{H}dz \tag{2.54}$$

where π_A is given by Eq. (2.50) for the particular polymer melt, Q by the desired final thickness and all other variables are known functions of z.

The haul-off wire tension F is given by

$$F = \int_l^L \left(\frac{dF}{dz}\right) dz + F_o \tag{2.55}$$

where F_o is the payoff tension. Introducing π_F (Eq. 2.27) yields

$$F = \int_l^L C\overline{\tau}\pi_F dz + F_o \tag{2.56}$$

The stresses are given by:

$$\text{at the wire} \qquad \tau_w = S_w\overline{\tau} = -\frac{1}{2}\pi_F(K+1)\overline{\tau} \tag{2.57}$$

$$\text{at the die wall} \qquad \tau_d = S_d\overline{\tau} \tag{2.58}$$

Of considerable interest as well is the maximum wire tension F_{max} given by:

$$F_{max} = \int_l^{z_o} C\overline{\tau}\pi_F dz + F_o \tag{2.59}$$

where z_o is the position before the die exit where dF/dz = 0 and the wire shear stress passes from a negative to a positive value, which means there is a tendency to push the wire out of the die, reducing the haul-off tension required. Since wire strength is an important factor, it is also necessary to know this maximum tension.

Further results from this analysis can be obtained under varying operating conditions. Fenner (1970) shows that for other speeds and temperatures, we have:

$$P = C_1 m_o V_w^n \tag{2.60}$$

$$F = C_2 m_o V_w^n + F_o \tag{2.61}$$

$$\tau_w = C_3 m_o V_w^n \tag{2.62}$$

$$\tau_d = C_4 m_o V_w^n \tag{2.63}$$

where C_1, C_2, C_3, C_4 are constants for a given wire radius and coating thickness and m_o is the apparent viscosity at unit shear rate and die operating temperature.

2.2.3 Nonisothermal Analysis

Winter (1977) seems to have made the first attempt to treat the nonisothermal problem using the LAT. His analysis takes into account convection and viscous dissipation effects within the die land and outside the die and shows the development of a temperature profile for a typical wire-coating operation. The nonisothermal analysis starts with the simplified equations:

$$Q = 2\pi \int_{r_i(z)}^{r_o(z)} v_z(r,z) r dr \tag{2.64}$$

$$\frac{dp}{dz} = \frac{1}{r}\frac{\partial}{\partial r}(r\tau_{rz}) \tag{2.65}$$

$$\rho C_p v_z \frac{\partial T}{\partial z} = k\frac{1}{r}\frac{\partial}{\partial r}\left(r\frac{\partial T}{\partial r}\right) + \tau_{rz}\frac{\partial v_z}{\partial r} \tag{2.66}$$

where a power-law is assumed for the shear stress τ_{rz}

$$\tau_{rz} = m\left(\frac{\partial v_z}{\partial r}\right)^n \tag{2.67}$$

and the consistency index m is an exponential function of temperature;

$$m = m_o \exp[-\mathrm{b}(T - T_o)] \tag{2.68}$$

b is a temperature shift factor and m_o the consistency index at the reference temperature T_o.

Winter (1977) discusses the relative importance of heat transfer mode at the boundaries in terms of the Biot modulus (Bi), which compares the relative magnitudes of surface convection and internal conduction resistances to heat transfer. It is expressed as:

$$\mathrm{Bi} = \frac{h_T R_w}{k} \tag{2.69}$$

where h_T is the heat transfer coefficient. A low Biot number (Bi<1) indicates low internal conduction resistance and heat transfer to the surroundings is subsequently poor (nearly adiabatic case). A high Biot number (Bi>100) indicates the opposite effect of poor resistance to external heat flow, with little heat retained internally (nearly isothermal case). Usual values in die flow are in the range 10-100. At the wire surface, an energy balance is required between the melt and the metallic wire. Finite difference solution (Winter, 1977) of the system of equations yields very high temperature rises close to the die wall where a region of low viscosity acts as a lubricant film and most of the polymer passes through the die in plug flow. On the other hand, the energy balance on the wire shows that within a very thin layer the melt regains its entrance temperature despite its contact with the much cooler wire. The average temperature increase for the melt was found to be about 3°C, and also the temperature of the wire stayed constant due to the extremely short residence time in the die. Furthermore, it was found that the temperature peak at the die exit wall levels off within a short distance (< 10 cm). Winter (1977) briefly extends his analysis to the cooling of the wire core as well as the coating melt.

2.3 Two-Dimensional Analysis

The need for a full analysis of wire-coating without making use of the lubrication approximation becomes evident because of the inability of the latter to describe the flow for large entrance angles and to accurately account for recirculation phenomena at the impact of the melt with the wire. Note that due to axisymmetry, the three-dimensional problem can be described by two independent variables, namely r and z . Thus for a cylindrical coordinate system, this analysis may be carried out as two-dimensional. A typical representation of a wire-coating die is shown in Figure 2.2.

The preceding equations (Eqs. 2.7- 2.11) are linked through the temperature and shear rate dependence of viscosity. The stress tensor, $\bar{\bar{\tau}}$, for a generalized Newtonian inelastic fluid is expressed in terms of a rate-of-strain tensor, $\bar{\bar{\dot{\gamma}}}$ as:

$$\bar{\bar{\tau}} = \eta \bar{\bar{\dot{\gamma}}} \tag{2.70}$$

where η is the non-Newtonian viscosity. Assuming incompressibility ($\nabla \cdot \bar{v} =$

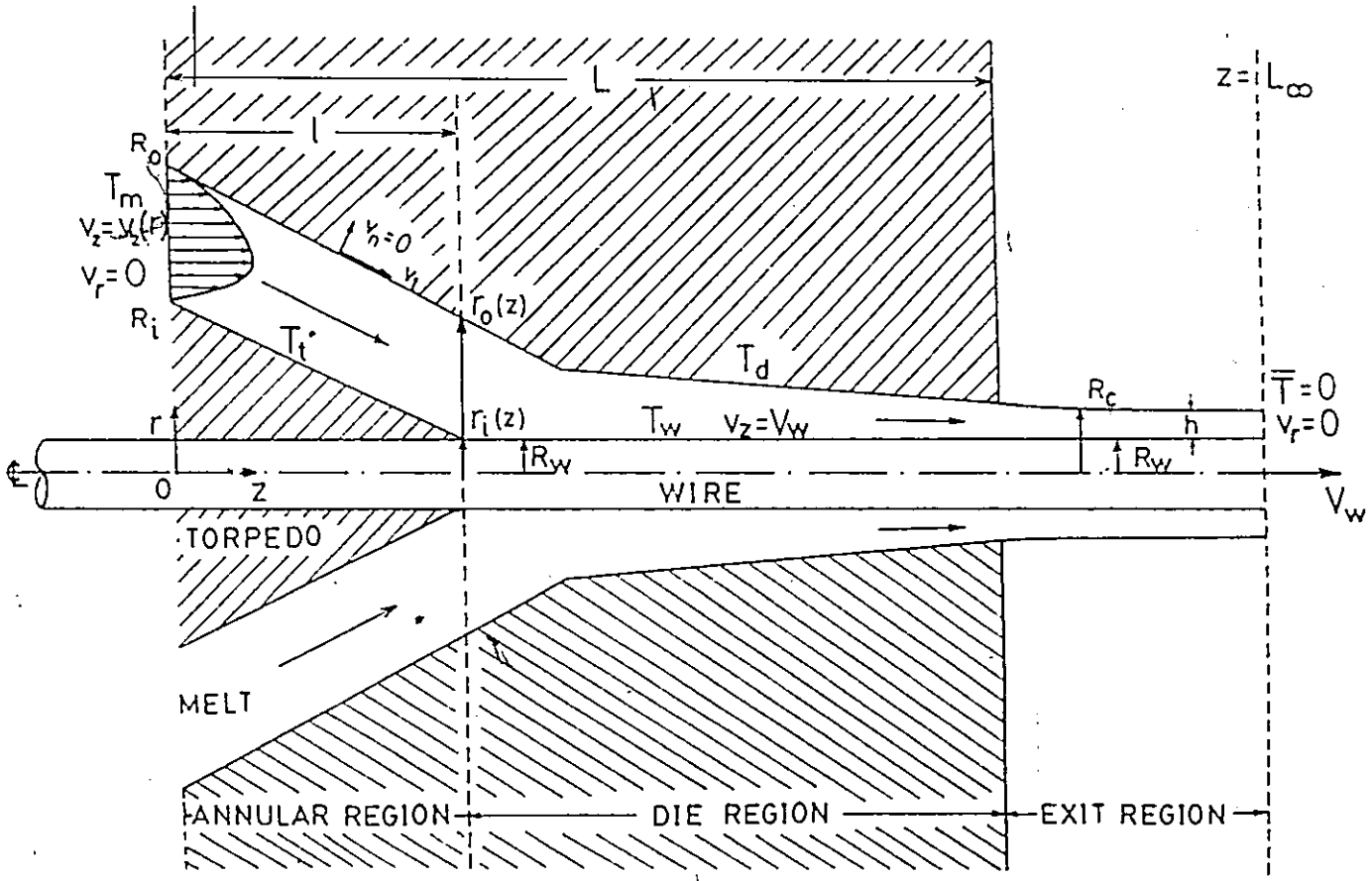

Figure 2.2: Notation for Flow and Heat Transfer Analysis without the Lubrication Approximation in a Wire-Coating Unit.

0), the components of the stress tensor can be expressed as:

$$\tau_{rr} = \eta\dot{\gamma}_{rr} = 2\eta\dot{\epsilon}_{rr} \quad (2.71)$$

$$\tau_{\theta\theta} = \eta\dot{\gamma}_{\theta\theta} = 2\eta\dot{\epsilon}_{\theta\theta} \quad (2.72)$$

$$\tau_{zz} = \eta\dot{\gamma}_{zz} = 2\eta\dot{\epsilon}_{zz} \quad (2.73)$$

$$\tau_{rz} = \tau_{zr} = \eta\dot{\gamma}_{rz} = \eta(\dot{\epsilon}_{rz} + \dot{\epsilon}_{zr}) \quad (2.74)$$

where $\dot{\epsilon}_{ij} = \partial v_i/\partial x_j$. The rate-of-strain tensor, $\bar{\bar{\dot{\gamma}}}$, is expressed in terms of the individual velocity gradients:

$$\bar{\bar{\dot{\gamma}}} = \begin{pmatrix} 2\frac{\partial v_r}{\partial r} & 0 & \frac{\partial v_r}{\partial z} + \frac{\partial v_z}{\partial r} \\ 0 & 2\frac{v_r}{r} & 0 \\ \frac{\partial v_z}{\partial r} + \frac{\partial v_r}{\partial z} & 0 & 2\frac{\partial v_z}{\partial z} \end{pmatrix}$$

Newtonian and Generalized Newtonian Fluids

For an incompressible fluid, Newton's law of viscosity states that the viscosity is constant at a given temperature and pressure, regardless of the stress or shear state of the fluid. The generalized Newtonian fluid however has a viscosity that has a functional dependence on the magnitude of the rate-of-strain tensor, $\bar{\bar{\dot{\gamma}}}$, in addition to temperature and pressure:

$$\bar{\bar{\tau}} = \eta\left(|\bar{\bar{\dot{\gamma}}}|\right)\bar{\bar{\dot{\gamma}}} \quad (2.75)$$

To obtain η as a scalar function of the rate-of-strain tensor, the invariants of this tensor must be found. Bird et al. (1960) explain the purpose and formulation of the three invariant quantities that lead to scalar quantities from the tensor. The assumption of an incompressible, viscometric flow effectively eliminates the first and third invariants, and the second invariant takes the form:

$$I_2 = (\bar{\bar{\dot{\gamma}}} : \bar{\bar{\dot{\gamma}}}) = \sum_i \sum_j \dot{\gamma}_{ij}\dot{\gamma}_{ji} \quad (2.76)$$

The magnitude $|\bar{\bar{\dot{\gamma}}}|$ is then given by:

$$|\bar{\bar{\dot{\gamma}}}| = \sqrt{\frac{1}{2}I_2} = \sqrt{\frac{1}{2}(\bar{\bar{\dot{\gamma}}} : \bar{\bar{\dot{\gamma}}})}$$

$$= \sqrt{2(\frac{\partial v_r}{\partial r})^2 + 2(\frac{v_r}{r})^2 + 2(\frac{\partial v_z}{\partial z})^2 + (\frac{\partial v_r}{\partial z} + \frac{\partial v_z}{\partial r})^2} \qquad (2.77)$$

Once this scalar value has been determined, it may be used in any one of many non-Newtonian shear-dependent viscosity models available, such as the power-law model.

The power-law model is an empirical relationship in which the viscosity is assumed to have a functional dependence on the shear state of the fluid. The relationship between the stress tensor and rate-of-strain tensor is

$$\bar{\bar{\tau}} = \left(m|\bar{\bar{\dot{\gamma}}}|^{n-1}\right)\bar{\bar{\dot{\gamma}}} \qquad (2.78)$$

The coefficient m is the consistency index and n is the power-law index. If $n < 1$, the fluid experiences a decrease in viscosity under increased shear rates (pseudoplastic behavior) and if $n > 1$, the viscosity will increase with greater shearing (dilatant behavior). For polymer melts we usually have $n < 1$ (shear-thinning behavior).

Other models can also be used to better describe the shear rate dependence of viscosity for polymer melts. For example, Carley et al. (1979) modelled the viscosity for two typical coating resins (plasticized PVC and LDPE) by using three regimes: a Newtonian regime at low shear rates, a transition regime at moderate shear rates and a power-law regime at high shear rates.

The link between viscosity and temperature is also important since during normal operation, significant temperature rises are expected. A common model, previously shown in Eq. (2.68), is often used:

$$\eta = \eta_0 \exp[b(T - T_0)] \qquad (2.79)$$

where b is determined for a given material, and η_0 is a reference viscosity at T_0.

Another model used by Carley et al. (1979) takes the form:

$$\eta = \eta_0 \exp\left[\left(\frac{E_r}{R_g}\right)\left(\frac{1}{T} - \frac{1}{T_0}\right)\right] \qquad (2.80)$$

where E_r is the activation energy at constant stress and R_g is the molar gas constant. Chapter 3 gives more information with regard to these equations.

2.4 Boundary Conditions

An appropriate set of boundary conditions is necessary for the solution of the flow equations. Referring to Figure 2.2, boundary conditions must be specified in all solid and free boundaries. These may be either "essential" (referring to the primitive variables, i.e. velocities and temperatures) or "natural" (referring to fluxes) boundary conditions.

In the annular region, a creeping annular flow occurs with no slippage along the solid surfaces. A fully developed velocity profile, $v_z(r)$, corresponding to a given volumetric flow rate, Q, is assumed at the entry. The flow rate is readily calculated at the exit by:

$$Q = \pi(R_c^2 - R_w^2)V_w \tag{2.81}$$

where R_c is the radius of the coated wire. The entering velocity profile is then computed by assuming Newtonian flow in an annulus, which has been analytically expressed by Bird et al. (1960):

$$v_z(r) = \frac{R_o^2}{4\mu}\frac{dp}{dz}\left[1 - \left(\frac{r}{R_o}\right)^2 + \left(\frac{1-\kappa^2}{\ln(1/\kappa)}\right)\ln\frac{r}{R_o}\right] \tag{2.82}$$

where κ is the ratio of inner to outer radius. The Newtonian profile may be used since the shear rates at the entrance are relatively small. From the computational viewpoint any profile corresponding to given Q is acceptable since it will rearrange itself within a short distance from its initial state to satisfy the particular flow geometry and boundary conditions.

The relatively large channel gap feeding the melt to the die helps prevent significant viscous heating, making the assumption of uniform entry temperature acceptable. Constant wall temperature is assumed throughout this section. Mathematically, these boundary conditions are expressed as follows:

$$v_z(r_i, z) = v_z(r_o, z) = 0 \quad , \quad 0 \le z \le l \tag{2.83}$$

$$v_r(r_i, z) = v_r(r_o, z) = 0 \quad , \quad 0 \le z \le l \tag{2.84}$$

$$T(r_i, z) = T(r_o, z) = T_d = T_i \quad , \quad 0 \le z \le l \tag{2.85}$$

$$v_z(r, 0) = v_z(r) \quad , \quad 0 \le z \le l \tag{2.86}$$

$$T(r, 0) = T_m \quad , \quad 0 \le z \le l \tag{2.87}$$

In the die region, where the melt meets the wire, the boundary conditions are:

$$v_z(r_i, z) = V_w \quad , \quad l \leq z \leq L \tag{2.88}$$
$$v_z(r_o, z) = 0 \quad , \quad l \leq z \leq L \tag{2.89}$$
$$v_r(r_i, z) = v_r(r_o, z) = 0 \quad , \quad l \leq z \leq L \tag{2.90}$$
$$T(r_i, z) = T_w \quad , \quad l \leq z \leq L \tag{2.91}$$
$$T(r_o, z) = T_d \quad , \quad l \leq z \leq L \tag{2.92}$$

When adiabatic conditions are assumed, then:

$$\left.\frac{\partial T}{\partial r}\right|_{r=r_i} = \left.\frac{\partial T}{\partial r}\right|_{r=r_o} = 0 \quad , \quad l \leq z \leq L \tag{2.93}$$

In the exit region, no mass or momentum flux will occur at any point normal to the surface, and adiabatic conditions may apply for the heat flux. Upon emerging from the die, the polymer melt will acquire everywhere the speed imposed on the wire. In addition, surface forces on the free boundary are set to zero in the absence of surface traction. These boundary conditions are expressed mathematically as:

$$\bar{n} \cdot \bar{v}(r_o, z) = 0 \quad , \quad L \leq z \leq L_\infty \tag{2.94}$$
$$\bar{n} \cdot \bar{\Gamma}(r_o, z) = 0 \quad , \quad L \leq z \leq L_\infty \tag{2.95}$$
$$v_z(r_i, z) = V_w \quad , \quad L \leq z \leq L_\infty \tag{2.96}$$
$$v_r(r_i, z) = 0 \quad , \quad L \leq z \leq L_\infty \tag{2.97}$$
$$T(r_i, z) = T_w \quad , \quad L \leq z \leq L_\infty \tag{2.98}$$
$$-k \left.\frac{\partial T}{\partial r}\right|_{r=r_o} = 0 \quad , \quad L \leq z \leq L_\infty \tag{2.99}$$

where $\bar{n}$ is the outward normal vector and $\bar{\Gamma}$ is the surface traction. Note that r_i refers to the inner torpedo wall up to the end of the annular section, after which it refers to the wire surface (R_w), and r_o refers to the outer die wall and free surface.

From the solution of the velocity field a great deal of information can be obtained. The components of the rate-of-strain and stress tensors are calculated, the vorticity, viscous dissipation term and an update for the

free surface. The latter is accomplished by considering what happens after the melt has exited the die. It must be true that at every point along the free surface no cross-flow occurs (i.e. flow normal to the surface). This is mathematically expressed by Eq.(2.94). Using this criterion, a method for determining the free surface of the melt has been proposed by Caswell and Tanner (1978). The following expression is derived from Eq.(2.94):

$$r_o(z) = r_o|_L + \int_L^z \left(\frac{v_r}{v_z}\right) dz \tag{2.100}$$

and is used to calculate iteratively the free surface. The numerical integration is carried out using Simpson's rule.

A force is exerted by the viscous melt on the wire as it passes through the die section. A significant force may cause rupture of the wire. To calculate this quantity, the shear stress at the wire surface is integrated over the wire surface as follows:

$$F = \int_A \tau_w dA = \int_l^{L_\infty} \tau_w 2\pi r dz \tag{2.101}$$

Initially, the drag of the wire will pull the melt with it, creating a negative shear stress (in the direction opposite to the flow). This then causes tensile action on the wire. However, when the melt velocity surpasses the wire speed, the stress then becomes reversed in direction. Therefore, calculation of the maximum wire tension exerted by the melt on the wire is found by:

$$F_{\max} = \int_A \tau_w dA = \int_l^{L_0} \tau_w 2\pi r dz \tag{2.102}$$

where L_0 is the axial position where $\tau_w = 0$.

To solve for and present visually the streamlines in the flow domain, solution for the stream function is required. In axisymmetric flows the stream function ψ is defined by:

$$v_r = -\frac{1}{r}\frac{\partial \psi}{\partial z} \tag{2.103}$$

$$v_z = \frac{1}{r}\frac{\partial \psi}{\partial r} \tag{2.104}$$

Stream function values can be obtained by solving *a posteriori* the Poisson equation:

$$\nabla^2 \psi = -\omega \tag{2.105}$$

where ω is the vorticity given by

$$\omega_{xr} = -\omega_{rx} = \frac{\partial v_x}{\partial r} - \frac{\partial v_r}{\partial z} \tag{2.106}$$

and has been calculated from the solution of the flow field. The stream function is normalized to yield a more meaningful flow field variable:

$$\psi^* = \frac{\psi - \psi_{\text{wall}}}{\psi_{\text{wire}} - \psi_{\text{wall}}} \tag{2.107}$$

where ψ_{wall} and ψ_{wire} are wall and wire stream function values, respectively. Note that ψ^* represents a fraction of the total melt flow rate, such that $0 < \psi^* < 1$. If ψ^* is outside the 0 to 1 interval, this would indicate that recirculation is occurring. The total flow rate may also be computed by using the stream function ψ according to:

$$Q = 2\pi \left(\psi_{wall} - \psi_{wire}\right) \tag{2.108}$$

Additionally, it should be noted that the energy equation with no convection satisfies a Poisson equation of the form:

$$k\nabla^2 T = -Q_d \tag{2.109}$$

The quantity Q_d is the viscous dissipation term ($Q_d = \bar{\bar{\tau}} : \nabla \cdot \bar{v}$). Note that Eq.(2.109) is equivalent to Eq.(2.105) when $Q_d = \omega$, $k = 1$ and $T = \psi$.

The Peclet number (Pe) of the system is also an important parameter and is defined as:

$$\text{Pe} = \frac{\rho C_p V_w R_w}{k} \tag{2.110}$$

which is a measure of the relative importance of convective heat transfer to conductive heat transfer. The Pe number in typical wire-coating operations ranges between 1000 and 20000. Such a Pe range is the highest encountered in any polymer processing operation.

2.5 Method of Solution

2.5.1 Lubrication Approximation Theory (LAT)

Unlike the case of a Newtonian fluid, power-law fluids have no exact solution, and therefore a numerical solution is required. Fenner's (1970) method

involved interpolation between characteristic curves generated for different K and n values, with π_Q appearing as an explicit variable on each graph. Interpolation between the curves would yield the information required for solution.

A thorough numerical solution of the dimensionless LAT equations gives more precise results however. An initial assumption of a $(\lambda K)^2$ value is required, and a dimensionless flow rate may be calculated. This quantity must agree with the actual (dimensionless) flow rate, otherwise alteration of the initial guess is required. A Newton-Raphson iterative technique may be used. In a certain region where the initial assumed value of $(\lambda K)^2$ is not appropriate, a bisection iterative method can be implemented. Such a numerical solution has been applied by Heng (1986), who solved the LAT equations using a FORTRAN computer program called LAT. This program has been used to obtain the LAT results of the present work.

2.5.2 Finite Element Method

The flow domain is initially discretized into numerous, small triangular subdomains called "finite elements". This is normally done automatically, unless a particular variation in the grid arrangement is required. The size or shape of each individual element need not be the same. Considering every element separately, a given contribution to the overall solution is determined, thus resulting in a "piecewise" approximation using the governing differential equations.

The solution of the equations along with the boundary conditions was carried out using the MACVIP finite element program developed for creeping viscoelastic flows (Mitsoulis et al, 1983). MACVIP implements a finite element formulation using the "primitive variable approach" and the "principles of virtual work" for planar or axisymmetric geometries. The primitive variable approach involves solving for radial and axial velocities (u and w, respectively) and the pressure (p). Each triangular element contains six nodes. The velocities u and w require solution at each node and pressure requires solution only at the three vertex nodes, as shown in Figure 2.3. Knowledge of the nodal quantities allows interpolation over the element to determine the value of a given field variable at any point. This is accomplished using continuous functions known as "interpolation" functions. Velocities are interpolated quadratically and pressures are interpolated lin-

early over the element domain. Secondary variables such as stresses, rates-of-strain, and stream function quantities can be determined from the known primitive variables. A more in-depth explanation of the principles behind the FEM can be found in the book by Huebner and Thornton (1982).

The analysis using MACVIP follows the procedure as outlined in the flowchart of Figure 2.4. A complete data file is composed of input data essential for proper simulation using the FEM. Such data includes material properties, operating and boundary conditions, information to allow construction of the finite element grid, geometric structure of the die, required number of solution or free surface iterations, and various flags to invoke or suppress certain capabilities of the program (such as nonisothermal or non-Newtonian analysis). Initially the finite element grid is constructed, after which all other data is incorporated. If the analysis is nonisothermal, temperature data is read in from an external file and used to calculate new viscosity values.

Since this method is based on solution contributions from area domains rather than individual points, the differential equations are rewritten in approximate integral form. Substituting the interpolation functions into these approximate integral equations and having set the boundary conditions, a set of simultaneous linear algebraic equations is created. The primitive variables are then found from the following expression:

$$\begin{bmatrix} [K_v] & [K_p] \\ [K_p]^T & [0] \end{bmatrix}_n \begin{pmatrix} \begin{pmatrix} u \\ w \end{pmatrix} \\ (p) \end{pmatrix}_n = \begin{pmatrix} (F) \\ (0) \end{pmatrix}_n \qquad (2.111)$$

The individual contributions from each element are found through integration of the individual terms of the FEM expressions corresponding to the conservation equations. Together they produce a symmetric "stiffness matrix", $[K]$, for each element n, with all contributions eventually added up and equated with the "load vector", F, that contains body forces, surface tractions and boundary conditions. These algebraic equations are solved by using the frontal method (Hood, 1976 and Taylor and Hughes, 1981). Since the viscosity is strain-rate dependent, a direct iteration scheme has been employed in the non-linear analysis. This direct substitution algorithm (Picard method) is based on the root-mean-square error (norm of the error) of velocities for successive iterations.

Iterations were initially performed until satisfactory convergence was

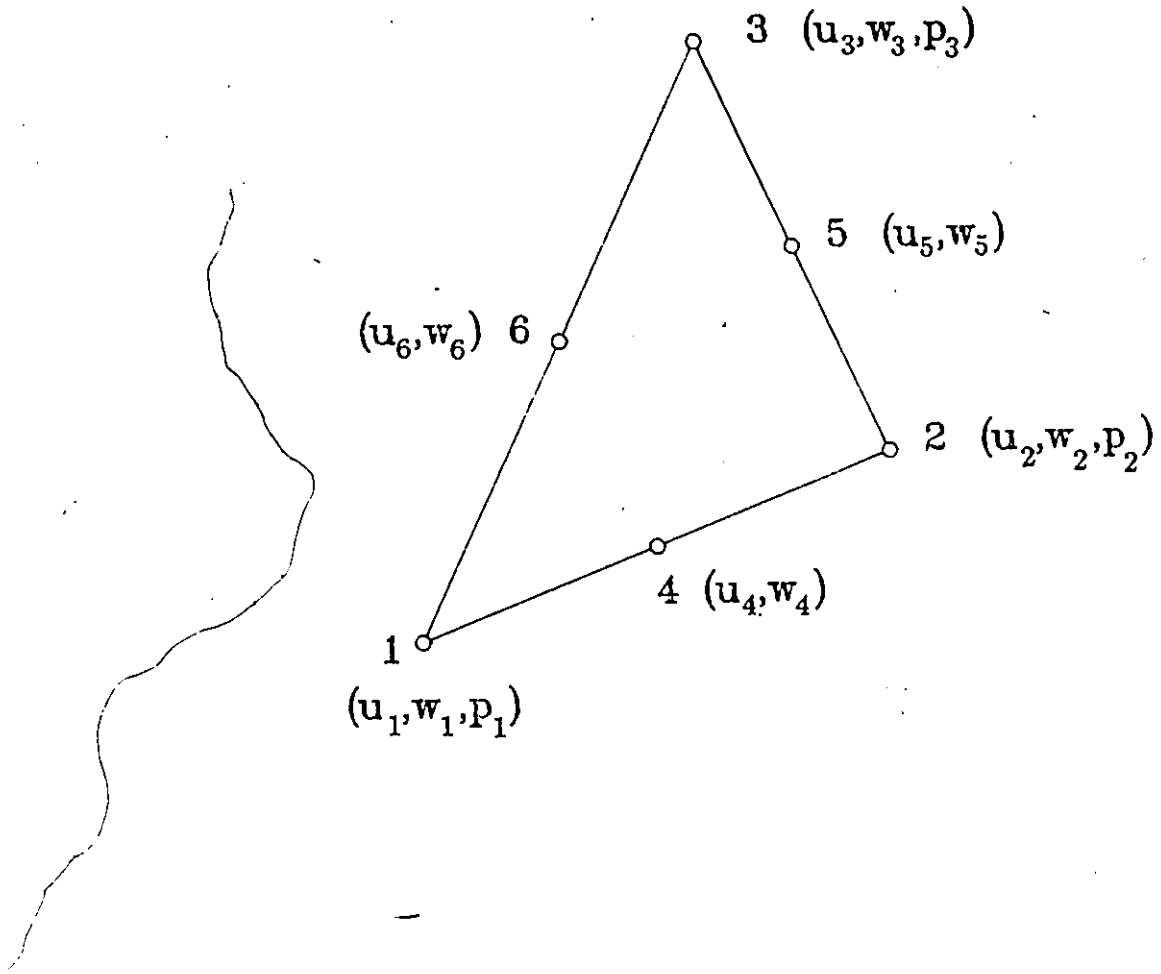

Figure 2.3: Typical Element Used in FEM Analysis.

achieved, after which the free surface was determined. Three iterations were normally sufficient with the first iteration being done by assuming a constant viscosity. The grid was then regenerated to account for the altered domain due to the inclusion of the free surface and the process for u-w-p solution was repeated. The free surface was solved for until little change was observed, usually requiring three attempts with last determination having no subsequent processing. Therefore, a total of five iterations was normally performed overall.

Computer time requirements for MACVIP vary due to various considerations such as number of iterations desired and the extent or intensity of the analysis. A denser grid will undoubtedly yield more precise data although the increase in CPU time required could make costs prohibitive. Therefore a balance must be struck between the two concerns: Overall CPU time for the five iteration process described above ranged between 114 and 121 CPU *secs*, with an average requirement of 24 CPU *secs* per iteration for the grids used in this study.

Figure 2.5 shows how the main program (MACVIP) interacts with other programs which have been designed to solve for other variables by using data created by the former. The solution for nodal temperatures in a nonisothermal analysis is done by the program POISSON FORTRAN. It requires the data files produced by the main program on coordinates (CWIRE DATA), velocities and pressures (SWIRE DATA), viscous dissipation (QWIRE DATA) and stresses (STWIRE). The POISSON FORTRAN program divides each 6-node element used for u-w-p formulation into 4 sub-elements with 3 nodes each.

As with the pressure determination, a linear approximating function is used for evaluation of temperatures over elements. This function is substituted into an integral form of the differential equation for the conservation of energy, which accounts for thermal variations due to convection, conduction, and viscous dissipation. From this, a linear system of finite element equations is obtained, expressed in the form

$$[K_T]\,[T^*] = [F_T] \tag{2.112}$$

where $[K_T]$ is the global heat stiffness matrix (unsymmetric), $[F_T]$ is the heat load vector incorporating all boundary conditions, and $[T^*]$ is the column matrix of the unknown nodal temperatures. The matrix solver used for solution is based on the Choleski decomposition method for non-

symmetric matrices. It was found that time requirements for execution were approximately 6 CPU *secs.*

Temperature oscillations were initially found to exist at moderate to high Peclet numbers (i.e. relatively high convection) by Mitsoulis (1984). To suppress these oscillations without making major grid density increases, a mathematical method called "upwinding" can be implemented. Basically, the contribution of the convective term is found through integration of the element matrices over the area of each triangle. This integration is performed at three midside nodes that are called the Gauss-Quadrature integration points. The upwinding technique serves to relocate these integration points so that the oscillations due to the convective term are minimized or eliminated. Some difficulties, however, arise from the fact that although upwinding suppresses the oscillations, it also introduces a certain degree of error into the computations. The upwinding process employed throughout this study is detailed further by Mitsoulis (1984).

After the final series of iterations has been completed by the main program, data is transferred to find the stream function values. This is accomplished by using the same program and format used to solve for temperatures, since mathematical description of the two are very similar (both satisfy the Poisson equation as seen earlier in this Chapter). Therefore by setting the thermal conductivity, k, equal to 1, eliminating the convection term and replacing the viscous dissipation with vorticity, quick determination of the stream function is accomplished using the POISSON FORTRAN program.

Finally, visual displays are created to illustrate the performance within the die by using the PLWIRE FORTRAN program. The stream function values are normalized, after which streamline patterns are produced by connecting points of equal value (i.e. contours). This procedure is also carried out for temperature values to give a presentation of isotherms. Other data, such as pressure, shear stresses, and wire tension are read in directly to quickly produce visual displays of their distributions in the die.

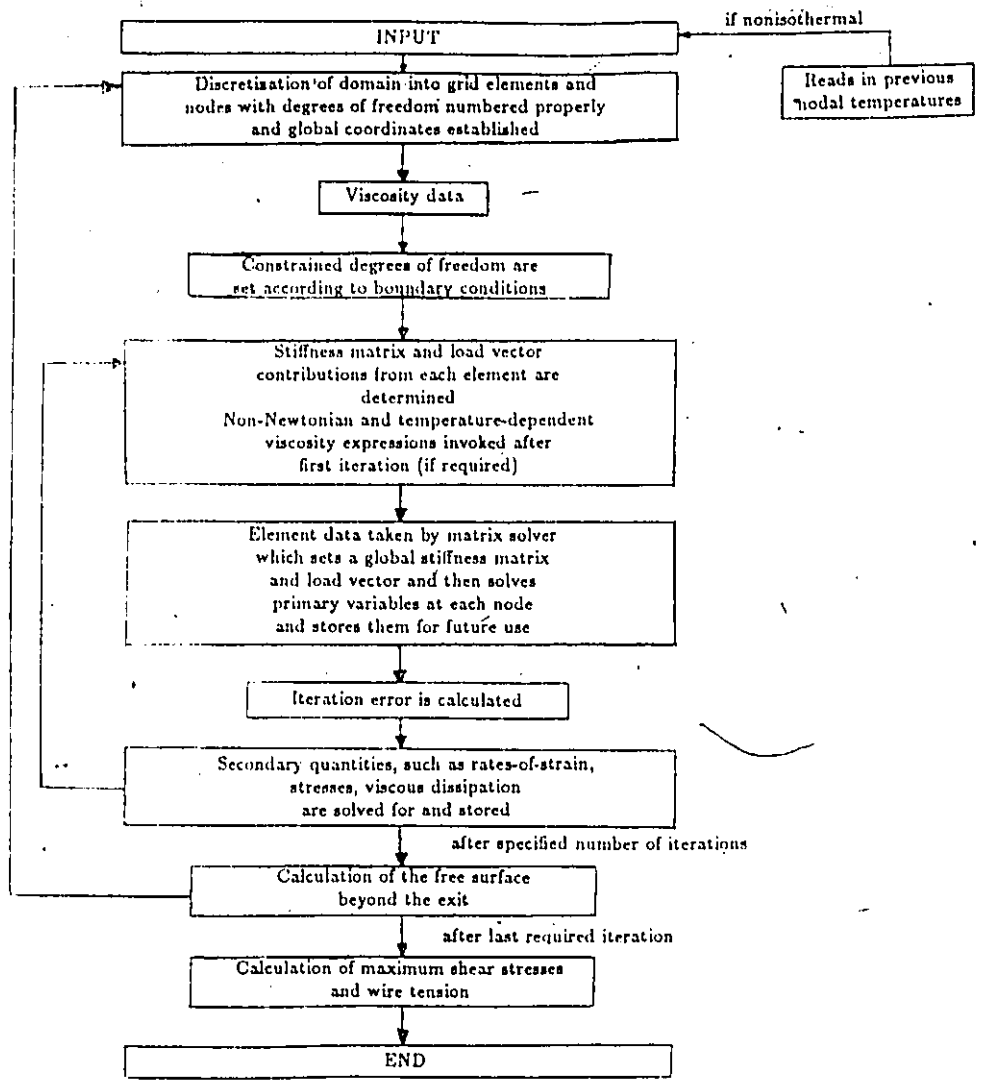

Figure 2.4: Flow Sheet for the Organization of Main Program (MACVIP).

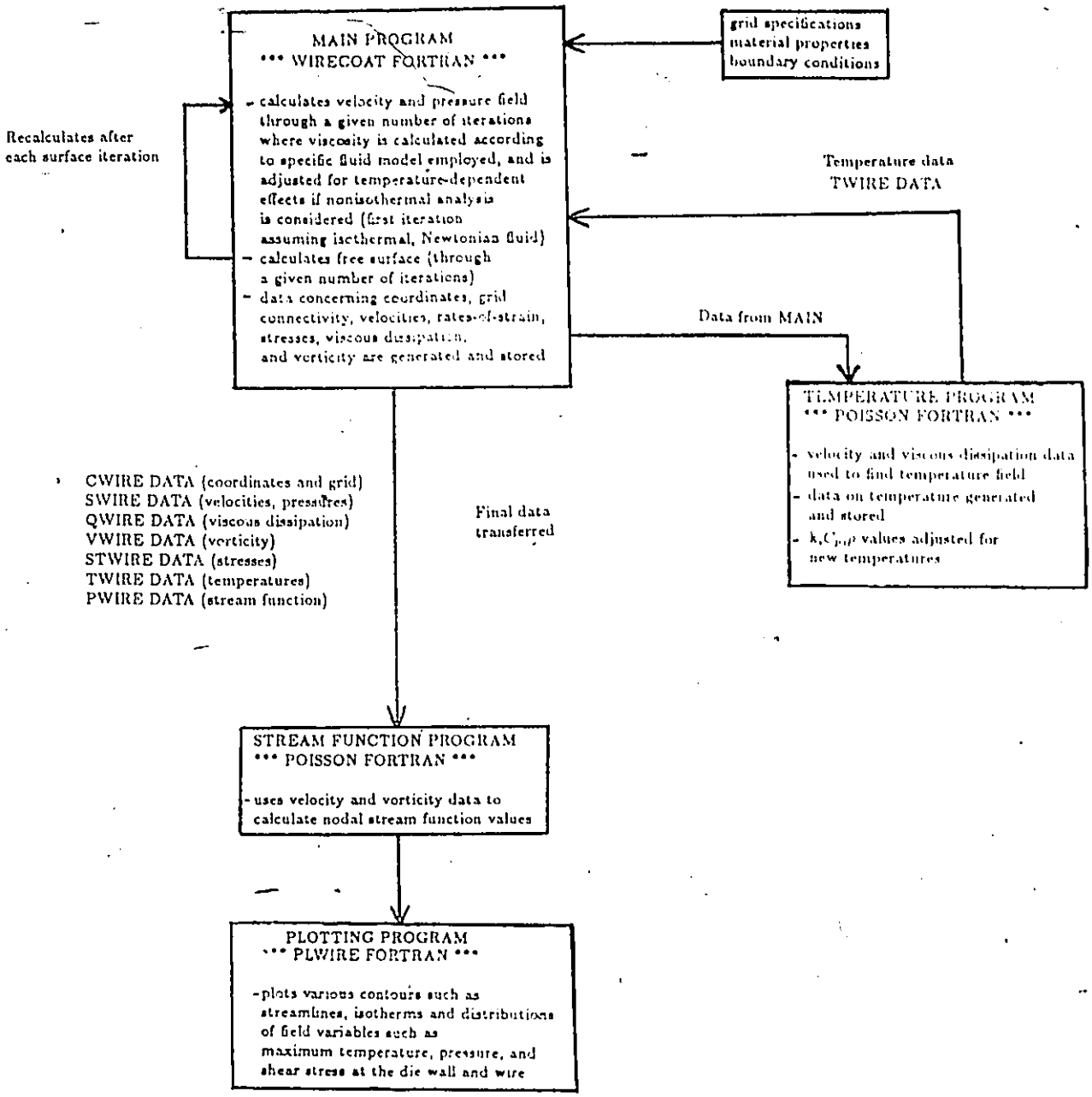

Figure 2.5: Sheet for the Overall Organization of all Programs Used.

Chapter 3

MATERIAL PROPERTIES

Low density polyethylene (LDPE) and plasticized polyvinyl-chloride (PPVC) are the primary coating materials under consideration due to their extensive commercial use. Material properties of these polymer melts such as viscosity, density, specific heat, and thermal conductivity are presented along with some characteristic critical values for stresses and temperatures useful in polymer processing.

3.1 Viscosity

The chemical structures of both LDPE and PVC are relatively basic,

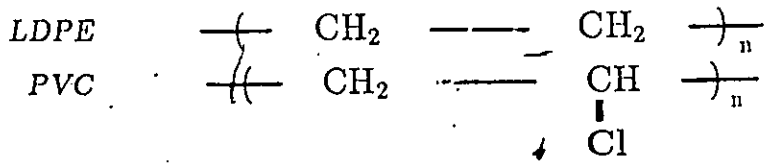

the repeat units of which are shown above. A detailed analysis of the chemical aspects of LDPE and PVC is given by Tadmor and Gogos (1979).

LDPE is a versatile plastic which can be modified with relative ease to enhance its properties. Given its relatively low cost, it enjoys great usage in comparison to other coating materials. PVC is more flexible than LDPE and has very good resistance to corrosion and flame. In addition, PVC has good electrical insulating properties but is much more thermally sensitive than LDPE.

At low shear rates, polymeric melts exhibit a generally constant viscosity, and thus they can be described adequately by the Newtonian model:

$$\eta = \mu = \text{constant} \tag{3.1}$$

where μ is the Newtonian viscosity.

These fluids, however, exhibit decreased viscosity at high shear rates ("shear-thinning" behavior). In wire-coating operations, very high shear rates are encountered that may reach 10^6 s^{-1} . The shear-thinning behavior is adequately represented by the power-law model which relates the viscosity η to the shear rate $\dot{\gamma}$ according to:

$$\eta = m\,|\dot{\gamma}|^{n-1} \tag{3.2}$$

where m is the consistency index and n is the power-law index.

To account for the entire shear rate range (i.e. Newtonian behavior at low shear rates and power-law behavior at higher shear rates) other models can be applied such as the Carreau or the Ellis model (Bird et al., 1977). Carley et al. (1979) have employed a three-equation model covering the entire shear range. This model includes a Newtonian regime at low shear rates, a transition regime at intermediate shear rates and a power-law regime for high shear rates. Upon specification of a Newtonian/transition shear rate value $\dot{\gamma}_N$ and a transition/power-law shear rate value $\dot{\gamma}_P$, the following equations were used:

$$\log\tau = \log\dot{\gamma} + \log\mu \qquad \dot{\gamma} \le \dot{\gamma}_N \tag{3.3}$$

$$\log\tau = a(\log\dot{\gamma})^2 + b(\log\dot{\gamma}) + c \qquad \dot{\gamma}_N \le \dot{\gamma} \le \dot{\gamma}_P \tag{3.4}$$

$$\log\tau = n(\log\dot{\gamma}) + \log m \qquad \dot{\gamma} \ge \dot{\gamma}_P \tag{3.5}$$

Eq. (3.3) is the Newtonian model and Eq. (3.5) is the power-law model, both expressed in logarithmic form. The given constants are found by requiring that the slopes be equal between the regions at the points of transition. The corresponding values are shown in Table 3.1. Note that τ is expressed in dynes/cm^2 and μ has the units of poise. Figures 3.1 and 3.2 illustrate the viscosity behavior over a large range of shear rates at different temperatures for LDPE and PPVC, respectively.

The temperature dependence of LDPE and PPVC was expressed by the Arrhenius relationship

$$\eta = \eta_0 \exp\left[\left(\frac{E_\tau}{R_g}\right)\left(\frac{1}{T} - \frac{1}{T_0}\right)\right] \tag{3.6}$$

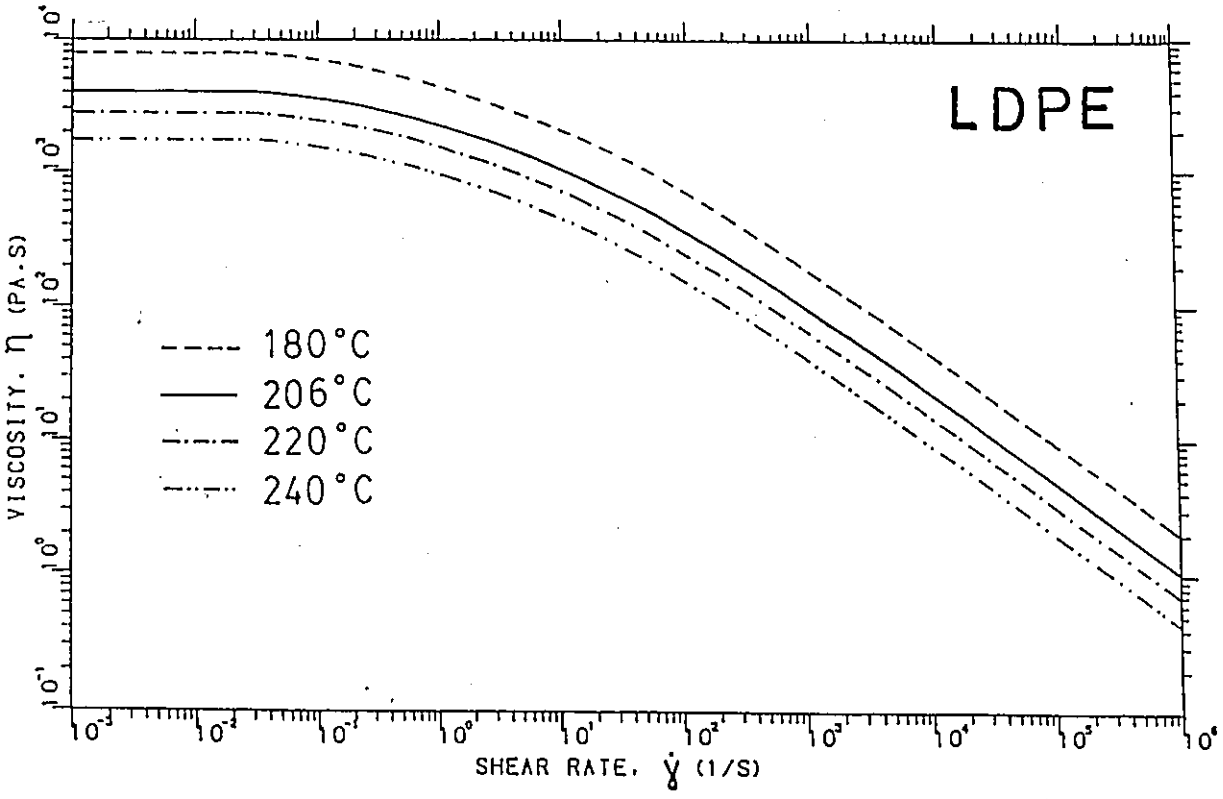

Figure 3.1: Viscosity Curve for LDPE (Carley et al., 1979).

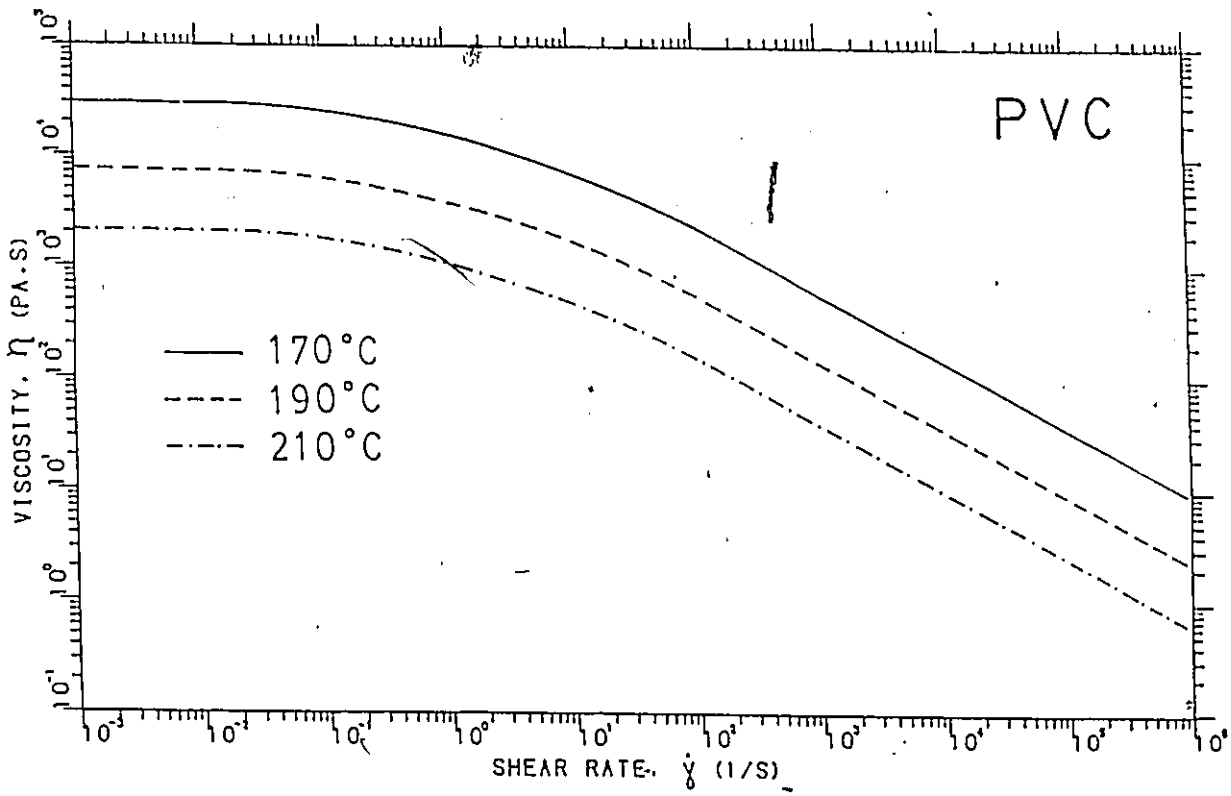

Figure 3.2: Viscosity Curve for PPVC (Carley et al., 1979).

Table 3.1: Parameters for Model Proposed by Carley et al. (1979).

Parameter	LDPE Value	PPVC Value
a	-0.06408	-0.06971
b	0.7437	0.7212
c	4.346	5.198
μ	40000	300000
$\log m$	5.004	5.568
n	0.333	0.400
$\dot{\gamma}_N$	$0.01s^{-1}$	$0.01s^{-1}$
$\dot{\gamma}_P$	$1600s^{-1}$	$201s^{-1}$
T	$206°C$	$170°C$

Table 3.2: Parameters for Temperature-Dependent Viscosity Model.

Variable	Units	LDPE	PPVC
E_τ	cal/gmol	11700	28400
η_0	poise	40000	300000
T_0	$°C$	206	170

where η_0 is the reference viscosity at a reference temperature T_0; E_τ is the activation energy at constant stress, and R_g is the molar energy constant ($R_g = 1.987$ cal/gmol·K). Table 3.2 gives the values employed in this analysis.

During this research an LDPE sample (Alathon 3535) was supplied from Du Pont Co., data from which was to be used in the analysis of the die presented by Haas and Skewis (1974). Experimental viscosity data was obtained using a capillary viscometer (Tzoganakis, 1986). Shear stress-shear rate curves were obtained at four different temperatures (190°C, 210°C, 230°C, and 250°C). The shear rate region was from about 2 s^{-1} to 2000 s^{-1}. The data was then corrected in terms of Rabinowitch and Bagley methods (McKelvey, 1962). The following viscosity function was used to curve-fit the data via linear regression analysis (Agur and Vlachopoulos, 1982):

$$\ln \eta = a_1 + a_2 \ln \dot{\gamma} + a_3 (\ln \dot{\gamma})^2 + a_4 T + a_5 T^2 + a_6 T \ln \dot{\gamma} \qquad (3.7)$$

where

$$a_1 = 10.6773 \qquad a_2 = -0.7615 \qquad a_3 = -0.0072$$
$$a_4 = 0.0035 \quad a_5 = -4.473 \times 10^{-5} \quad a_6 = 0.00113$$

Figure 3.3 shows the experimental data points and the corresponding viscosity curves in the shear region from $1s^{-1}$ to $10^6\ s^{-1}$. To test the LAT for power-law fluids, the following power-law relations were also obtained by curve-fitting the data:

$$\text{at } 190°C \quad \tau = 18184\dot{\gamma}^{0.3994} \tag{3.8}$$
$$\text{at } 210°C \quad \tau = 14459\dot{\gamma}^{0.4051} \tag{3.9}$$
$$\text{at } 230°C \quad \tau = 10241\dot{\gamma}^{0.4378} \tag{3.10}$$
$$\text{at } 250°C \quad \tau = 6967\dot{\gamma}^{0.4629} \tag{3.11}$$

In the above equations, the shear stress is expressed in Pa.

3.2 Density

The density of LDPE is a function of temperature, and is expressed according to Raff and Allison (1956) as:

$$\rho = [1.143 + (0.00089)T]^{-1} \qquad T \geq 127°C \tag{3.12}$$

where T is the temperature in °C, and ρ is expressed in g/cm^3. This relationship was used by Endo (1976) in his research and it is also employed in this work. Clogswell (1972) gives data concerning density of molten LDPE with moderate branching, reporting 0.746 g/cm^3 at 210°C, as compared with 0.752 g/cm^3 from the above relationship. Basu (1981) presents another density relationship for LDPE as a linear function of temperature (1 atm):

$$\rho = 0.8772 - 0.00059T, \qquad T \geq 150°C \tag{3.13}$$

The density from this expression at 210°C is calculated to be 0.753 g/cm^3, which is in excellent agreement with the value found using Eq. (3.12). The ambient temperature (23°C) density of LDPE is given by Basu (1981) as 0.918 g/cm^3. Overall, the density will depend on the chemical structure of the particular type of polymer used.

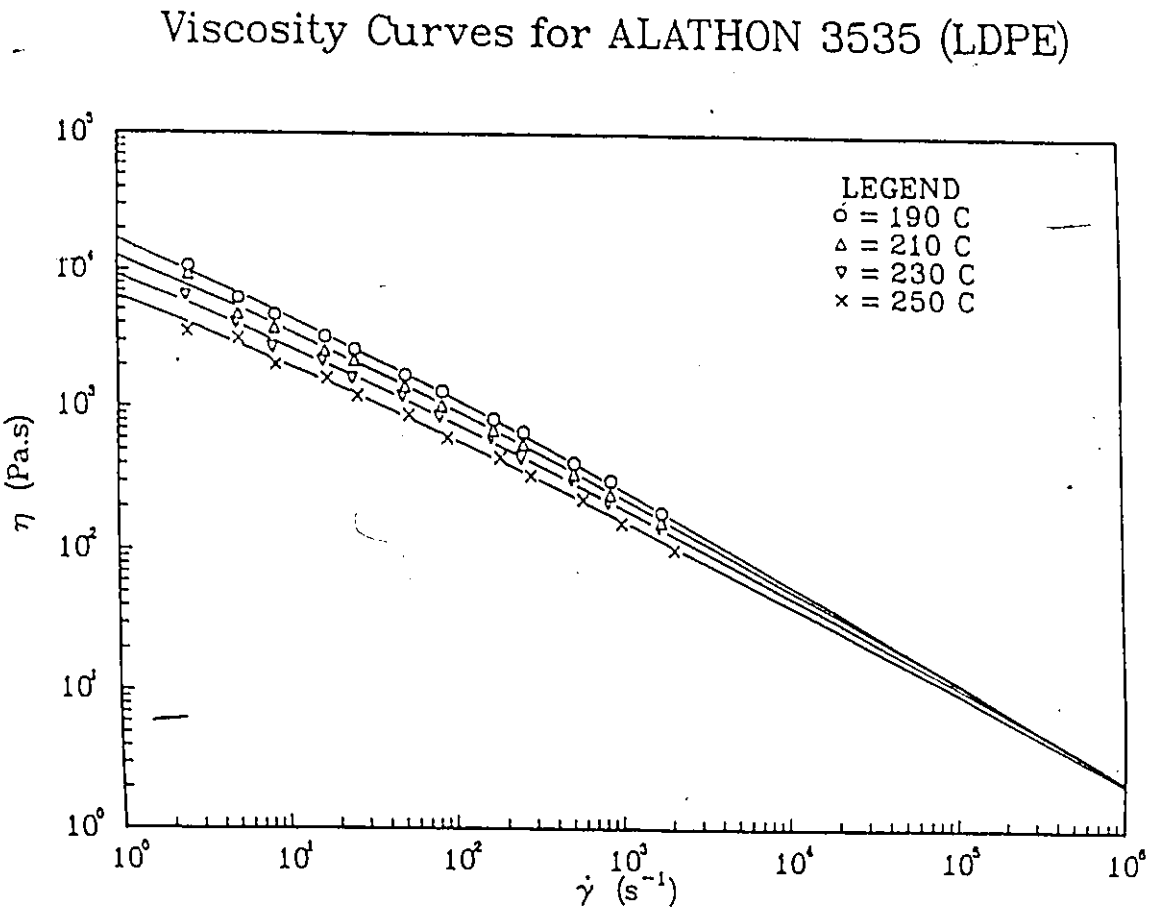

Figure 3.3: Viscosity Curve for a Commercial Wire-Coating LDPE Melt (Alathon 3535) Supplied by Du Pont Co. Experimental Data and Least-Squares Fit.

For this research, the method of assuming the density for PVC used by Endo (1976) was employed. In lieu of available data, 90% of the density at 25°C was taken to represent the density at 170°C (1.05 g/cm^3). Cogswell (1972) gives a density of 1.39 g/cm^3 at 190°C for a rigid grade of PVC, and this may possibly be more accurate but it is not definitely known.

3.3 Thermal Conductivity

Limited information on thermal conductivity values is available in the literature for polymer melts. Lack of data for LDPE in the molten state for this particular property means that a satisfactory value must be assigned. Endo (1976) cites a thermal conductivity value, k, at room temperature (23°C) as $k = 0.0032886$ J/cm · s ·°C. Basu (1981) uses virtually the same value in his research and therefore it will also be used in this work. Furthermore, the thermal conductivity value for PVC used by Endo (1976) is $k = 0.0014226$ J/cm · s ·°C for the entire temperature range, and this is also used in the present computations. Since the temperature dependence of k is relatively weak, little error will be introduced by introducing constant values.

3.4 Specific Heat

Specific heats for polymer melts are functions of temperature. The following linear relationships, quoted by Endo (1976), are given by Dole et al. (1952) for LDPE and Koleske and Wartmen (1969) for PVC, respectively:

$$LDPE \quad C_p = 2.079 + 0.003376T \tag{3.14}$$

$$PVC \quad C_p = 0.857 + 0.00362T \tag{3.15}$$

Temperature T is expressed in °C and C_p is expressed in J/g ·°C. Basu (1981) also makes use of Dole's correlation in his research.

3.5 Critical Stress

An important consideration in wire-coating operations is the stress allowable before the onset of "melt fracture". Melt fracture occurs when a fluid

is subjected to shear stresses that are too large to allow smooth coating of a wire. This critical stress value depends upon the material used. Vlachopoulos and Chan (1977) and Vlachopoulos and Alam (1972) have done work in this area, and the latter study presents expressions to calculate critical shear stress values for a variety of materials, including LDPE. The critical stress values are functions of molecular weight and temperature, and for LDPE the following expression was found to apply:

$$\frac{\tau_{cr}}{T_{abs}} = 1317 + \frac{1.005 \times 10^8}{MW} \tag{3.16}$$

where τ_{cr} is the critical shear stress (dynes/cm^2), T_{abs} is the absolute temperature, and MW is the molecular weight of the resin. Figure 3.4 shows the critical shear stress values as a function of temperature with the upper curve representing an LDPE resin with a molecular weight of 50000 and the lower curve of a molecular weight of 90000. The two curves represent typical extremes for LDPE molecular weights. It is also of importance to note that these expressions were obtained from data generated for a 90-degree entrance angle. Hence, there is evidence that properly designed tapers may allow the critical stress values to be exceeded without necessarily leading to melt fracture.

The only available critical shear stress data on PVC is given by Agassant (1980) and is presented in Figure 3.5. Higher temperatures will increase the critical stress even though the actual stresses will be lowered as a result of the decreased viscosity. The molecular weight for this particular PVC sample was not specified.

3.6 Thermal Degradation

Large temperature rises in the melt cause concern with respect to thermal stability of the polymer. An extensive literature search has shown limited information for polymer melts, but studies of polymer melt flows gave implicit information. For example, LDPE has been tested over a wide variety of temperatures (150 - 300°C) and apparently does not degrade within that range. Hammond (1960) has stated that LDPE operation above 227°C is desired since it improves the finish of the final coating. On the other hand, PVC was never found to be used at temperatures above 210°C, and it is ex-

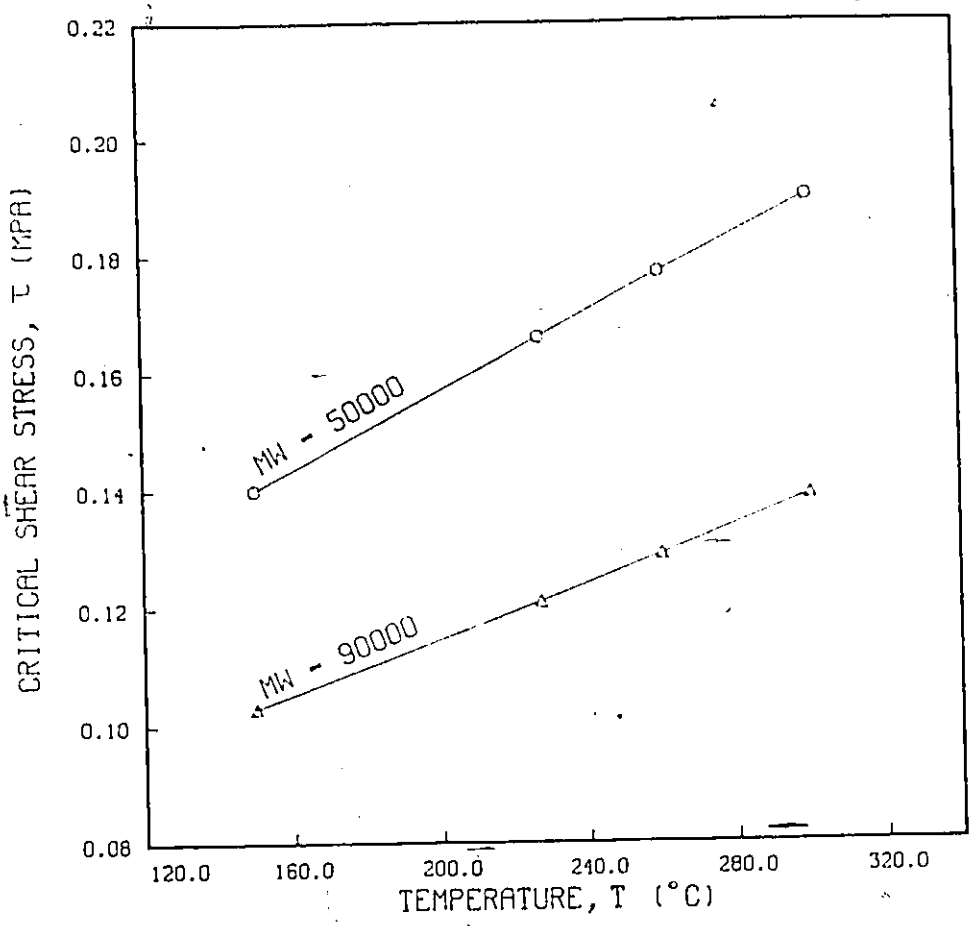

Figure 3.4: Critical Shear Stress vs. Temperature for LDPE (Vlachopoulos and Alam, 1977).

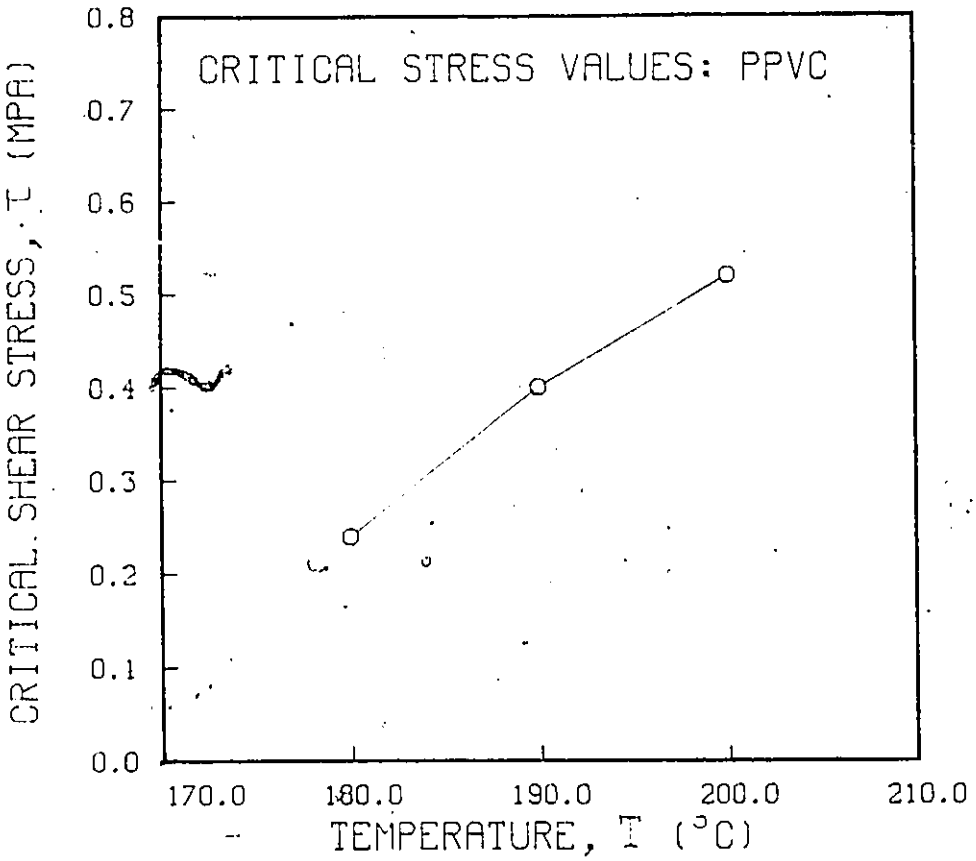

Figure 3.5: Critical Shear Stress vs. Temperature for PVC (Agassant, 1980).

pected that significant degradation occurs around and above this temperature. Griff (1968) states that the normal operating temperature using PVC compounds is somewhere around 185°C. The decomposition mechanism involves the elimination of hydrogen chloride molecules after which oxidation occurs at the double bonds, leading to possible discoloration of the polymer. Furthermore, simultaneous cross-linking of the resin yields subsequent deterioration of material properties and possible extrudate roughness. Heat stabilizing compounds are available to assist in helping to combat this problem although the choice of a particular one must satisfy specific criteria for a given set of circumstances. Further information on the sensitivity of PVC melts is found in work by Owen (1967), Collins and Daniels (1974), and Collins (1978).

Chapter 4

ANALYSIS OF FENNER'S DIE

A particular die design is examined by using both LAT and FEM analysis. The LAT is applied for Newtonian and power-law fluids under isothermal conditions. Results obtained from the FEM are compared with LAT results for verification. The FEM analysis is then extended to nonisothermal conditions, and a series of parametric studies is done for both LDPE and plasticized PVC.

4.1 Introduction

The die configuration given by Fenner (1970) is shown in Figure 4.1. There are two distinct regions: the region around the torpedo (Section Y-Y) and the die region (Section X-X). The polymer melt will contact the bare wire where the torpedo comes to an abrupt end (Section A-A).

Analyses undertaken by Fenner (1970) are for isothermal conditions, assuming either Newtonian or power-law constitutive models. The effect of viscous dissipation was not examined. Extension to nonisothermal analysis is important in order to obtain results in a more realistic environment and also show the relative influence that internal heat generation has on previous isothermal findings.

For this die, both an LDPE and a plasticized PVC resin will be considered as the principal coating materials. This analysis assumes a wire radius of 0.025 cm with a constant coating thickness of 80% the wire radius for a

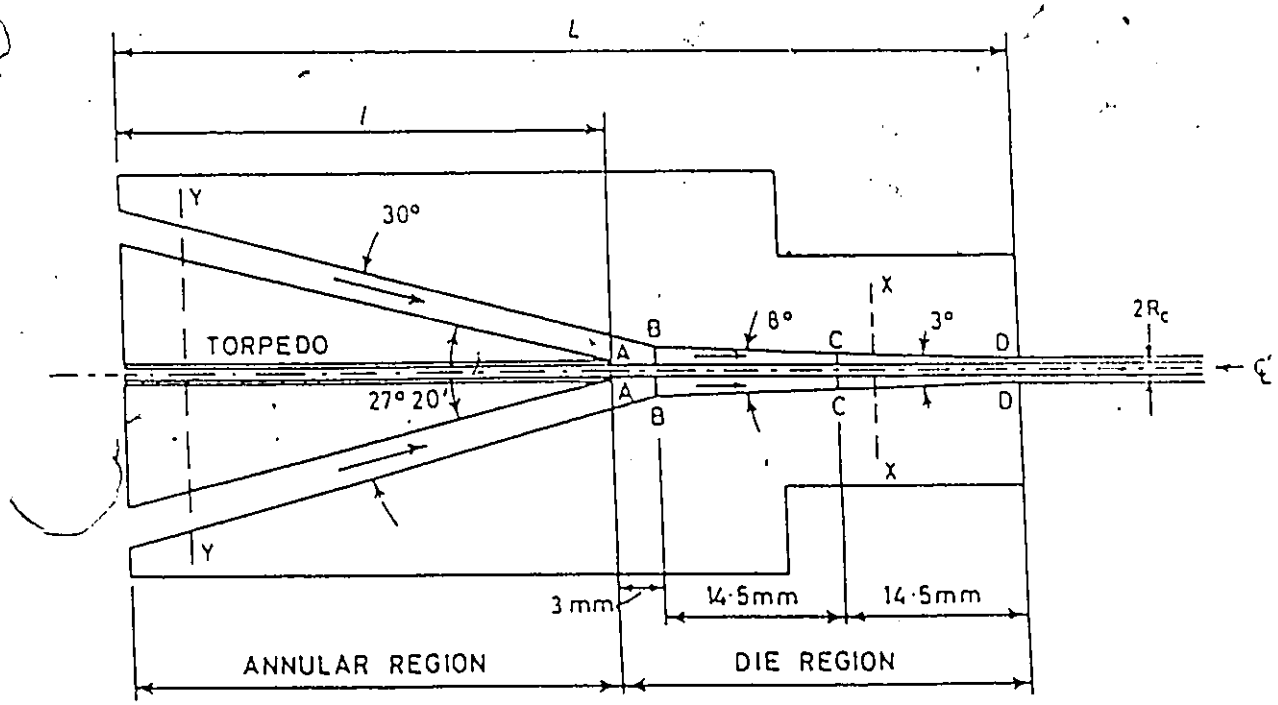

Figure 4.1: Fenner's Wire-Coating Die Unit

final radial thickness of 0.045 cm at the exit. The difference between the melt and ambient resin density is not considered in this particular analysis.

4.2 LDPE: Isothermal Analysis

This analysis assumes that the containing surfaces remain at a fixed temperature along the die and that the temperature of the LDPE melt stays unchanged. This assumption is carried through for both Newtonian and power-law fluids.

4.2.1 Lubrication Approximation Theory

The LAT has been applied to this system for fluids having different power-law indices. The results are generated by using the LAT FORTRAN program. For the LAT analysis, Heng (1986) used 30 axial divisions in the die region and 100 axial divisions in the annular region, with 100 vertical divisions for every axial location. These conditions are acceptable since it is found that a three-fold increase in total number of divisions yields differences under 1% while nearly doubling the execution time required. It was found that execution time for the Newtonian case took approximately 3 CPU *secs*, whereas in the case of a power-law fluid the execution time was about five times greater. Figure 4.2 shows the pressure distribution in dimensionless form for different fluids (n = 1.0, 0.75, 0.50, and 0.25).

It can be seen that for the Newtonian case (n = 1), the entry pressure in dimensionless form was found to be around 31.1 and a pressure build-up in the die section reached a dimensionless value of 42.2. The positive pressure gradient that exists in the die region corresponds to a development of a velocity profile showing flow in the opposite direction, beginning with the fluid nearest the die wall. This partial recirculation of flow is very undesirable, having an adverse effect on the quality of the final product. The exact extent and intensity of recirculation cannot be readily determined in the LAT analysis.

The previous figure shows two interesting aspects with respect to the behavior of power-law fluids. First, the dimensionless entry pressure for the n = 0.50 fluid exceeds that of the n = 0.75 fluid, and the n = 0.25 fluid surpasses all fluids. Secondly, the pressure build-up in the tapered

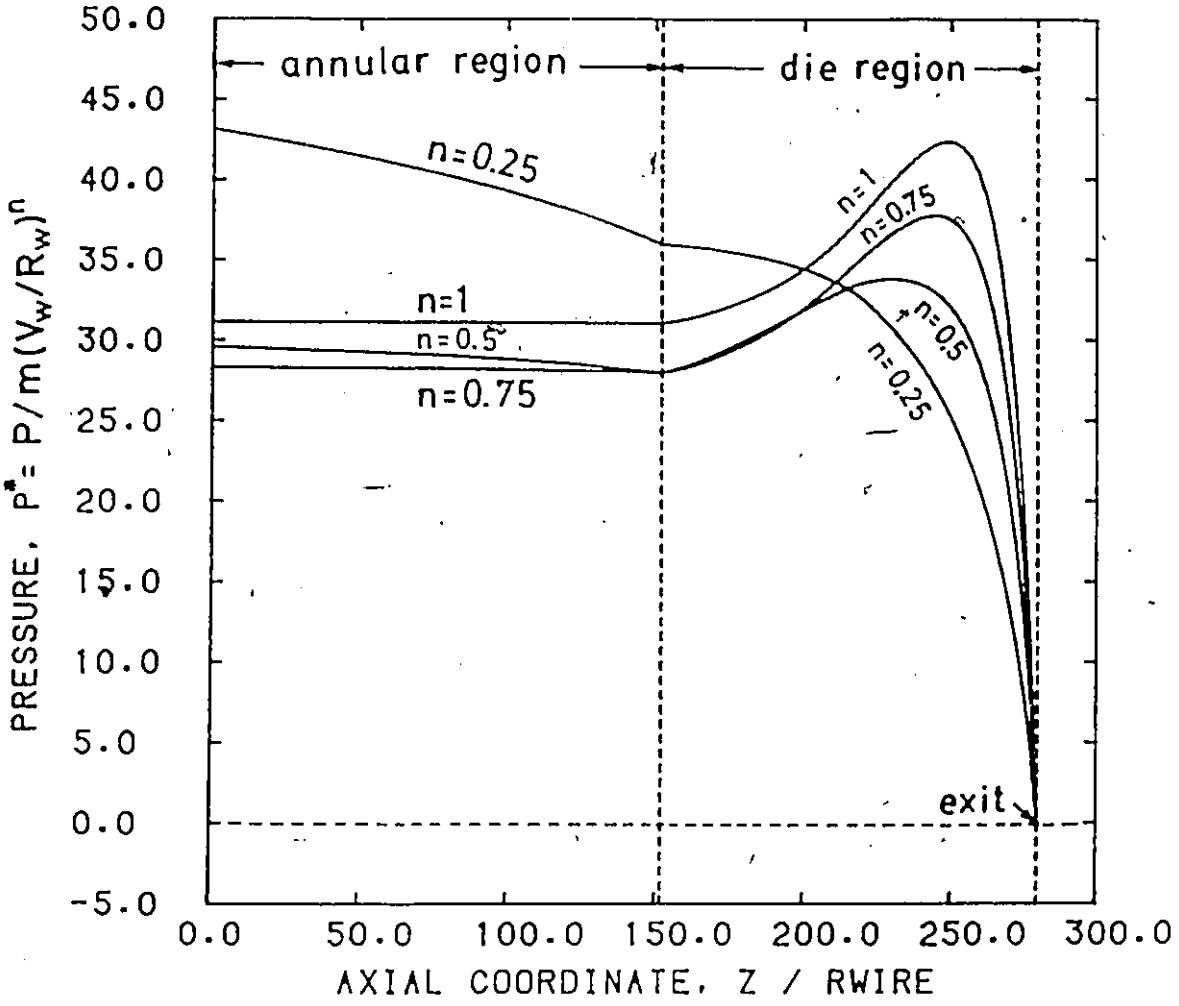

Figure 4.2: Dimensionless Pressure Distribution along Fenner's Wire-Coating Unit for Power-law Fluids (Lubrication Approximation Theory).

region decreases steadily with the power-law index, and it is seen that at n = 0.25 the pressure exhibits a consistent, monotonic drop. The pressure distribution of each fluid is linked with the nature of the flow field found to exist in each case (e.g. the occurrence of backflow). More detailed discussion of this is made in the FEM analysis section.

Because of the rearrangement of the velocity profile throughout the length of the die, the shear stresses will also change continually along the axial length. Figure 4.3 gives the dimensionless shear stress distribution at the wire and die wall. The wire tension is also calculated from knowledge of the shear stress state along the wire, and is presented in dimensionless form in Figure 4.4.

Fenner used the LAT method to analyze his die design considering an LDPE melt following power-law behavior with n = 0.48. The consistency index was not given by Fenner, and therefore it needed to be calculated. Using the value of inlet pressure (27 MPa) cited for a speed of 510 cm/s, the consistency index was found to be m = 0.00745 MPa $\cdot s^n$. Fenner considered two speeds, 510 cm/s and 2040 cm/s, under isothermal conditions (300°C). Several performance quantities were found including inlet pressure, shear stresses and wire tension. These results present a basis for comparison with the FEM analysis under similar conditions.

4.2.2 Finite Element Analysis

The finite element grid employed to compute the required quantities is shown in Figure 4.5. This particular grid was initially tested under Newtonian isothermal conditions to verify the adequacy of the finite element discretization. Mitsoulis (1986) found that this grid, consisting of 240 triangular elements for velocities-pressure and 567 nodes, gave results virtually identical to those obtained from grids having 264 and 300 elements. (The number of elements for solution of temperatures and streamlines is necessarily four times greater, totalling 960 elements). Due to symmetry, only half the domain need be considered for the calculations. Many elements were concentrated near the impact zone and the die exit, where the stresses will have the greatest magnitude. This grid covers a total length of 7.4 cm (or 296 wire radii), extending 0.4 cm beyond the exit. Such an exit length is adequate to satisfy the natural boundary conditions on the free surface.

It was found that for a Newtonian fluid under isothermal conditions,

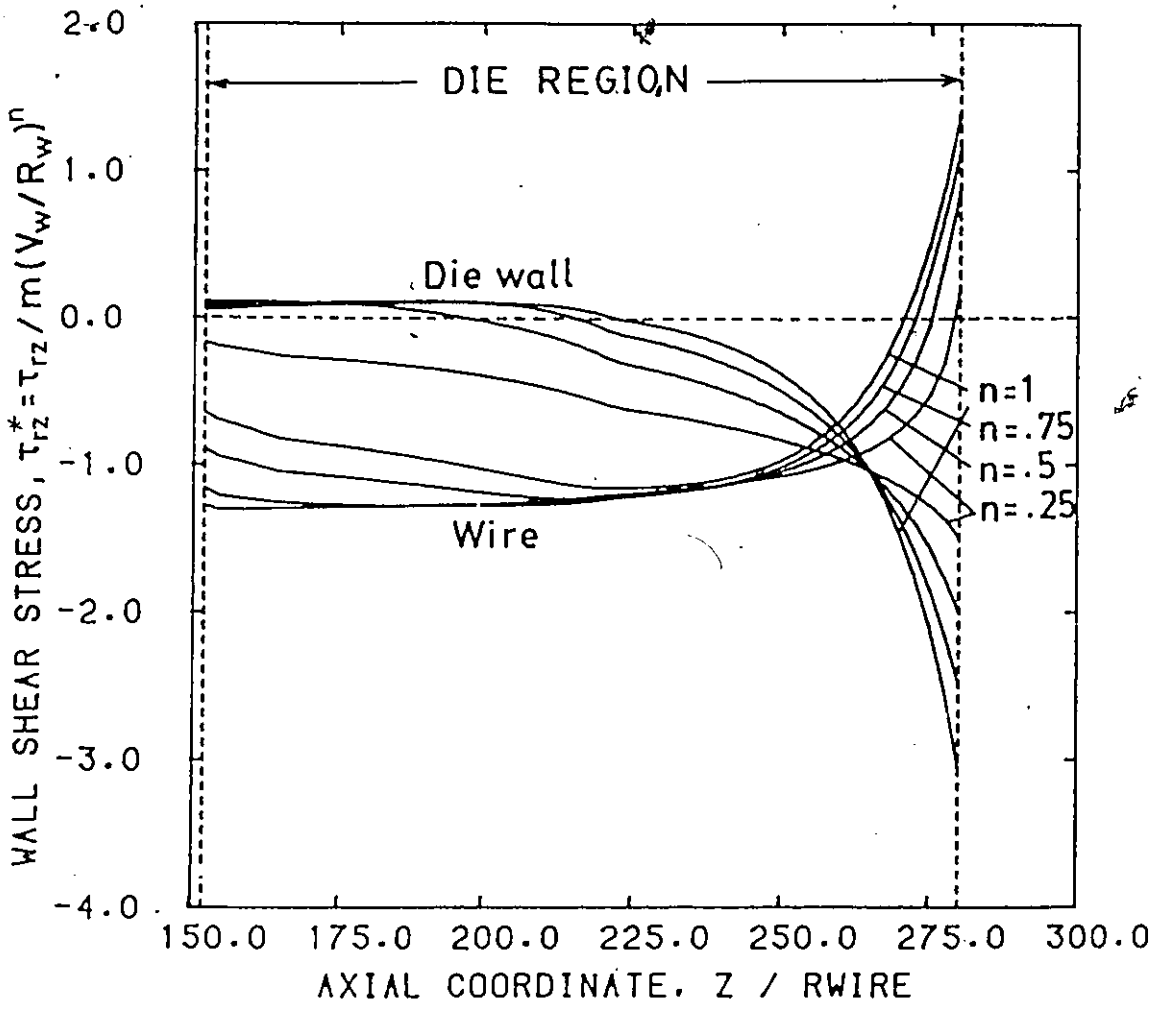

Figure 4.3: Dimensionless Shear Stress Distribution along the Die Wall and the Wire in the Die Region of Fenner's Die (Lubrication Approximation Theory).

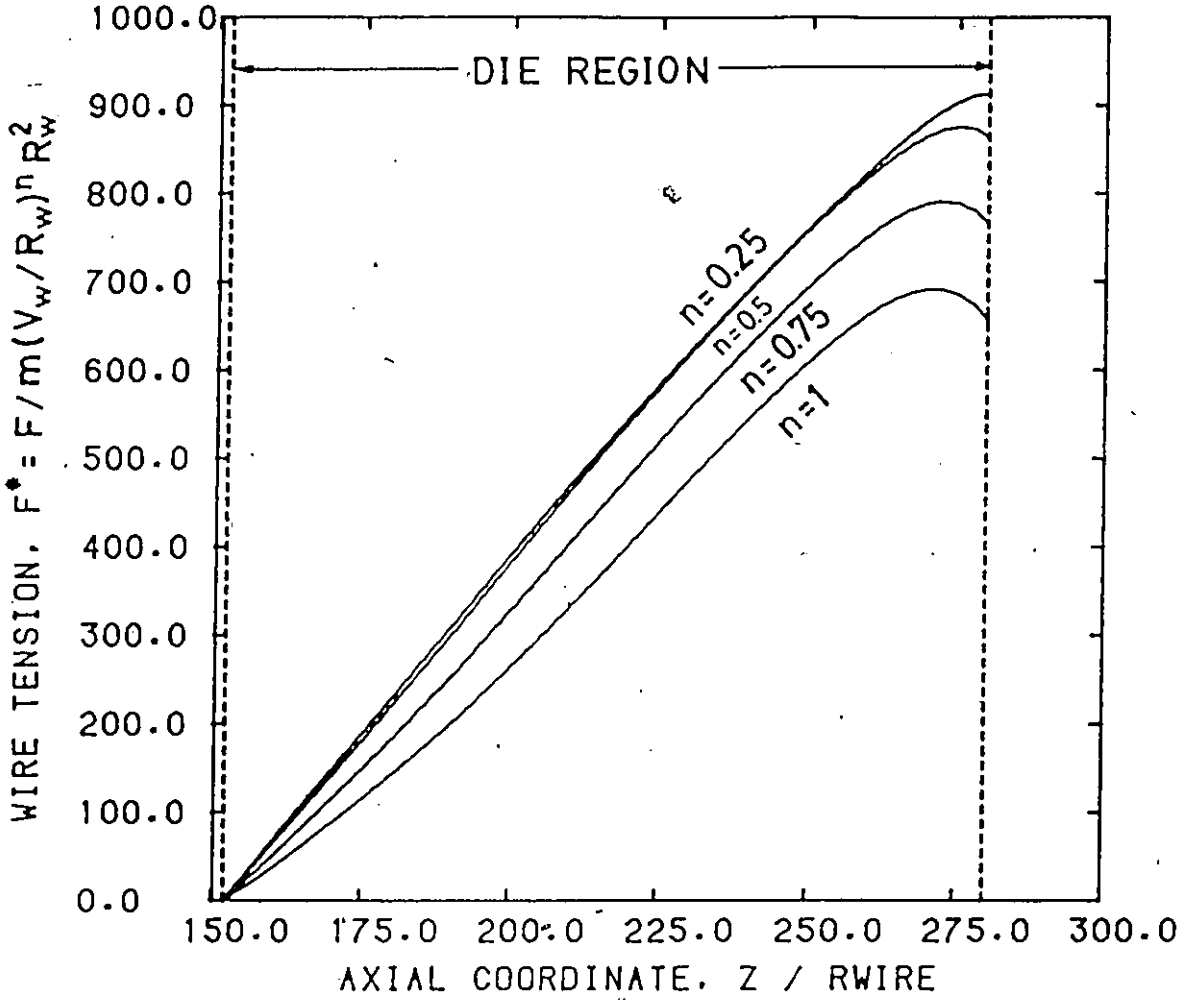

Figure 4.4: Dimensionless Wire Tension in the Die Region of Fenner's Die (Lubrication Approximation Theory).

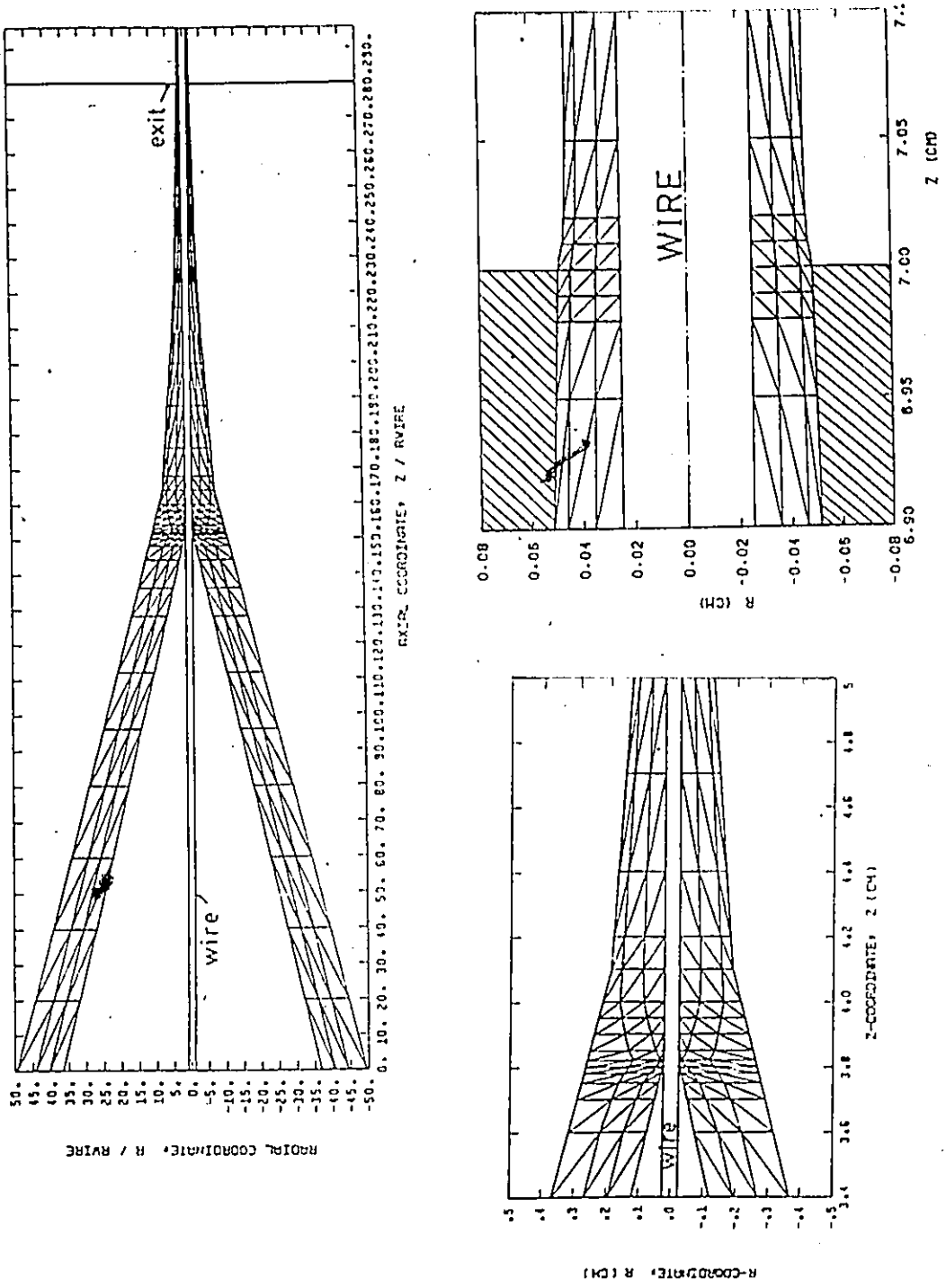

Figure 4.5: Finite Element Grid for Velocity-Pressure in Fenner's Die

an area of intense recirculation existed. Computations showed that about 120% of the flow rate recirculates within the die in a region located just after impact. Figure 4.6 gives a visual representation of the flow field. Using FEM analysis, Caswell and Tanner (1978) generate results that support the existence of recirculatory behavior under these conditions, but give no numerical values to their streamlines. Figure 4.7 compares in dimensionless form the pressure distributions along the axial length for both studies. The discrepancies were traced to the modelling of the impact zone with finite elements as discussed below.

It was found that the FEM results were very sensitive with respect to the nature of the discretization in the impact region, and relatively insensitive to the number of radial divisions employed. Figure 4.8 illustrates two different types of arrangements considered. The first shows a clearance gap between the end of the torpedo (at 3.8 cm) and the wire surface (at 3.82 cm). In reality, a free surface will occur in this minute area just before the melt contacts the wire (at 3.82 cm). It was found that for a Newtonian fluid, a dimensionless entry pressure of 34.2 was thus generated, exceeding the LAT and Caswell and Tanner's (1978) predictions by about 10%. The second type of arrangement shown best modelled the LAT approach, placing the node at the surface of the emerging wire (at 3.8 cm), thus eliminating the clearance gap. Setting the node at 3.82 cm to the wire velocity, the results obtained effectively matched both the LAT and Caswell and Tanner's analysis. Nevertheless, in the remainder of calculations the first arrangement was adopted, since it better represents the clearance gap found in actual operations.

The effect of shear-thinning was then studied by considering several fluids described by the power-law model, with each fluid having a different index (n = 0.25, 0.35, 0.50, 0.75). The flow patterns developed within the die will depend primarily upon power-law indices of the coating fluid, as well as wire radius and coated radius requirements under isothermal assumptions. In Figure 4.9, the pressure distribution in dimensionless form for each fluid is shown, assuming a clearance gap between the end of the torpedo and the wire surface. The extent of recirculation decreased when shear-thinning behavior was greater (smaller n values). It was found that below n = 0.35, no secondary flow existed. At indices where recirculation occurred, pressure build-ups were present in the die region, the magnitudes of which extended above inlet pressure values. However, at n = 0.35, the

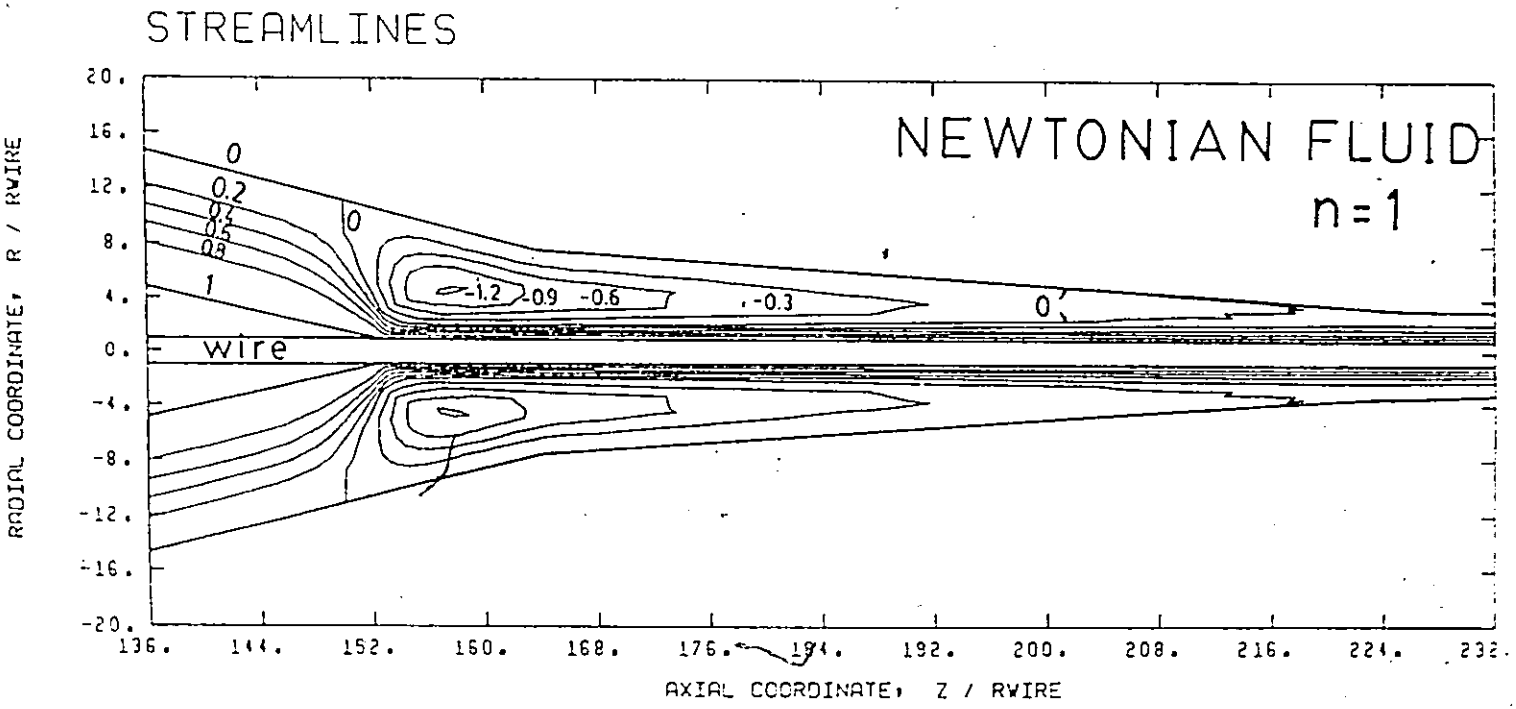

Figure 4.6: Streamline Pattern for a Newtonian Fluid in Fenner's Die

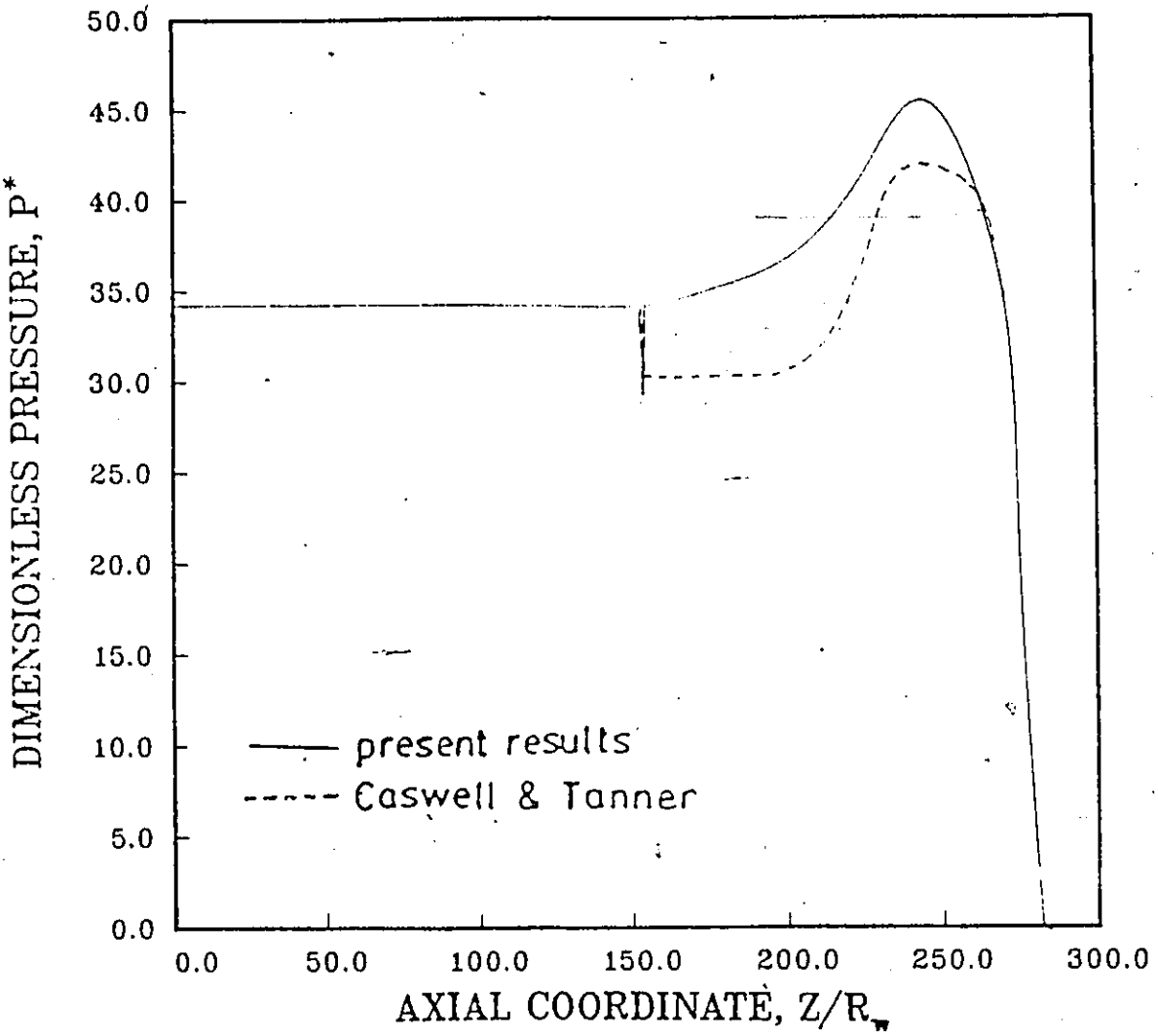

Figure 4.7: Dimensionless Pressure Distribution for a Newtonian Fluid: Comparison with Previous Work (Caswell and Tanner, 1978).

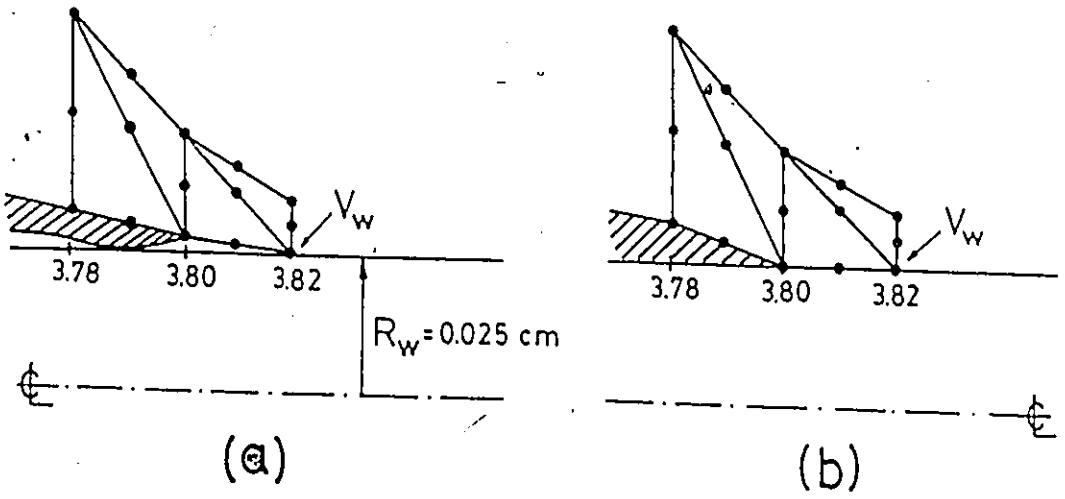

Figure 4.8: Finite Element Modelling of the Impact Region

die region back-pressure had sufficiently decreased, allowing a larger inlet pressure (i.e. driving force) to develop. Generation of design specifications that yield monotonic pressure drops must be a primary objective in the design of wire-coating dies.

Caswell and Tanner (1978) extended their analysis of Fenner's die to include a shear-thinning fluid with n = 0.50. It was suggested that the effect of shear-thinning on the extent of the recirculation zone was small but no comment was made concerning any effect on the intensity of recirculation, which is of more immediate importance to proper coating performance. The flow field generated for a similar case with n = 0.48 is shown in Figure 4.10. Flow reversal still exists, with up to 14% of the total flow rate recirculating. The characteristic shear-thinning behavior of the coating fluid has effectively decreased the intensity of recirculation which was about 120% for a Newtonian fluid (Figure 4.6). However, note that the size of the zones where recirculation occurs are in fact about the same.

In addition to the flow recirculation, it is interesting to examine the values of the other performance variables. It is noted that these values were quite high. The shear stress values range between 1-4 MPa, which easily exceeds critical values for LDPE melts (around 0.1-0.2 MPa), therefore indicating possible melt fracture. Since it is likely that this die has been used in actual operation under high speeds with LDPE, the elimination of both recirculation and likely melt fracture (i.e. shear stress reduction) must be possible under certain conditions.

A comparison between axial pressure distributions obtained by the LAT and FEM, under the same conditions and using the same fluid model employed by Fenner (1970), is shown in Figure 4.11. The two curves are almost identical up to the tapering zone, after which the pressure predicted by the LAT falls below the FEM curve. The LAT fails to account for the effects of the singularities (e.g. high stresses at the impact and exit), thus causing the backpressure to be underestimated. Other pertinent quantities such as shear stresses and haul-off tension are shown in Table 4.1.

The isothermal assumption, while facilitating a quick and approximate solution, can only be considered as approximate since viscous dissipation effects can give temperature increases within the melt. The energy conservation equation must be included to make the analysis and related results more realistic. A nonisothermal analysis is therefore required so better observations can be made.

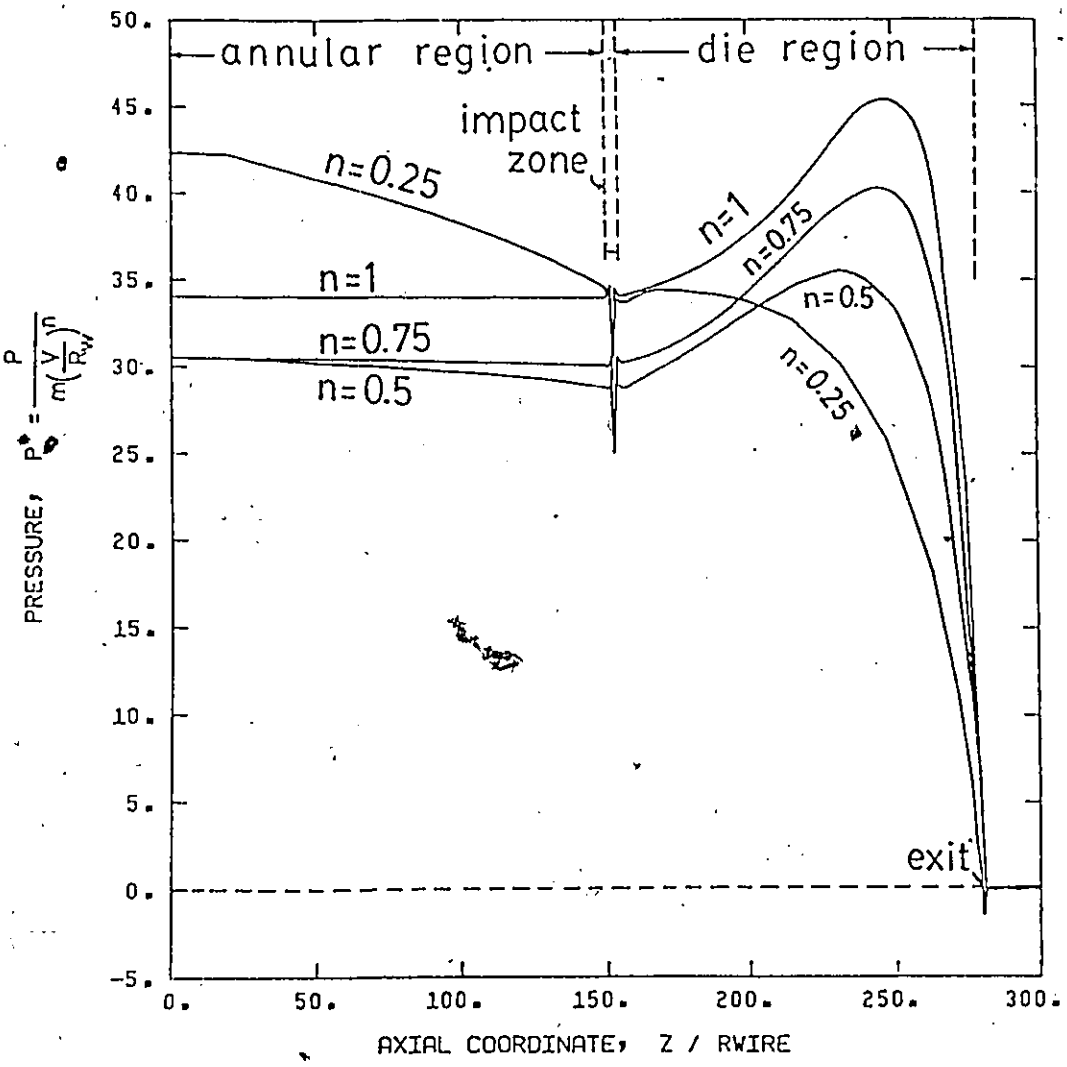

Figure 4.9: Pressure Development for Power-Law Fluids in Fenner's Die

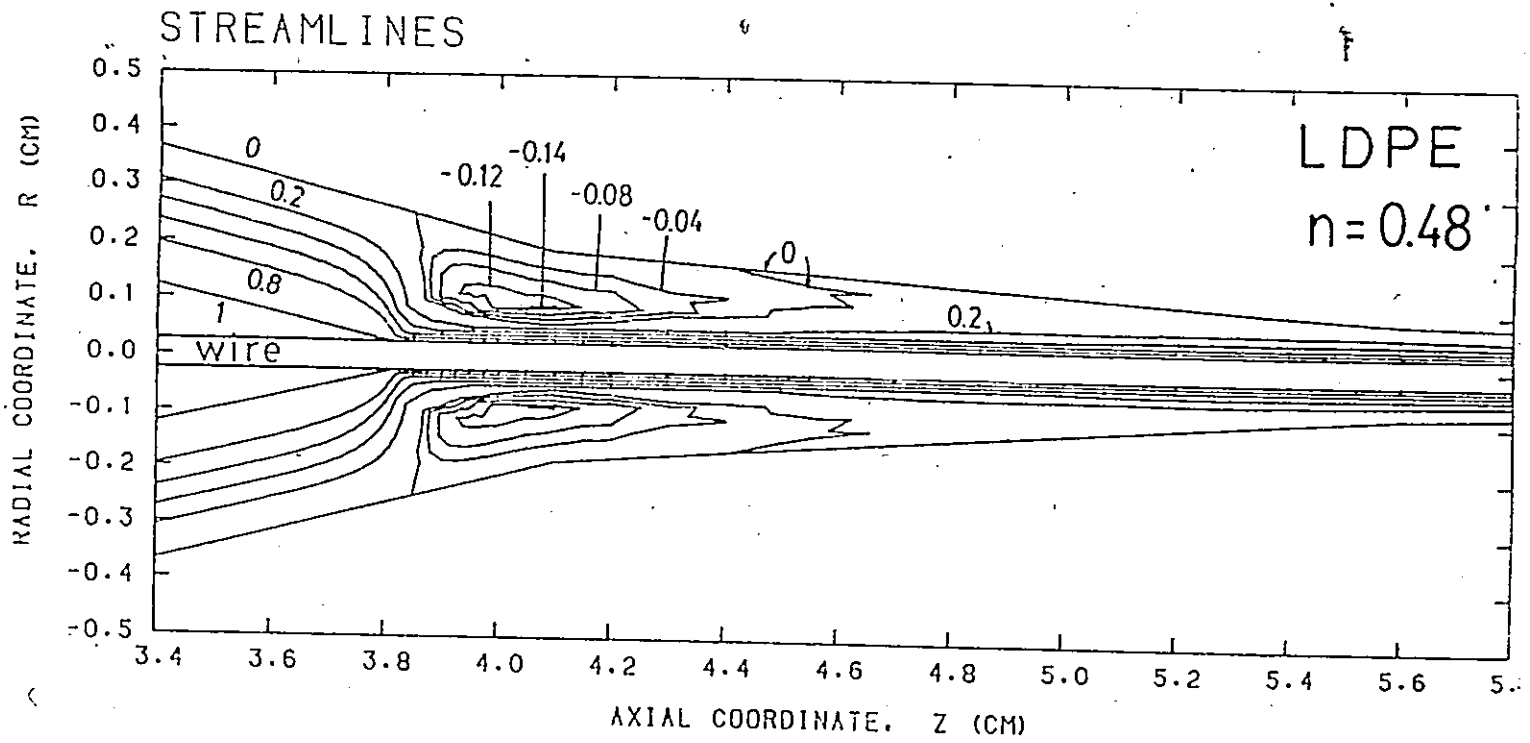

Figure 4.10: Flow Field in the Die Region of Fenner's Die under Isothermal Conditions for a Power-law fluid Using FEM (V_w= 510 cm/s, n = 0.48).

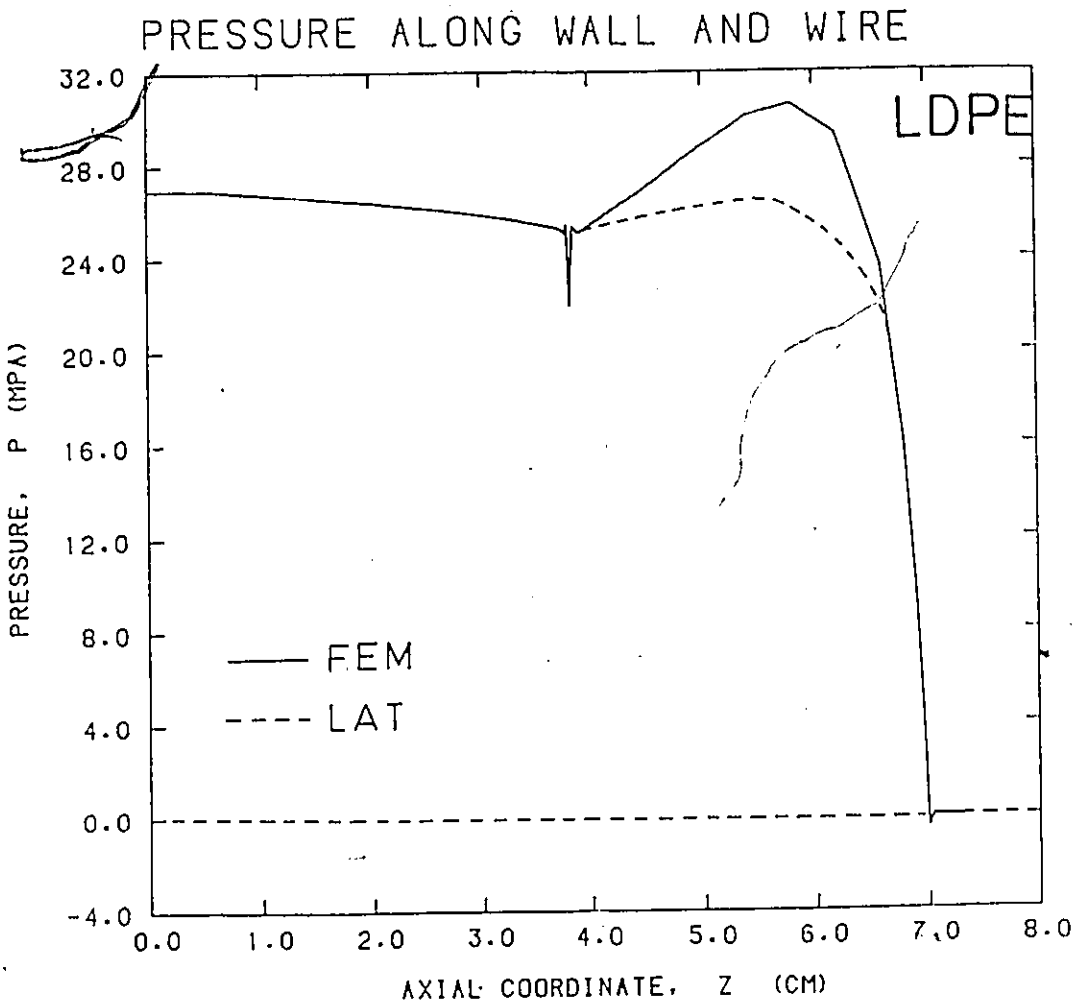

Figure 4.11: Axial Pressure Distribution Predicted from the LAT and FEM for a Power-law Fluid in Fenner's Die (V_w = 510 cm/s, n = 0.48).

Table 4.1: Comparison between Predictions from the LAT and FEM for a Power-law Fluid ($\tau = 0.00745\dot{\gamma}^{0.48}$MPa) in Fenner's Die for Different Wire Speeds under Isothermal Conditions (R_w= 0.025 cm.).

	V_w= 510 cm/s				V_w= 2040 cm/s			
Variable	LAT		FEM		LAT		FEM	
Inlet Pressure ΔP (MPa)	27.0		27.0		53.0		52.7	
Maximum Pressure P_{max} (MPa)	27.0	5.8*	30.6	5.8*	53.0	5.8*	59.5	5.8*
Haul-off Tension F (N)	17.0		40.2		33.0		78.2	
Maximum Tension F_{max} (N)	20.0	6.6*	40.4	6.9*	38.0	6.6*	78.6	6.9*
Maximum Shear Stress at Wire $\tau_{w,max}$ (MPa)	0.83	7.0*	1.44	3.8*	1.58	7.0*	2.81	3.8*
Maximum Shear Stress at Die Wall $\tau_{d,max}$ (MPa)	1.03	7.0*	2.01	7.0*	2.00	7.0*	3.91	7.0*

*Location (in cm) where the maximum value is observed.

4.3 LDPE: Nonisothermal Analysis

This analysis assumes that the metal surfaces (wire and die and torpedo walls) are kept at a constant temperature which is equal to the temperature of the entering melt. Solution of the energy equation was required to account for the heating effect due to viscous dissipation in the melt.

Carley et al. (1979) examined the coating of a No. 22 AWG wire (R_w = 0.032 cm) using speeds between 254 cm/s to 3048 cm/s (500 ft/min to 6000 ft/min) and a melt entry temperature of 227°C. Hammond (1960) has found that temperatures for wire-coating grade LDPE resins should be in excess of 227°C to improve the luster and gloss of the final coating.

On the basis of the above information, runs were undertaken in Fenner's die with R_w = 0.025 cm at three different temperatures: 227°C, 260°C, and 300°C. The speeds set for the wire ranged between 250 cm/s to 3000 cm/s. The metal surfaces (wire and die) are kept constant at the melt entry temperature. Winter (1975) has claimed that this assumption is not entirely correct, since the real state of these surfaces is somewhere between isothermal and adiabatic. However, Basu (1981) has shown that the results are not greatly affected within the die for either set of conditions. Additionally, Carley et al. (1979) report a relatively small increase in pressure drop (approximately 7.5%) when the die wall was treated as isothermal instead of adiabatic.

The runs were performed for the LDPE melt obeying the viscosity function as given by Carley et al. (1979) (Figure 3.1). Throughout these runs, it was found that a small zone of flow recirculation was present, involving 1 to 2% of the total flow rate. Recirculation becomes less pronounced under conditions of lower speeds and higher temperatures. Figure 4.12 gives an example of the flow pattern found at 2000 cm/s and 227°C, showing the flow recirculation just after impact.

In addition to the occurrence of minor secondary flow, further important information can be derived from this nonisothermal analysis. Figure 4.13 shows the temperature field under the same conditions. As expected, the greatest dissipation occurs near the die exit, where flow conditions are the most intense. The basic temperature pattern found to exist in the melt for all runs is presented in Figure 4.14, which shows various steady-state temperature profiles at selected axial locations after the melt-wire impact. The wire surface radius has been normalized to zero. It is seen that as the exit

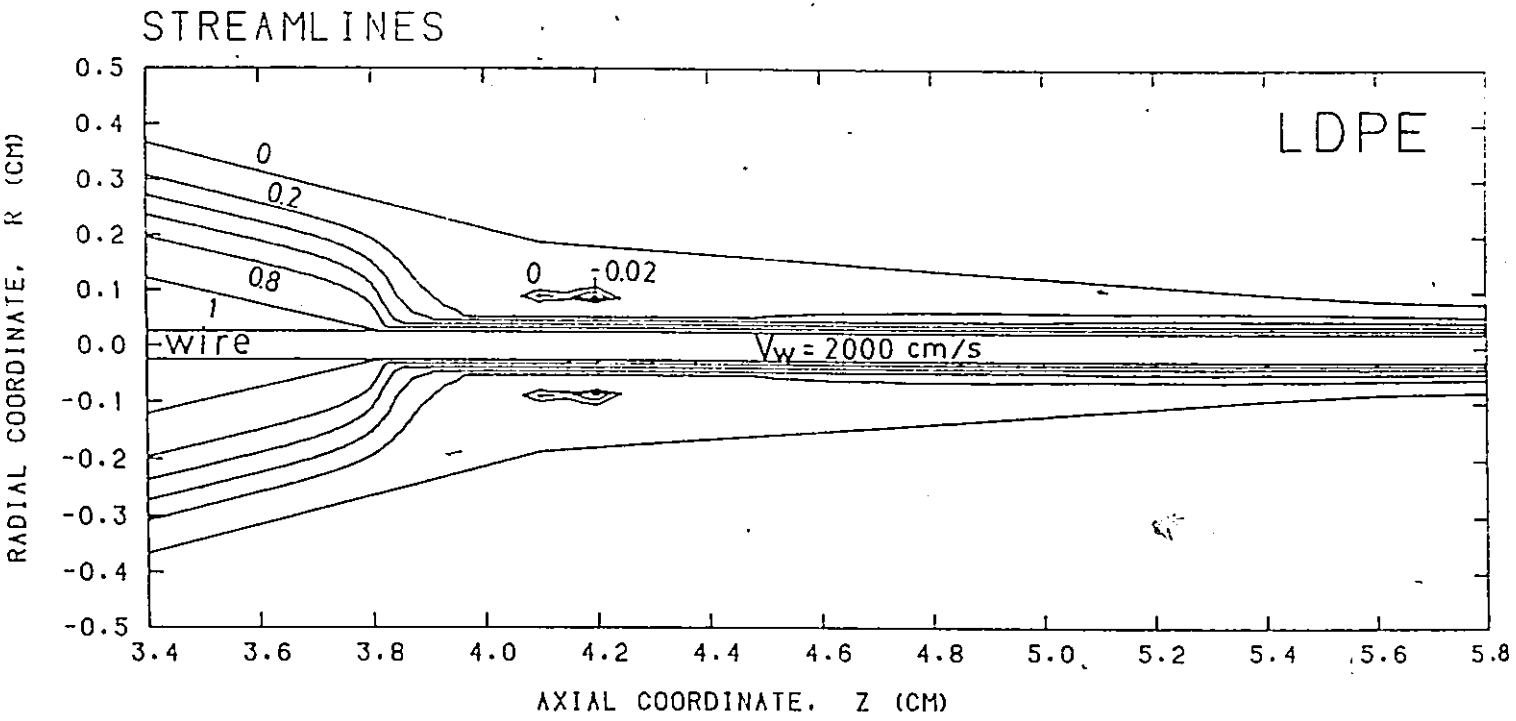

Figure 4.12: Streamline Pattern in Fenner's Die for LDPE under Non-isothermal Conditions ($\tilde{V}_w$ = 2000 cm/s, T = 227°C).

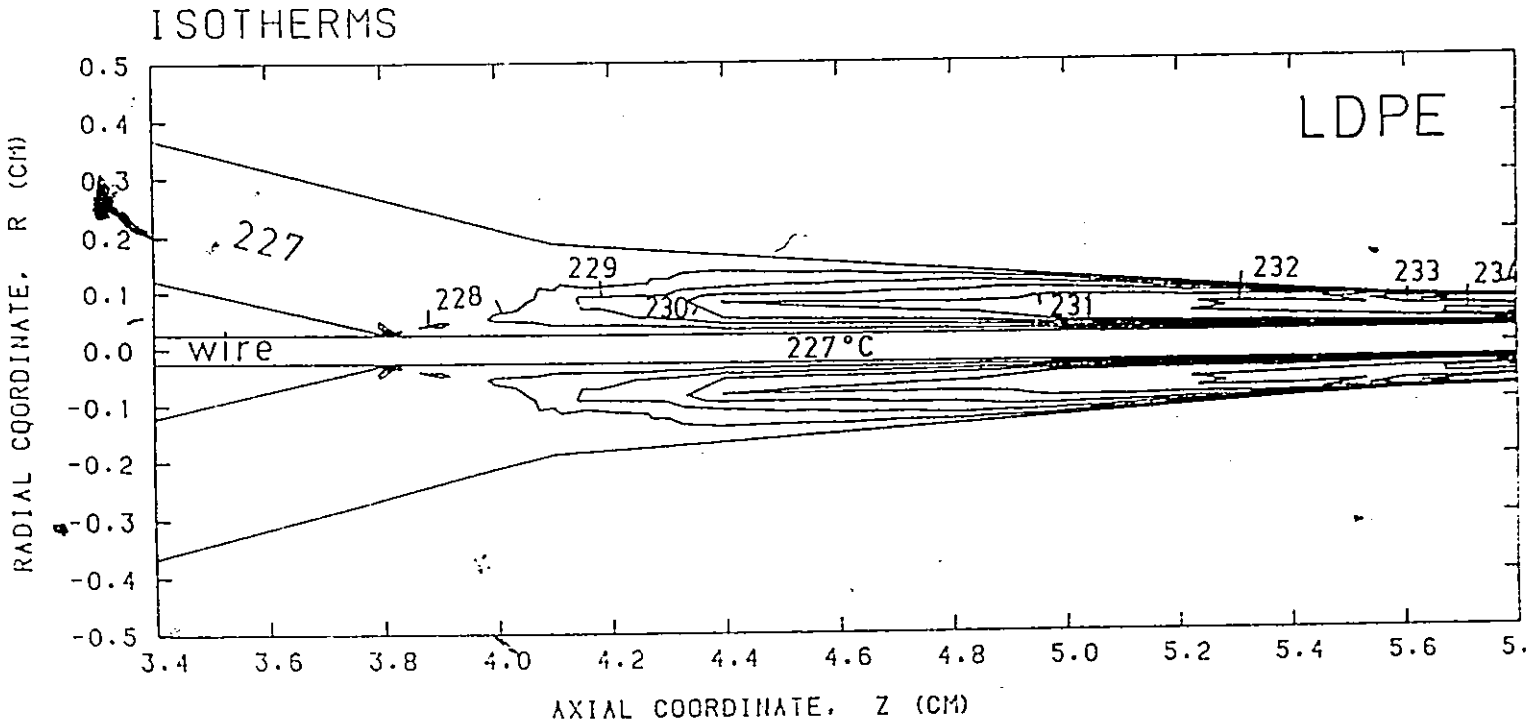

Figure 4.13: Isotherms in Fenner's Die for LDPE under Nonisothermal Conditions (V_w = 2000 cm/s, T = 227°C).

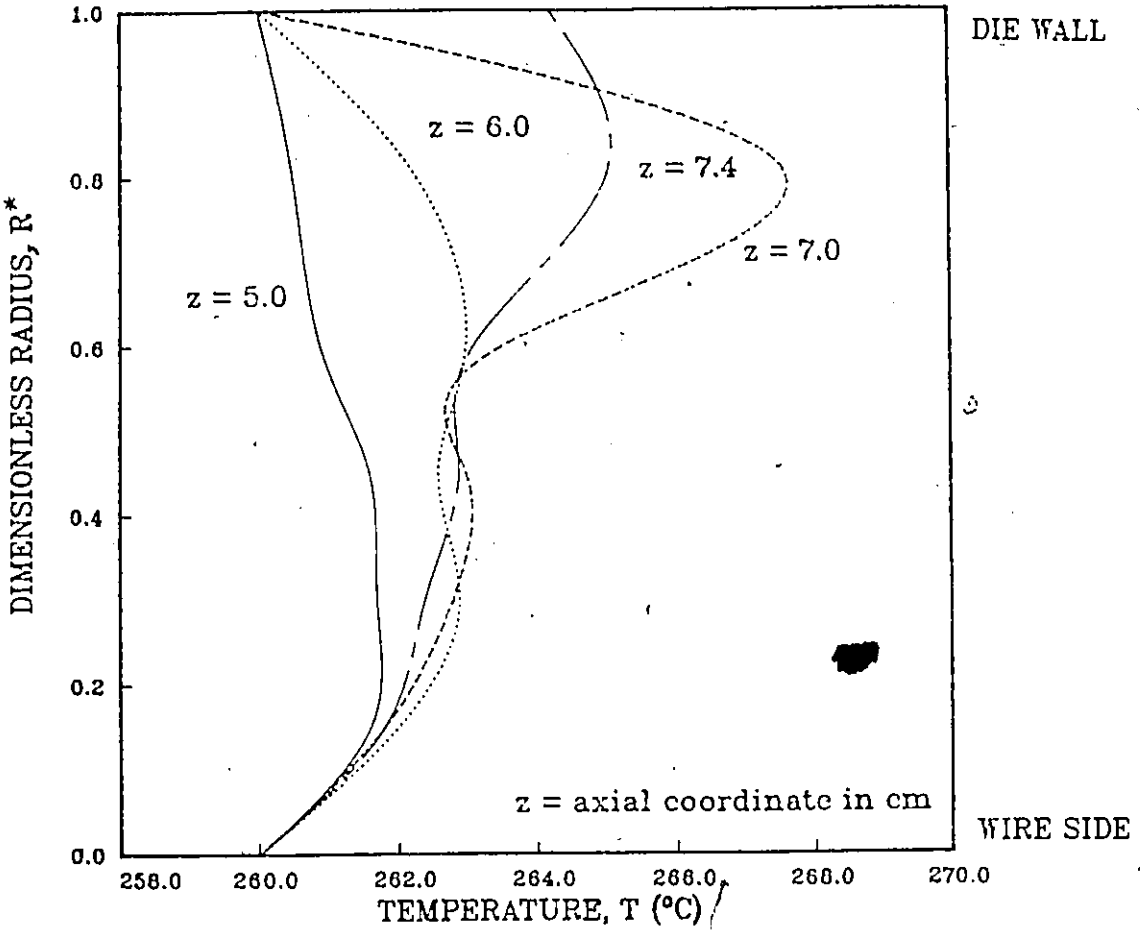

Figure 4.14: Temperature Profiles for LDPE in Fenner's Die (V_w= 1000 cm/s, T = 260°C).

is approached, the temperature maxima become greater and move closer to the die wall, where shear stress values are the greatest. Natural adiabatic conditions after the exit (z = 7.0 cm) reduce the maximum value by virtue of heat flow out to the coated surface. Figure 4.15 shows the occurrence of maximum temperatures at each radial division considered throughout the entire length of the die. The temperature increases more towards the exit of the die, with the melt temperature dropping quickly upon emergence (where natural adiabatic conditions come into effect). An overall temperature rise of 24.2°C is found to exist in this case. It was found that a nonisothermal analysis at 300°C yielded a temperature field showing little thermal variation, becoming essentially isothermal. This is attributable to lowered viscosity resulting from the higher temperature, which then serves to reduce the overall severity of the conditions inside the die. A total rise of only 7.7°C was computed for conditions of 3000 cm/s and 300°C, with lower speeds causing even smaller temperature increases. Figure 4.16 shows the effect of wire speed on the resulting maximum temperatures. Higher wire speeds will undoubtedly lead to greater temperature rises. The occurrence of significant temperature increases within the polymer melt demonstrates the need to consider nonisothermal conditions if a realistic performance analysis is to be made.

Shown in Figure 4.17 is the axial pressure development, where an inlet pressure of 2.7 MPa is predicted. The decreased magnitude of the pressure build-up is indicative of a smaller amount of recirculation. The magnitude of this build-up is essentially dependent on the extent of recirculation. Figure 4.18 shows how wire speed affects the required inlet pressure, with these results generated at a die temperature of 227°C. Figure 4.19 gives the general correlation between pressure and temperature at different wire speeds. Conditions of higher wire speeds and lower temperatures will naturally require larger overall pressures. It appears that pressure requirements are more sensitive to operating temperature than wire speed.

Close examination of shear stress data is required if possibility of melt fracture is to be detected. Melt fracture is probably avoided if the greatest shear stress magnitude does not exceed a characteristic critical value (Chapter 3). Figure 4.20 shows the expected maximum shear stresses expected to occur at the wire surface and die wall for a given wire speed at 227°C, and Figure 4.21 illustrates the influence of temperature on predicted maximum die wall shear stress values at different wire speeds, supporting

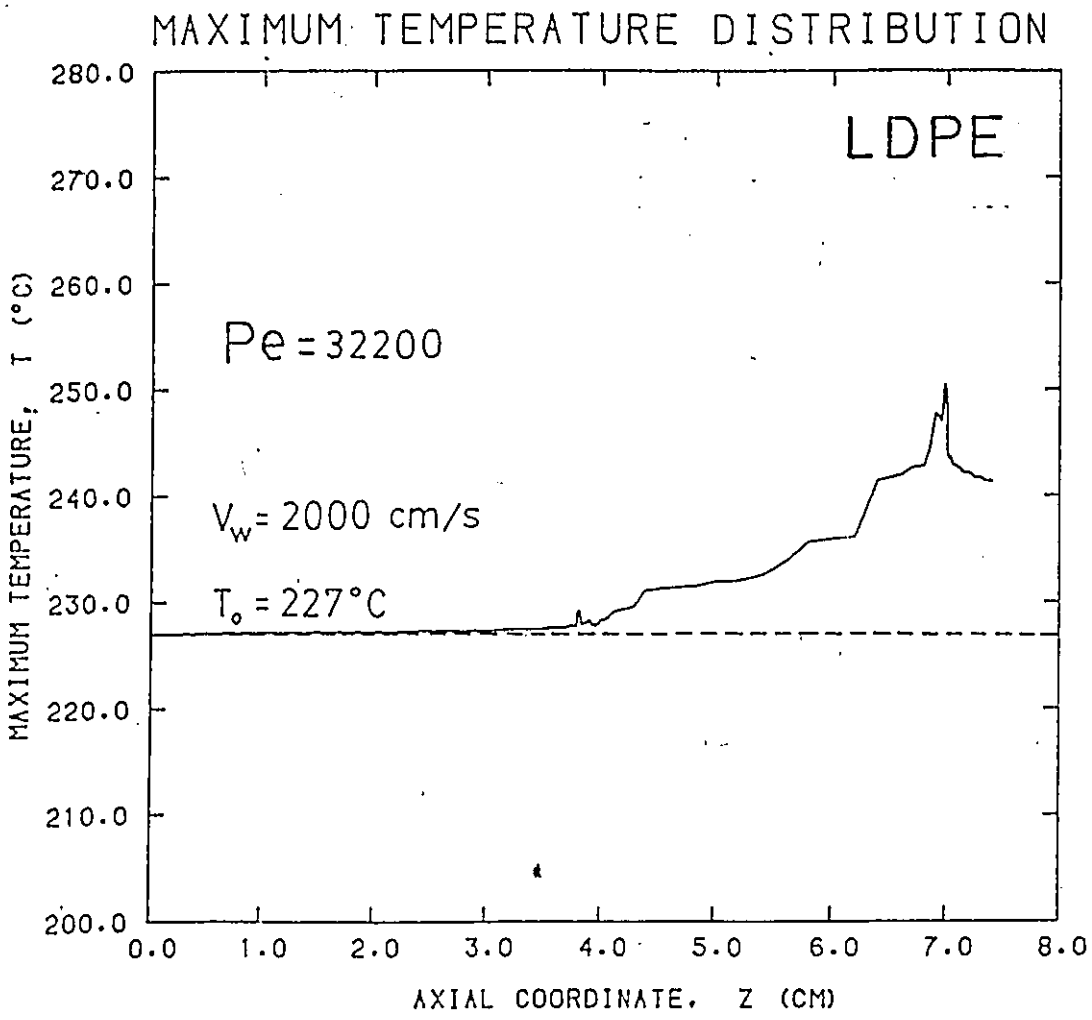

Figure 4.15: Maximum Temperature Distribution for LDPE in Fenner's Die (V_w= 2000 cm/s, T =227°C).

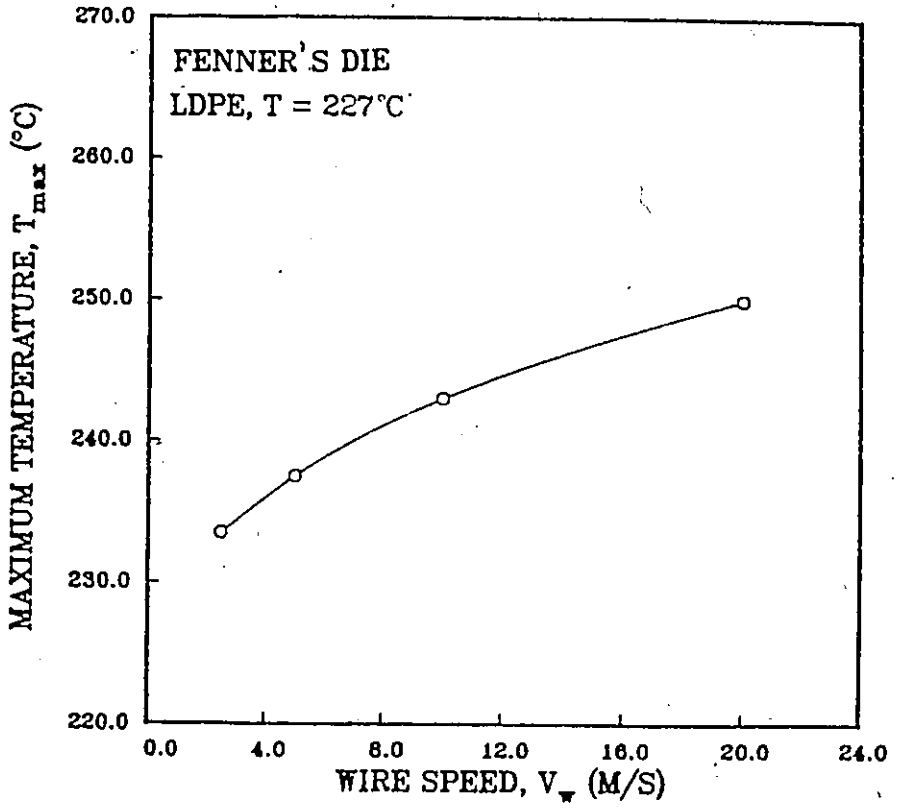

Figure 4.16: Maximum Temperature vs. Wire Speed for LDPE in Fenner's Die (T = 227°C).

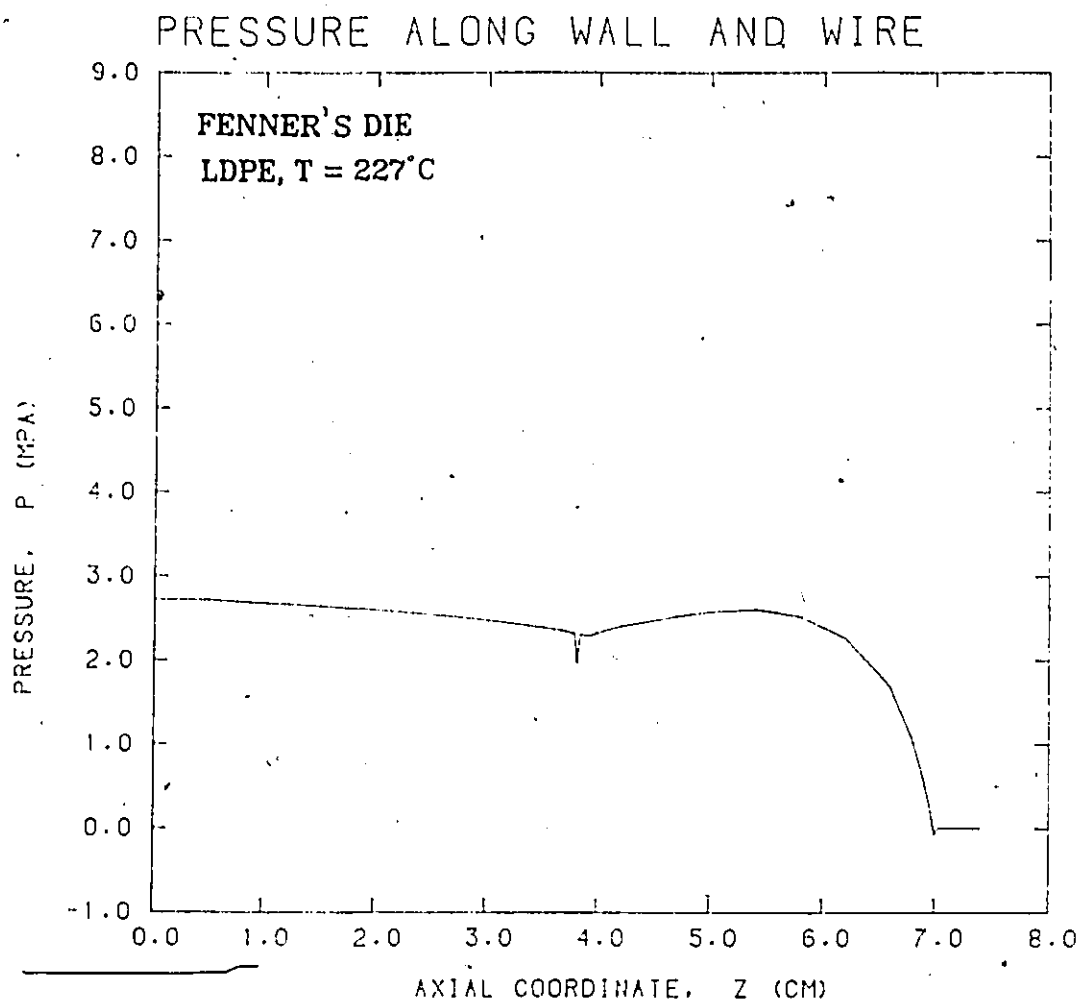

Figure 4.17: Pressure Distribution for LDPE in Fenner's Die (V_w= 1000 cm/s, T = 227°C).

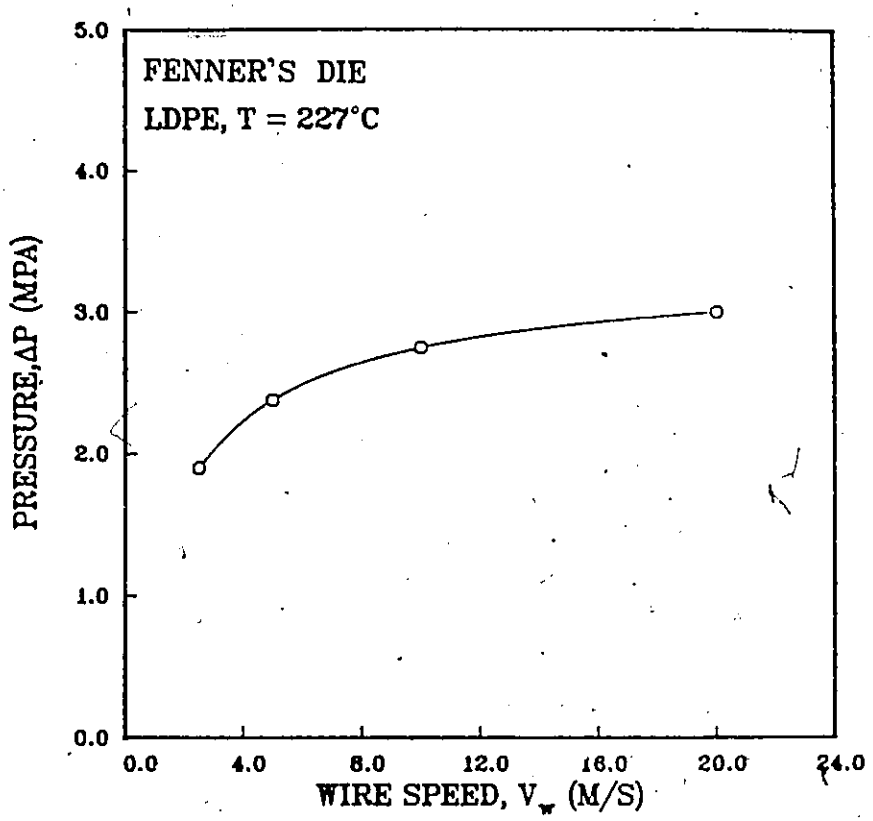

Figure 4.18: Pressure vs. Wire Speed for LDPE in Fenner's Die (T = 227°C).

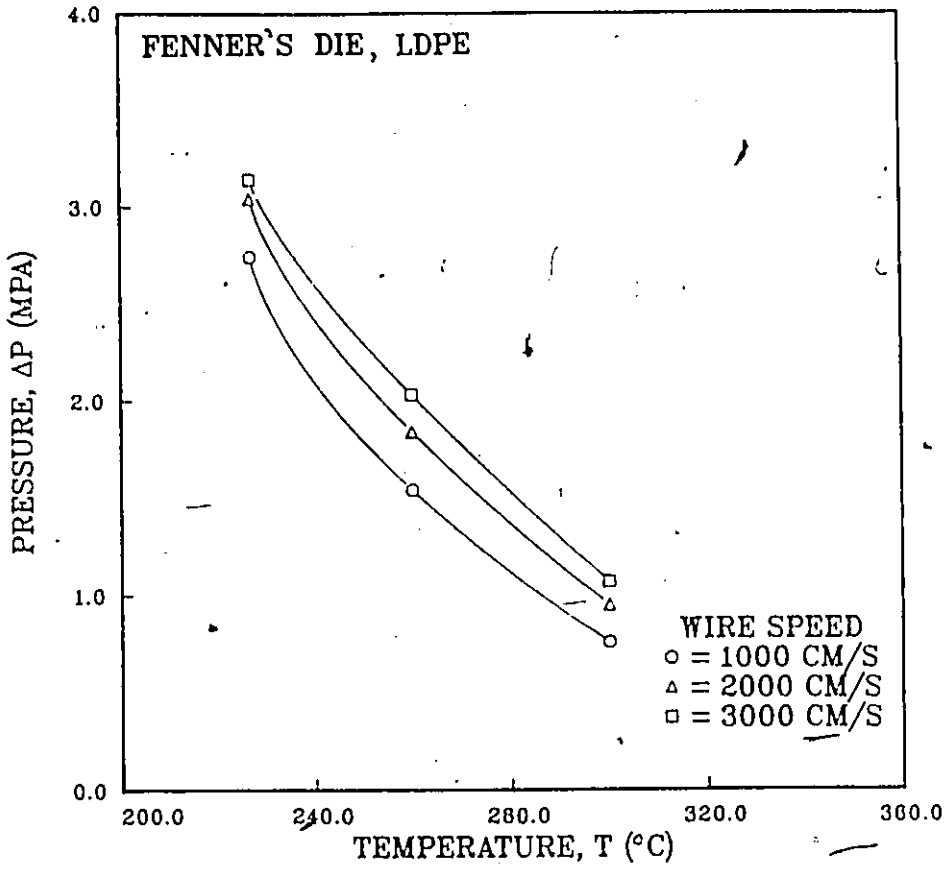

Figure 4.19: Pressure vs. Operating Temperature at Different Wire Speeds for LDPE in Fenner's Die.

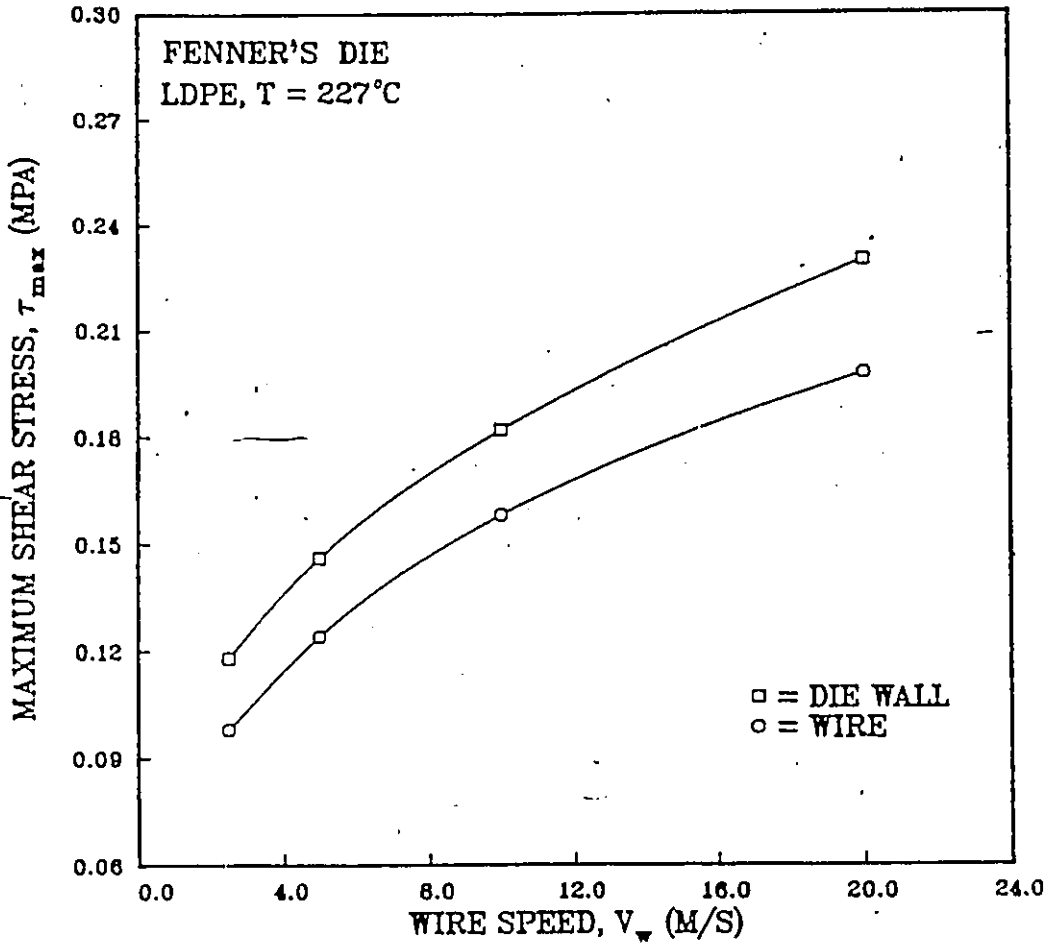

Figure 4.20: Maximum Shear Stress vs. Wire Speed for LDPE in Fenner's Die (T = 227°C).

the expectation that the less viscous fluid existing at a higher temperature will experience smaller shear stress. As detailed in Chapter 3, the critical shear stress values are calculated to range from 0.13 MPa to 0.19 MPa for temperatures between 227°C and 300°C. Note that at higher speeds of 2000 cm/s and 3000 cm/s (at 227°C) the critical shear stress value would be exceeded, possibly leading to melt fracture of the coating material. However, Hammond (1960) has suggested that higher temperatures will naturally reduce maximum stress values below the critical range. Figure 4.22 shows the axial shear stress development along both the wire surface and the die wall for 2000 cm/s and 227°C. The maximum wire shear stress occurs at the melt-wire impact (0.2 MPa) due to the stress singularity present when the melt speed at the wall changes from zero to the wire speed. The velocity gradient increases at the die wall as the external pressure imposed on the flow becomes more significant (i.e. a flatter velocity profile) thus giving a stress magnitude at the exit of 0.23 MPa. Shear rate maxima in this coating die are found to range from 2.3 x 10^5 s^{-1} at 1000 cm/s to essentially triple this to 7.0 x 10^5 s^{-1} at 3000 cm/s (at 260°C). These large shear rates suggest that for any proper simulation, the rheological model must be a comprehensive one, having acceptable accuracy up to very high shear rates.

The existence of recirculation for LDPE is rather small, the greatest magnitude being 2.5% of the total flow rate (at 3000 cm/s and 227°C). But even small amounts of recirculation would likely cause surface roughness. A strategy to overcome this may include altering the operating conditions and/or the geometric die design. In the latter case, reduction of the flow area would effectively eliminate unneeded space in the die that would allow for recirculation to occur. One method of achieving this is alteration of the "gum space" (Haas and Skewis, 1974). An optimum gum space is a lateral distance between the torpedo and die wall, adjusted by fixing the torpedo position. This concept is examined further in Chapter 6. For this particular analysis, the die configuration remains unchanged, but a new, thicker wire, No. 22 AWG, is introduced (R_w= 0.032 cm) to generate the same effect (i.e. reduce the area available for flow). The wire is still assumed to require an 80% coat (R_c = 0.0576 cm).

Runs were performed using the new No. 22 AWG wire at 260°C and at three different wire speeds: 1000 cm/s, 2000 cm/s, and 3000 cm/s. Table 4.2 compares several important variables found from both wire radii

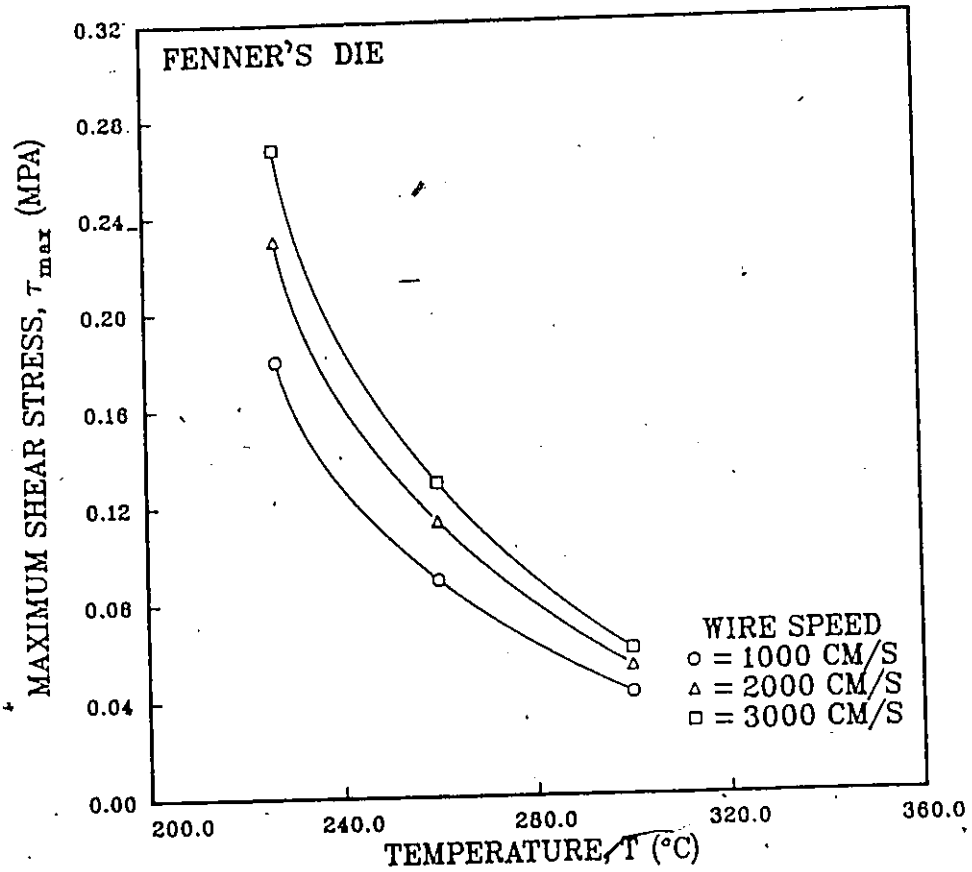

Figure 4.21: Shear Stress vs. Operating Temperature at Different Wire Speeds for LDPE in Fenner's Die.

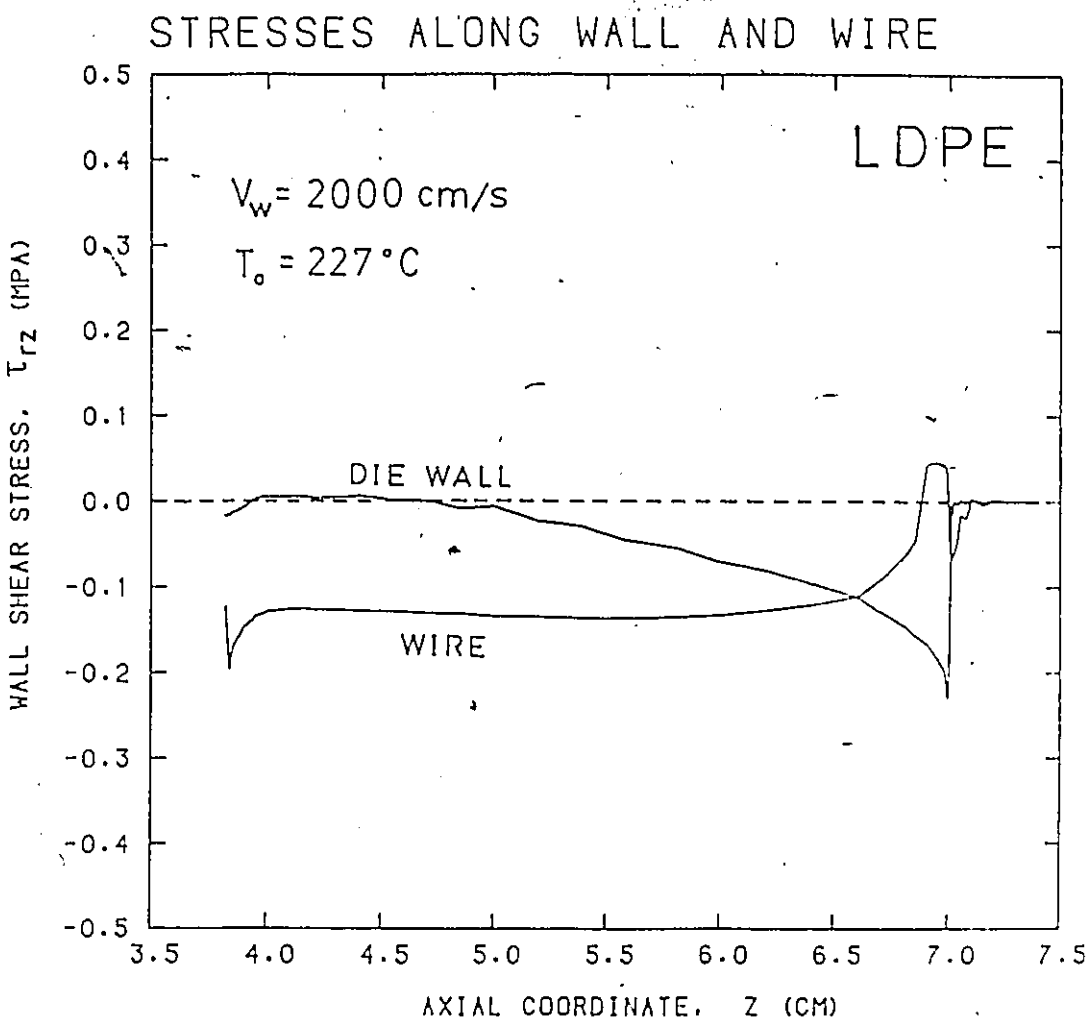

Figure 4.22: Shear Stress Development for LDPE in Fenner's Die (V_w= 2000 cm/s, T = 227°C).

Table 4.2: Comparison of Design Variables for Two Different Wire Radii at T = 260°C for LDPE in Fenner's Die.

Radius R_w (cm)	Speed V_w (cm/s)	Pressure ΔP (MPa)	Max. Temp. T_{max}(°C)	Max. Shear Stress $\tau_{w,max}$ (MPa)
0.025	2000	1.842	272.0	0.1127
0.032	2000	6.911	286.5	0.1848

considered. The reduced flow area will result in higher shear stresses occurring at the same wire speed, therefore leading to greater viscous dissipation and subsequently greater temperature increases. A comparison of maximum temperatures predicted at different wire speeds is shown in Figure 4.23 for a die entry temperature of 260°C.

It is logical to expect that a greater inlet pressure is required, as evidenced by the 275% increase for the case shown in the previous table. The effect of the wire speed on the pressure is detailed in Figure 4.24 with Figure 4.25 showing the axial pressure development at 2000 cm/s. The pressure build-up in the die region is noticeably less intense for this particular wire. Furthermore, from examination of the streamline pattern shown in Figure 4.26, it is evident that flow recirculation has been effectively eliminated.

The continuous rearrangement of the z-velocity profile along the axial direction is presented in Figure 4.27. It is evident that near the impact region a drag-type profile exists with the wire speed as the maximum. The effect of the die geometry on the melt flow can then be observed as there is a dramatic change in the nature of the profile with maxima moving away from the wire surface and the melt velocity exceeding that of the wire. In addition, it can be seen that the velocity gradient near the die wall steadily grows steeper as the exit is approached, producing high rates-of-strain.

To investigate the shear stress state, and therefore melt fracture, Figure 4.28 illustrates how shear stress values increase when the radius of the wire is enlarged from 0.025 cm to 0.032 cm. It is observed that the shear stress value predicted for 260°C and 2000 cm/s (0.185 MPa) actually exceeds the critical shear stress thought to cause melt fracture. However, it must be recalled that critical stress data was derived from tests in which the melt was subjected to a sudden contraction, that is an entry angle of

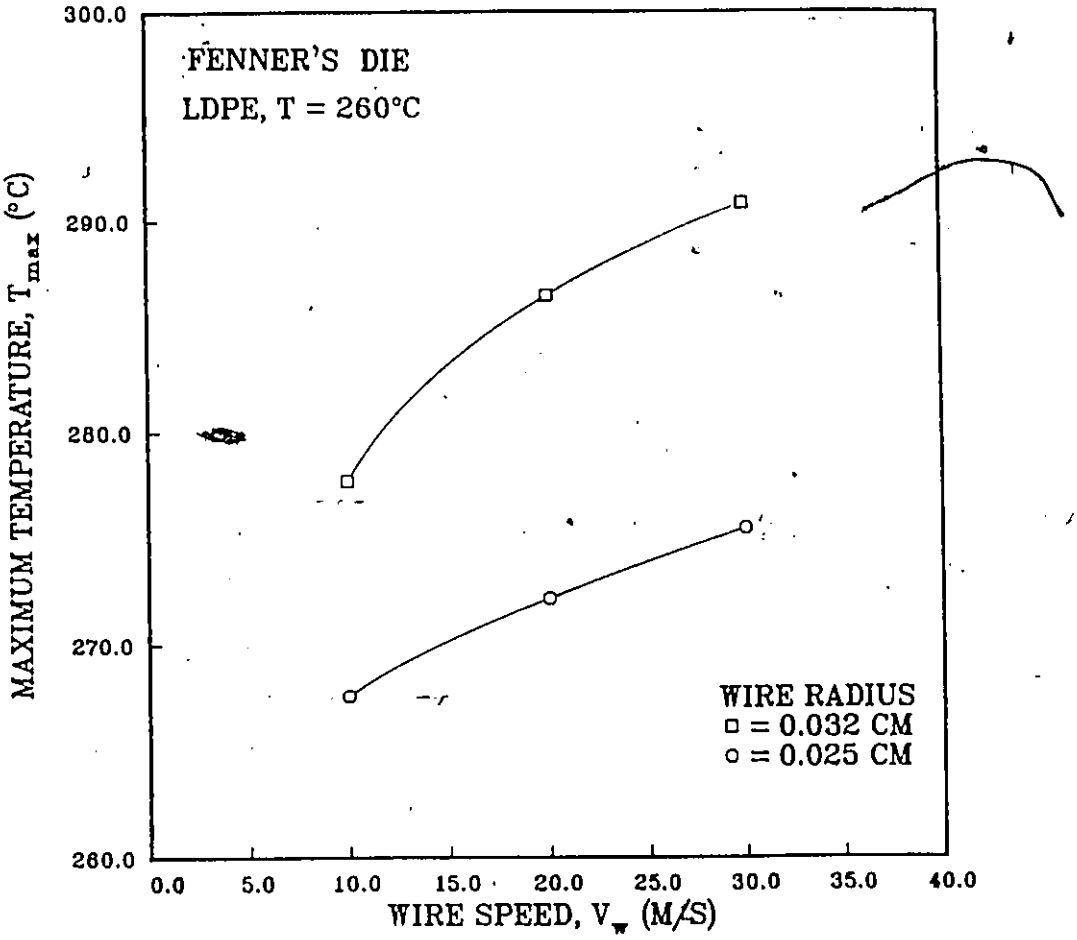

Figure 4.23: Maximum Temperature vs. Wire Speed for LDPE in Fenner's Die for Two Different Wires (T = 260°C).

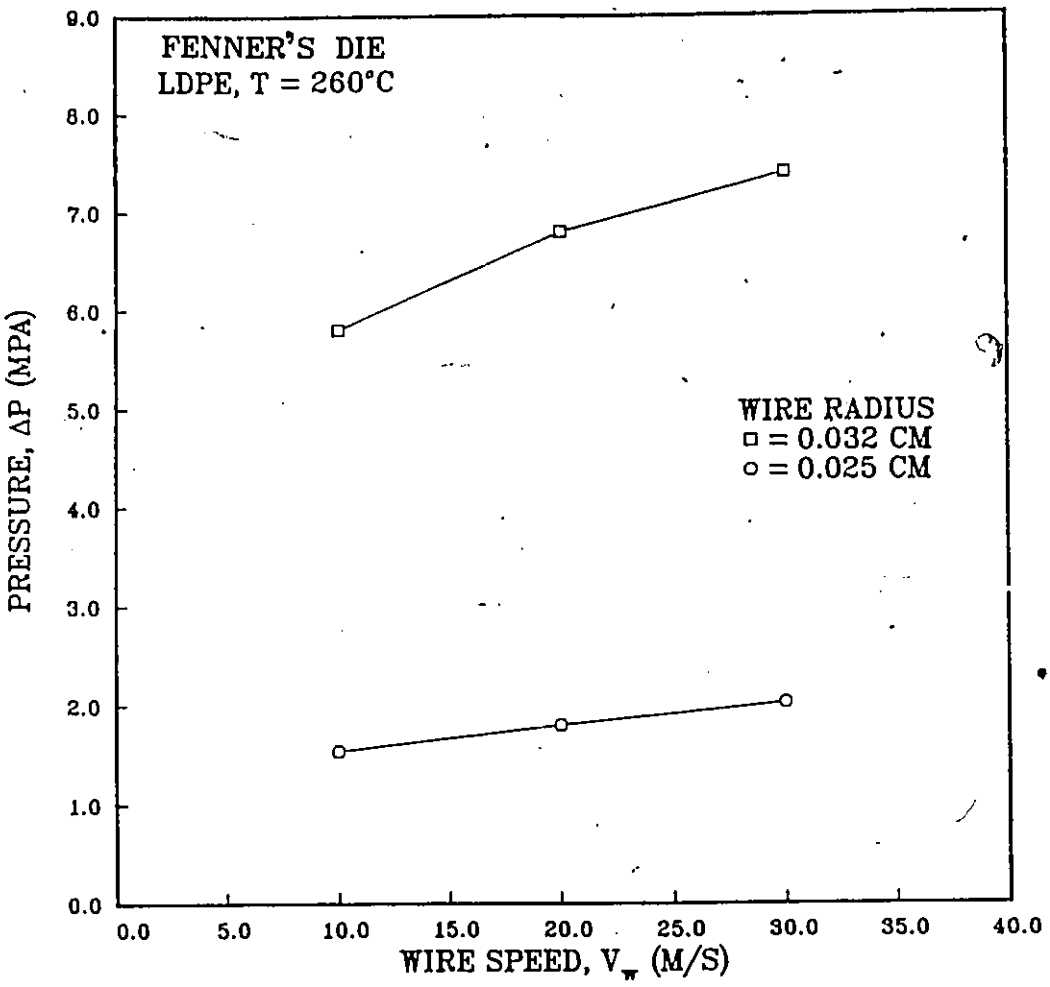

Figure 4.24: Pressure vs. Wire Speed for LDPE in Fenner's Die for Two Different Wires (T = 260°C).

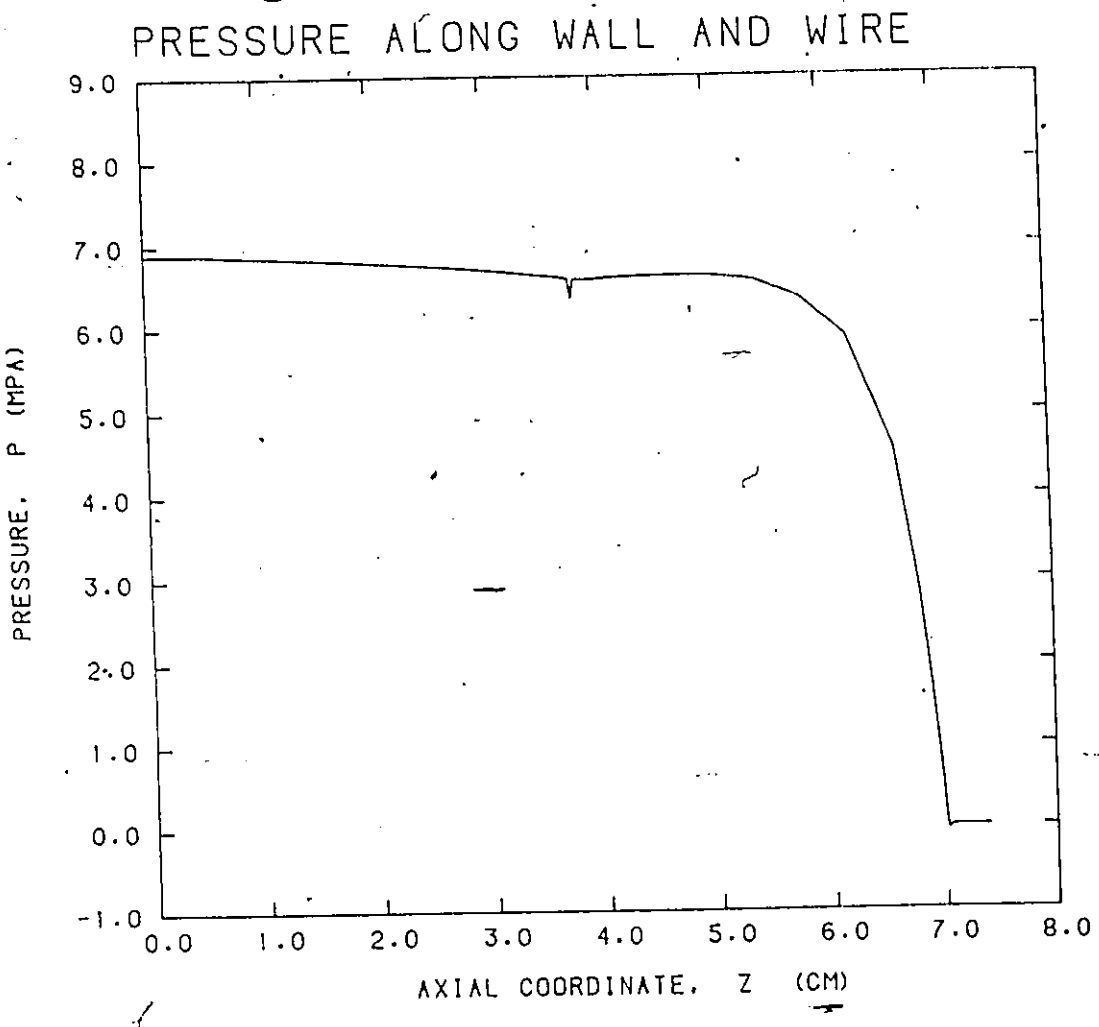

Figure 4.25: Pressure Development for LDPE in Fenner's Die with R_w= 0.032 cm (V_w= 2000 cm/s, T = 260°C).

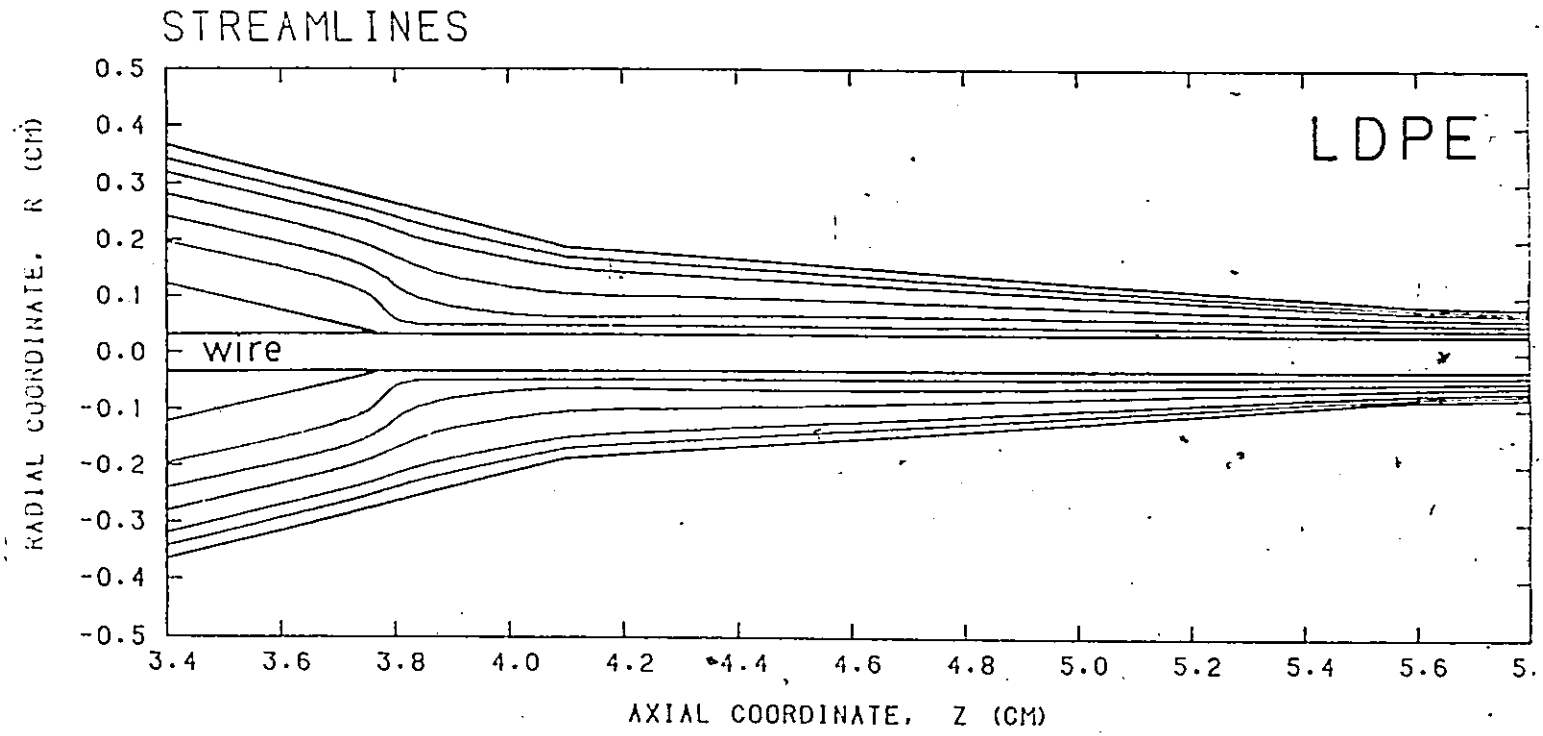

Figure 4.26: Streamline Pattern for LDPE in Fenner's Die with R_w= 0.032 (V_w= 2000 cm/s, T = 260°C).

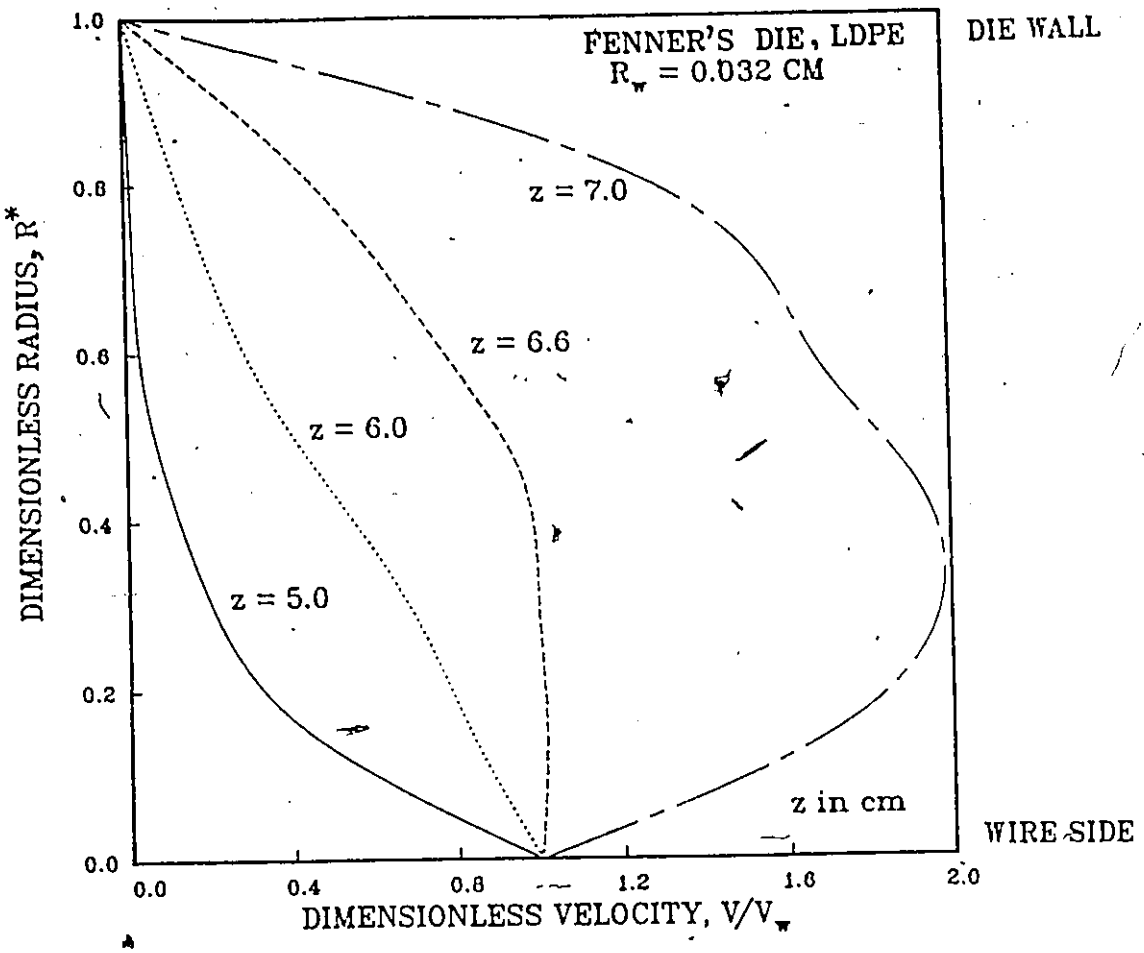

Figure 4.27: Velocity Profiles for LDPE in Fenner's Die with R_w= 0.032 cm (V_w= 2000 cm/s, T = 260°C).

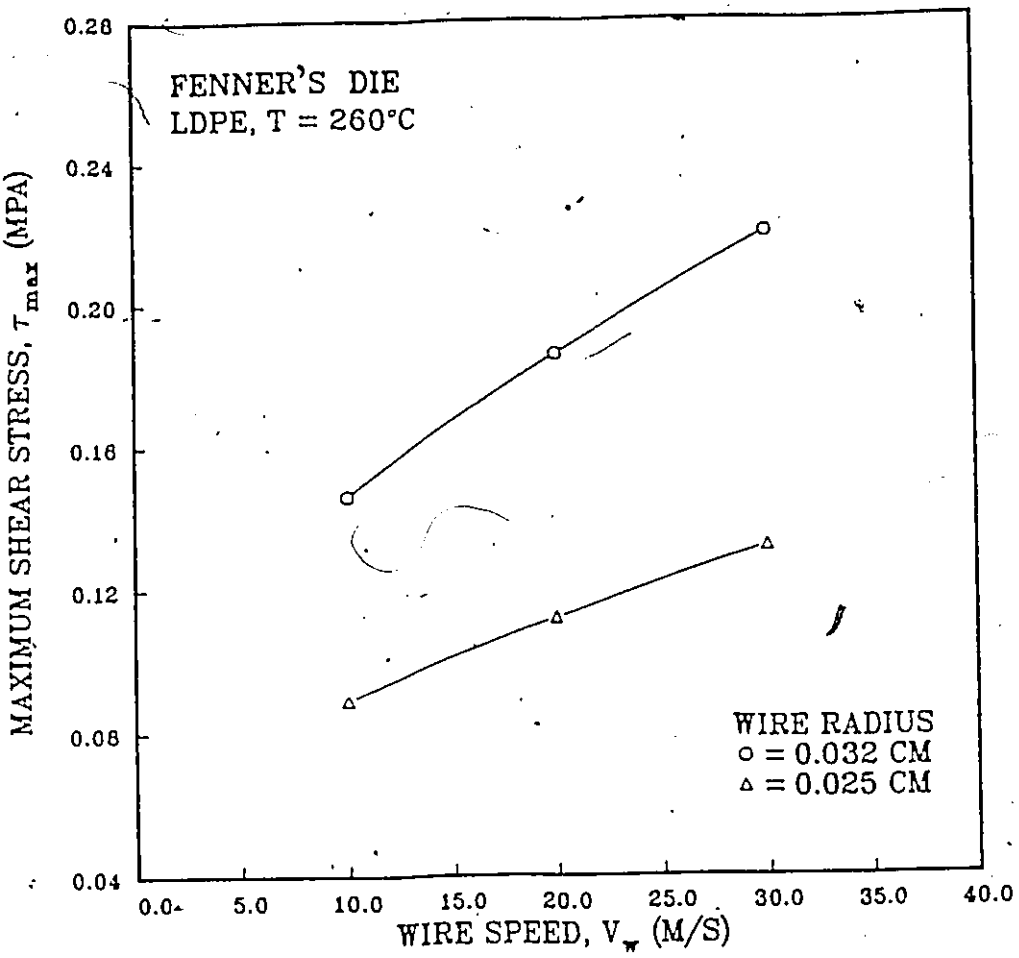

Figure 4.28: Maximum Shear Stress vs. Wire Speed for LDPE in Fenner's Die (T = 260°C)

90-degrees. In this tapered geometry, melt fracture occurrence is far from certain. In fact, Haas and Skewis (1974) have suggested that melt fracture depends also upon the die design (e.g. tapering, length) and can possibly be avoided at shear stresses well exceeding critical values. This makes prediction of melt fracture a difficult task. Nevertheless, a logical response to counteract high shear stress development would involve reduction in the speed of operation, effectively lowering the magnitude of shear stresses well below the critical level.

4.4 PPVC: Nonisothermal Analysis

Runs using PPVC as the coating substance were performed at three different temperatures: 170°C, 180°C, and 200°C. At each temperature, wire speeds of 100 cm/s, 150 cm/s, and 200 cm/s were examined, these speeds being of the same order of magnitude as those used by Carley et al. (1979). The wire radius was set at 0.025 cm and the coating thickness taken to be 80% of the wire radius. The viscosity function was given by Carley et al. (1979) (Figure 3.2).

The first set of runs for different speeds at 170°C gave results that indicated that such conditions were totally unrealistic. Entrance pressures were found to be negative (-0.75 MPa at 100 cm/s) throughout and very large temperature rises were generated that would lead to major thermal degradation.

The previous runs were repeated for 180°C, yielding results that were more realistic in the physical sense, although they were still not acceptable. Upon inspection of the entrance pressures, it was found that while the lower speeds produced pressures slightly greater than zero, speeds greater than 200 cm/s gave negative pressures. This is shown in the pressure-wire speed relationship illustrated in Figure 4.29 for both 180°C and 200°C. Furthermore, the pressure distribution at both these temperatures for a wire speed of 200 cm/s is shown in Figure 4.30. Note the large pressure build-up in the die section at 180°C which is indicative of significant recirculation.

The occurrence of significant flow recirculation is clearly shown in the streamline pattern of Figure 4.31, which predicts recirculation of around 20% of the total flow rate. Figure 4.32 shows that the higher operating temperature serves to decrease the magnitude of flow recirculation, in this

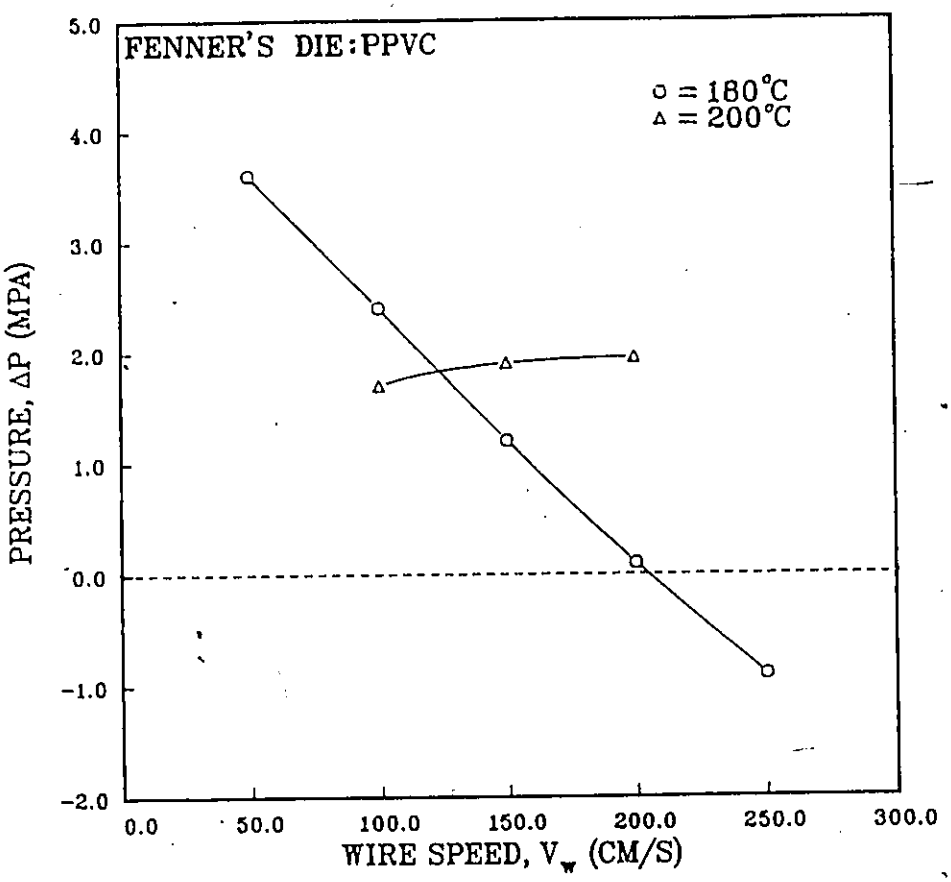

Figure 4.29: Pressure vs. Wire Speed for PPVC in Fenner's Die at 180°C and 200°C.

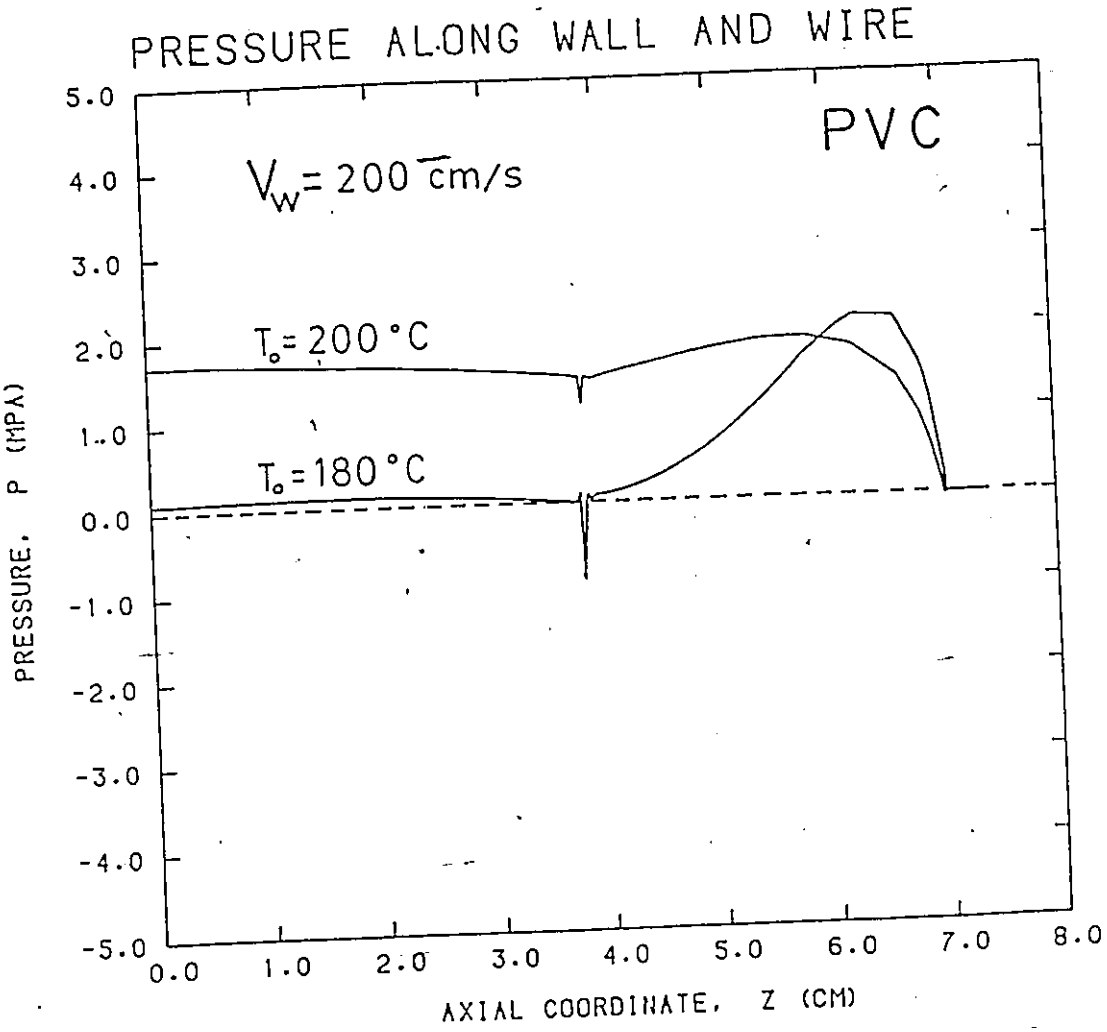

Figure 4.30: Pressure Development for PPVC in Fenner's Die at 180°C and 200°C (V_w= 200 cm/s).

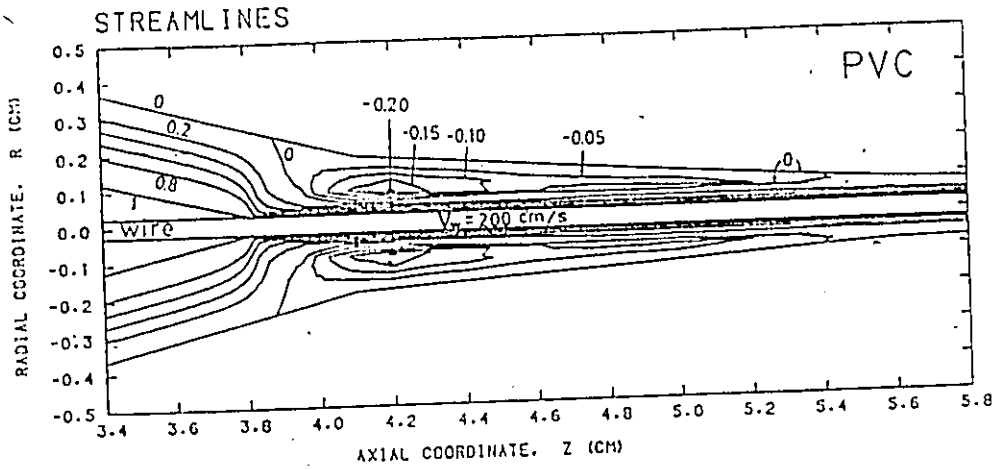

Figure 4.31: Streamline Pattern for PPVC in Fenner's Die (T = 180°C, V_w= 200 cm/s).

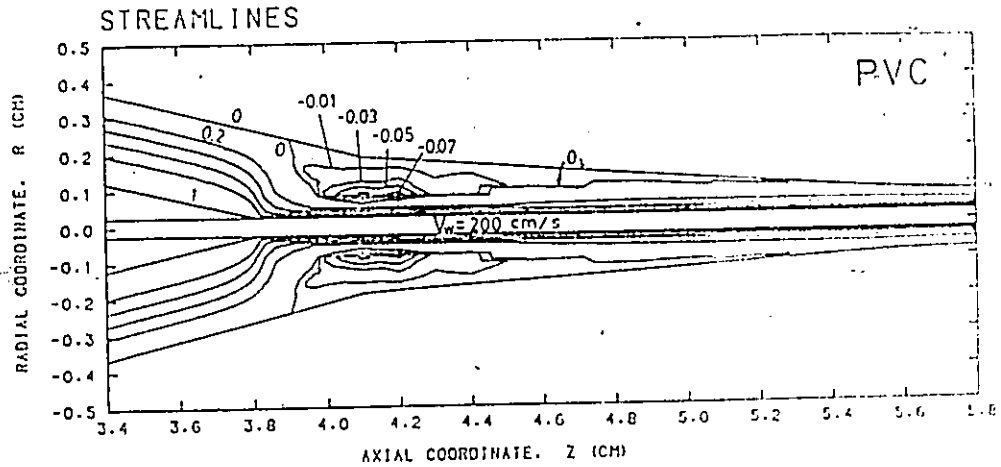

Figure 4.32: Streamline Pattern for PPVC in Fenner's Die (T = 200°C, V_w= 200 cm/s).

Table 4.3: Maximum Temperature for PPVC in Fenner's Die (180°C).

Wire Speed (cm/s)	Maximum Temperature (°C)
100.0	199.9
150.0	206.0
200.0	210.3

case to about 7%, due to the overall lowered fluid viscosity. The isothermal results for PPVC gave a total flow recirculation of 5% at 200 cm/s and 180°C. This illustrates the relative inadequacy of assuming isothermal conditions when analyzing wire-coating operations. Figure 4.33 shows that greater speeds will lead to more intense recirculation, and more importantly that decreasing the speed will not alone eliminate flow reversal at 180°C.

Temperature fields were generated at both 180°C and 200°C (for 200 cm/s) and are illustrated in Figures 4.34 and 4.35, respectively. It is seen that maximum temperatures will exist near the die orifice, where the viscous dissipation is the greatest. The temperature field for the 200°C case is much smoother than that of the 180°C case. This is also clear from the maximum temperature distribution, shown in Figure 4.36. The overall temperature rise must be monitored closely since PVC exhibits degradation tendencies at temperatures around 210°C and above. Temperature increases in the flow have a dependence on the wire speeds employed as detailed in Table 4.3.

The difference in maximum temperatures is not great, however operating at 200 cm/s (and perhaps 150 cm/s) would probably lead to significant degradation of the resin. In addition, shear stresses were found to range between 0.3 MPa to 0.49 MPa for the different wire speeds considered. Critical shear stress values have been correlated with temperature by Agassant (1980), and these values ranged from 0.24 MPa at 180°C to 0.67 MPa at 210°C. Therefore, operations at 180°C could possibly lead to the occurrence of melt fracture. Figure 4.37 presents shear stress results at different wire speeds for 180°C and 200°C.

Results obtained at 200°C were better, although degradation effects at this temperature are likely. Temperature differences under these conditions are found to be less pronounced, reducing the tendency for recirculatory behavior of the fluid. This is supported by the pressure distribution curve for 200 cm/s (Figure 4.30) showing a less severe positive pressure gradient

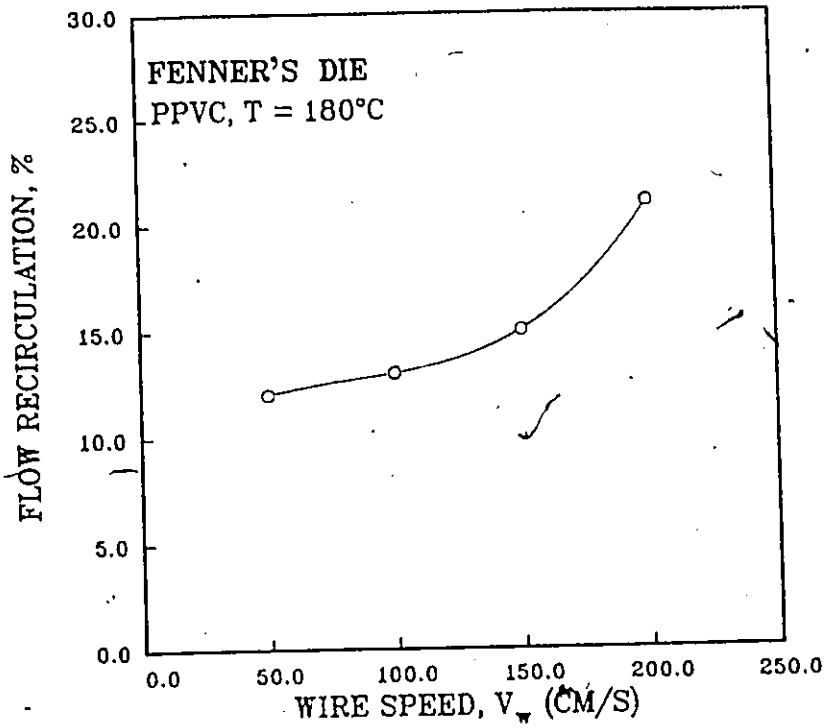

Figure 4.33: Recirculation vs. Wire Speed for PPVC in Fenner's Die at 180°C.

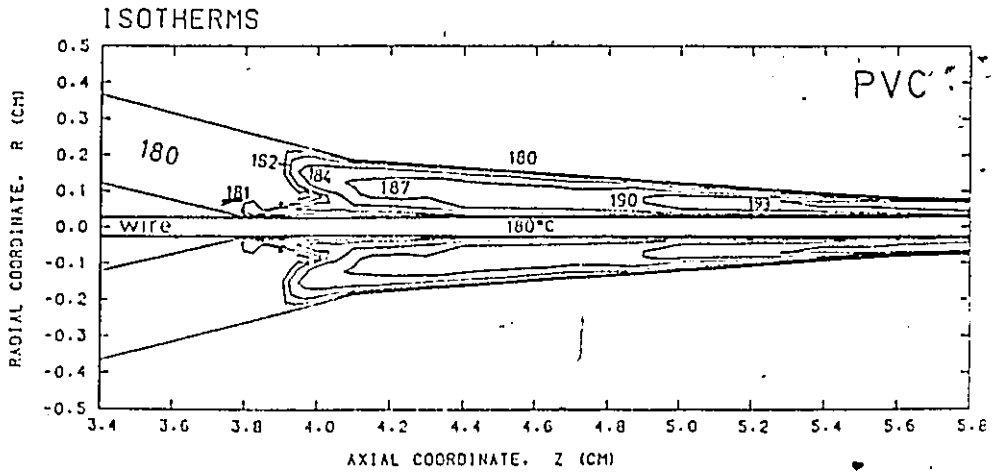

Figure 4.34: Temperature Field for PPVC in Fenner's Die (T = 180°C, V_w= 200 cm/s).

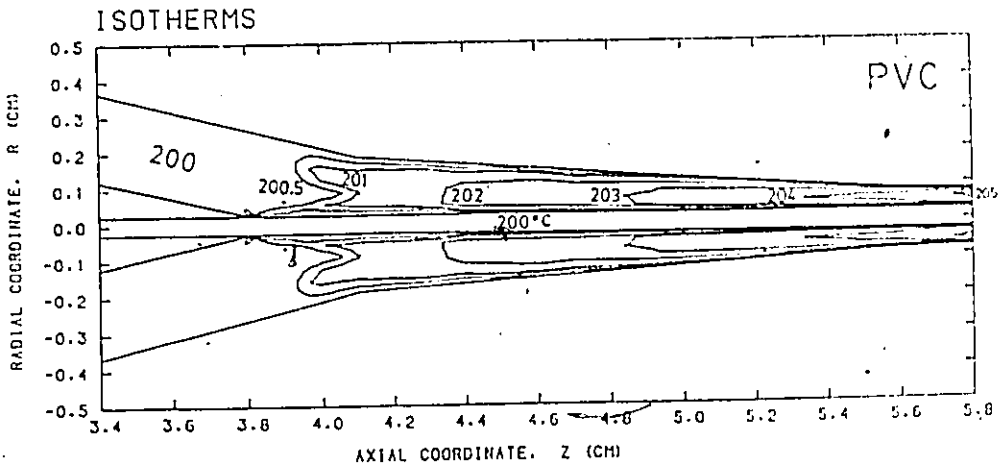

Figure 4.35: Temperature Field for PPVC in Fenner's Die (T = 200°C, V_w= 200 cm/s).

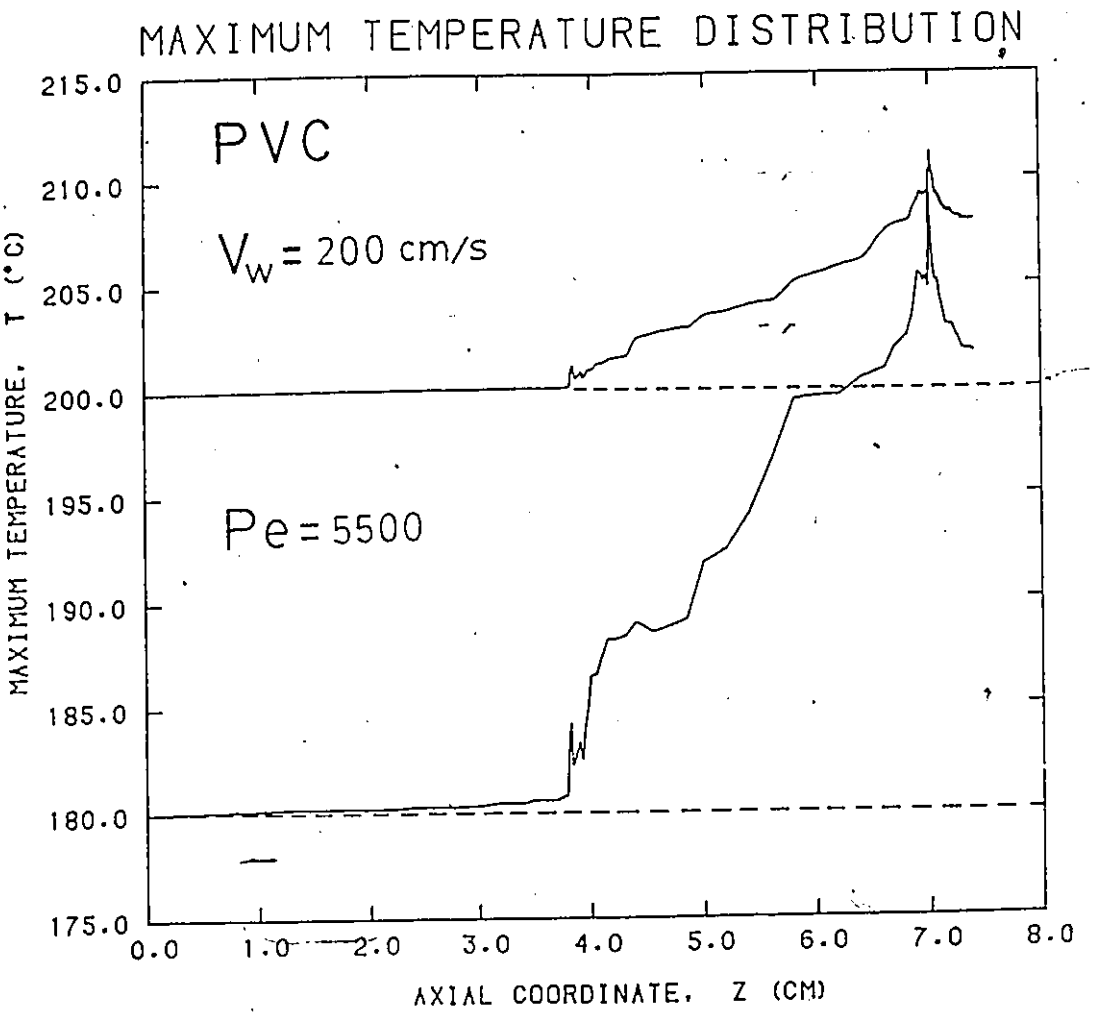

Figure 4.36: Maximum Temperature Distribution for PVC under Non-isothermal Conditions in Fenner's Die (V_w= 200 cm/s).

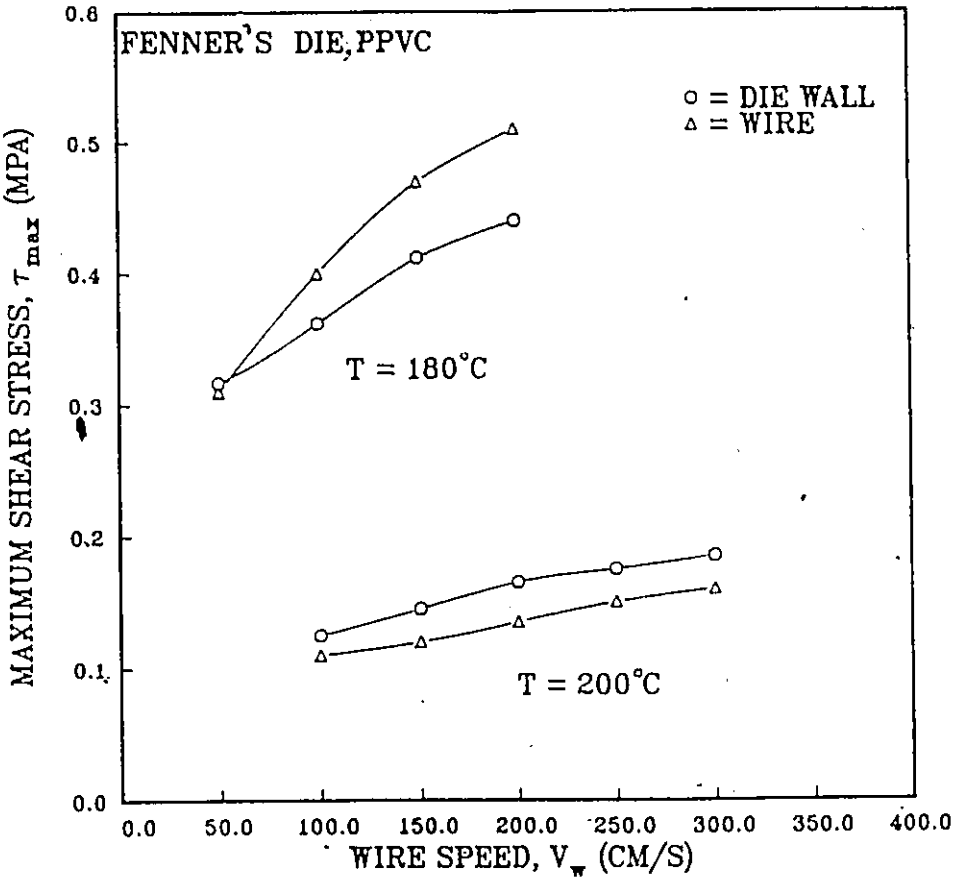

Figure 4.37: Shear Stress vs. Wire Speed for PPVC in Fenner's Die at 180°C and 200°C .

at this temperature. It is clear, however, that backflow will occur.

Examination of the shear stresses at 200°C show that they do not exceed the forementioned critical values. These values remain reasonably small, primarily due to an overall decrease in viscosity of the melt. A summary of results, found in Table 4.4, generally shows the effect of both nonisothermal conditions and higher temperatures on various performance variables.

The amount of recirculation occuring in Fenner's die for PPVC is unacceptably high. The high viscosity of this resin, coupled with its sensitivity to high temperatures strongly suggests that a smaller die length is required for successful wire-coating operations using PPVC. Therefore, another die design would be required to handle PPVC, and this is the subject of the next chapter.

4.5 Concluding Remarks

The use of the LAT, while only giving an isothermal, one-dimensional perspective, does yield a good deal of important information. It provides us with a quick and preliminary estimate of performance data. The existence of flow recirculation is readily deduced using this method. In addition, the results from the LAT analysis are required so that those obtained by the FEM analysis may be compared for agreement in the most limiting cases. This will ensure the correctness of the FEM simulation. The discrepancy observed in this chapter was primarily the cause of an assumed clearance gap in the FEM analysis, a realistic assumption not incorporated in the LAT method. It is of interest that the results obtained near the impact are very sensitive with respect to the nature of the modelling (i.e. element structure) in that region.

Both LDPE and plasticized PVC were examined in this die design. LDPE performance results were acceptable when a 0.025 cm wire was employed, except for a small flow recirculation being evident throughout all runs. To remedy this, an increased wire radius was assumed and this effectively eliminated flow recirculation while giving reasonable results for other performance variables. It is likely, therefore, that Fenner's die was designed to handle LDPE for coating small telephone wires.

Results using plasticized PVC were found to be rather poor under almost every condition. It is felt the large die size is inappropriate for PPVC.

Table 4.4: Comparison between Predictions from Isothermal and Non-isothermal Analysis for a Plasticized PVC Melt in Fenner's Die (V_w= 200 cm/s).

Variable	Isothermal 180° C	Nonisothermal 180° C	Nonisothermal 200° C
Inlet Pressure ΔP (MPa)	10.76	0.22	1.72
Maximum Pressure P_{max} (MPa)	11.15 5.4*	2.10 6.2*	1.87 5.8*
Haul-off Tension F (N)	15.46	12.63	3.81
Maximum Tension F_{max} (N)	15.52 6.9*	12.91 6.9*	3.83 6.9*
Maximum Shear Stress at Wire $\tau_{w,max}$ (MPa)	0.52 3.8*	0.52 3.8*	0.14 3.8*
Maximum Shear Stress at Die Wall $\tau_{d,max}$ (MPa)	0.68 7.0*	0.43 7.0*	0.16 7.0*

*Location (in cm) where maximum value is observed.

Its greater viscosity also leads to greater heat dissipation and due to its strong thermal sensitivity, it is very likely that the polymer would be subjected to significant thermal degradation if used in Fenner's die.

Chapter 5

ANALYSIS OF CASWELL AND TANNER'S DIE

A particular die design is studied by using both the LAT and FEM analysis. The LAT is applied for both Newtonian and power-law fluids assuming isothermal conditions. These findings are used to verify the results obtained by the FEM. The FEM is then extended to nonisothermal conditions for an extensive study using plasticized PVC.

5.1 Introduction

Caswell and Tanner (1978), in addition to pioneering the application of the FEM in the simulation of the wire-coating process, also established criteria from which a new design could be constructed. Pressure considerations and secondary flow effects were designated as the two principal concerns.

The new die design put forward by Caswell and Tanner (also referred to as Caswell's die in this study) is detailed in Figure 5.1. It was constructed by using the LAT to give desired velocity profiles at certain axial distances in the die. At impact, the best velocity profile would be one having no backflow within the largest gap possible. The large gap at this point would assist in suppressing the development of high shear rates. To prevent pressure rising downstream from impact, this gap would have to be quickly reduced to yield a less severe profile, basically determined by the motion of the wire. This drag profile should then be eliminated to give a more "plug-like" velocity, thus easing the fluid drag exerted on the wire. The total

length of the die region was selected to provide a sufficient overpressure to prevent cavitation in the impact zone while also preventing the possibility of wire stretch, with either case yielding an unacceptable product. From this, Caswell and Tanner (1978) deduced the basic dimensions. The authors reasoned that this design would give no secondary flow while maintaining a positive pressure at the impact point. In addition, a blunt nose was used in order to model the effect of machining tolerances and wear. Caswell and Tanner (1978) note that the sharp nose used in Fenner's die is a suitable model only for thick wires. The wire considered has a radius of 0.025 cm with a coating requirement of 80% of the wire radius to give a product of 0.045 cm at the exit. In the present study of Caswell's die the coating material is assumed to be a plasticized PVC resin, the properties of which are found in Chapter 3. Again, the density difference between the exiting hot melt and the final cold coating is not considered.

5.2 Isothermal Analysis

This analysis assumes that the containing surfaces remain at a fixed temperature along the die and that the temperature of the LDPE melt stays unchanged. This assumption is carried through for both Newtonian and power-law fluids.

5.2.1 Lubrication Approximation Theory

The analysis of wire-coating performance was initially carried out for Newtonian and power-law fluids under isothermal conditions using the LAT. Power-law indices examined were n = 0.75, n= 0.50, and n=0.25, while n = 1 gives the Newtonian case. Figure 5.2 illustrates the dimensionless pressure distribution within this die for all cases considered. It is evident that maximum pressure values exist at the inlet for each fluid, therefore indicating the absence of recirculatory behavior. In all cases a relatively small discontinuity exists immediately after impact, this being basically due to the blunt nose of the torpedo. Subsequent pressure drop in the parallel land section will show almost linear behavior since there is no taper. Shear stress distribution at the die wall and wire surface is presented (in dimensionless form) in Figures 5.3 and 5.4, respectively. In addition, Figure

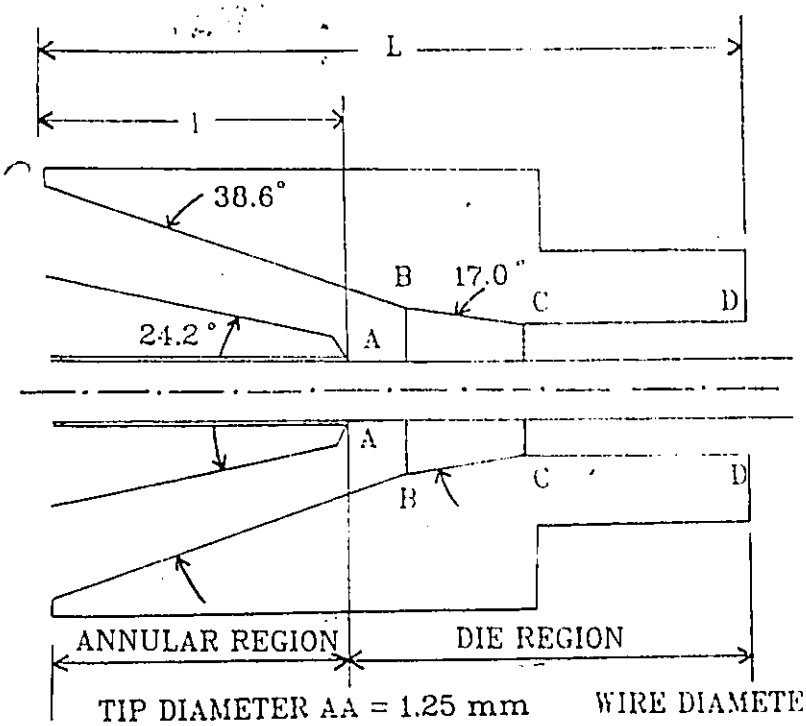

TIP DIAMETER AA = 1.25 mm
DIAMETER BB = 1.40 mm
DIAMETER CC = 1.10 mm
DIAMETER DD = 1.09 mm

WIRE DIAMETER = 0.50 mm
TORPEDO LENGTH, l = 2.5 mm
OVERALL LENGTH, L = 5.9 mm

Figure 5.1: Die Design Given by Caswell and Tanner (1978).

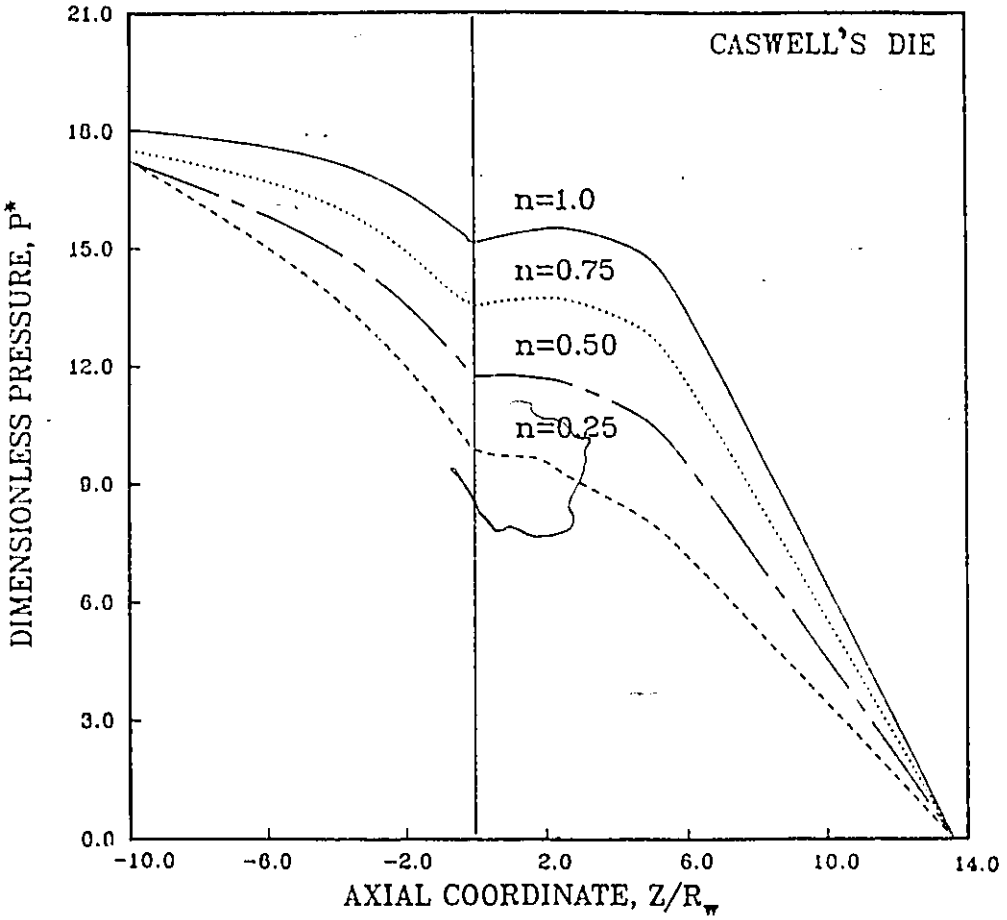

Figure 5.2: Dimensionless Pressure Distribution in Caswell's Die Using LAT.

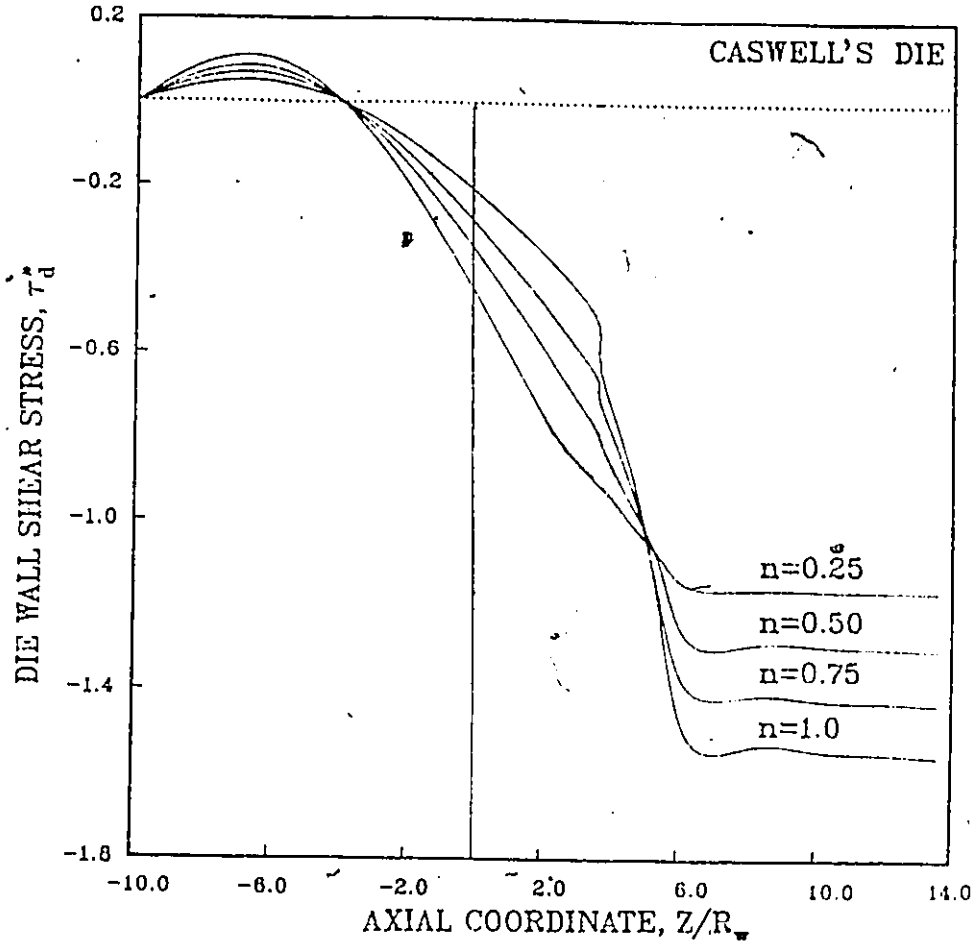

Figure 5.3: Dimensionless Shear Stress Distribution at Die Wall in Caswell's Die Using LAT.

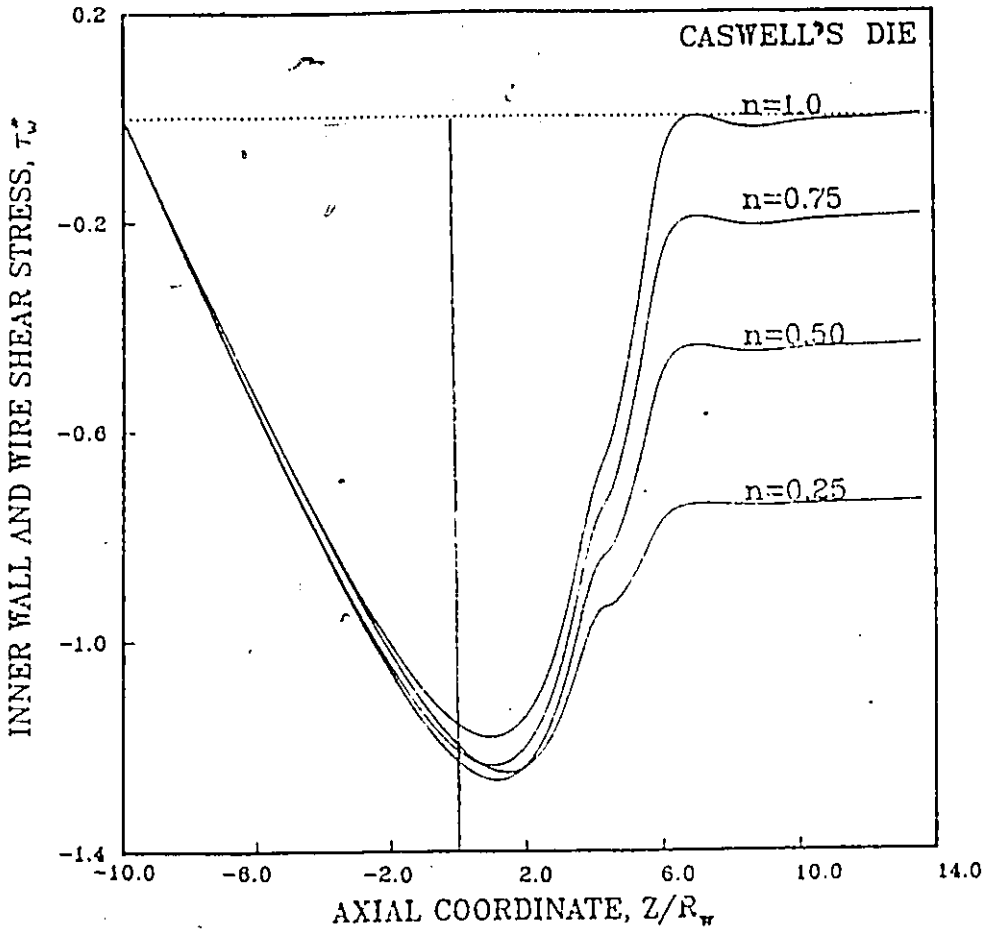

Figure 5.4: Dimensionless Shear Stress Distribution at Wire in Caswell's Die Using LAT

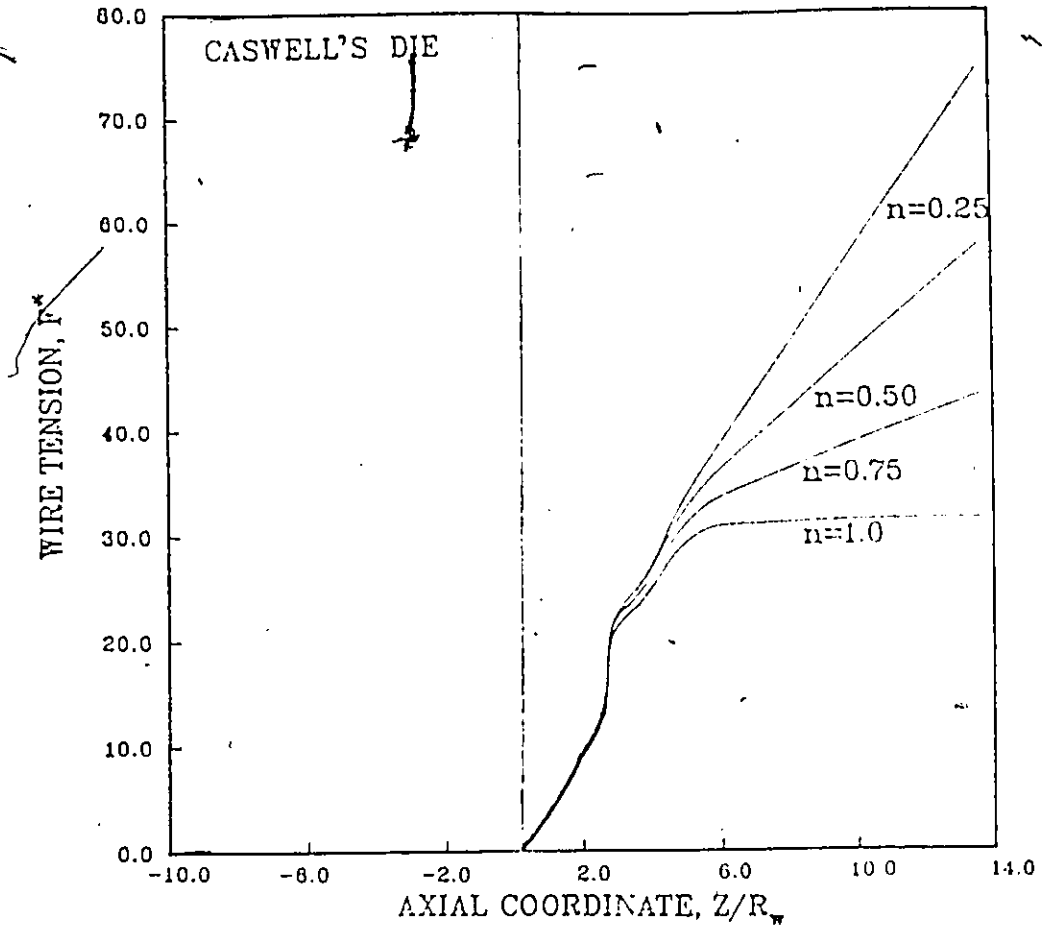

Figure 5.5: Dimensionless Wire Tension in Caswell's Die Using LAT.

5.5 shows the development of the wire tension throughout the die section, again in dimensionless form.

5.2.2 Finite Element Method

The finite element grid used in the simulations is shown in Figure 5.6. The grid contains a total of 240 elements for velocities-pressure computations and 567 nodes. The flow domain was extended to a total of 30 wire radii as compared to 24 wire radii used by Caswell and Tanner. A longer distance has been considered after the exit to better account for exit effects (i.e. satisfying the natural boundary conditions on the free surface). The domain has been selectively discretized with a denser grid used in regions where singularities are known to exist.

An initial run was made assuming a Newtonian fluid under isothermal conditions and having a coating requirement of $h = h_m = 0.8R_w$, these conditions having previously been employed in the LAT analysis thereby providing a basis for comparison. The FEM computations yield a smoothly streamlined flow field with no evidence of backflow as shown by Figure 5.7. This is in agreement with the LAT predictions. The pressure distribution obtained is compared with that found from the LAT in Figure 5.8. The discrepancy between the two distributions can be attributed to several factors. As previously observed, results are quite sensitive to the grid arrangement used in the impact region. Furthermore, the LAT can only be considered as an approximation since it is only one-dimensional by nature, and loses accuracy when the angle of convergence is greater than 10 degrees, which is the case near the impact. Thus the LAT does not account for the radial pressure contribution occurring in the impact zone. A discrepancy also exists between the LAT results and those of Caswell and Tanner (1978) but is smaller in magnitude. The relatively small difference between the results of the latter and the current findings is likely due to differences in the grid density employed.

5.3 Nonisothermal Analysis

This analysis assumes that the metal surfaces (wire and die and torpedo walls) are kept at a constant temperature which is equal to the entering

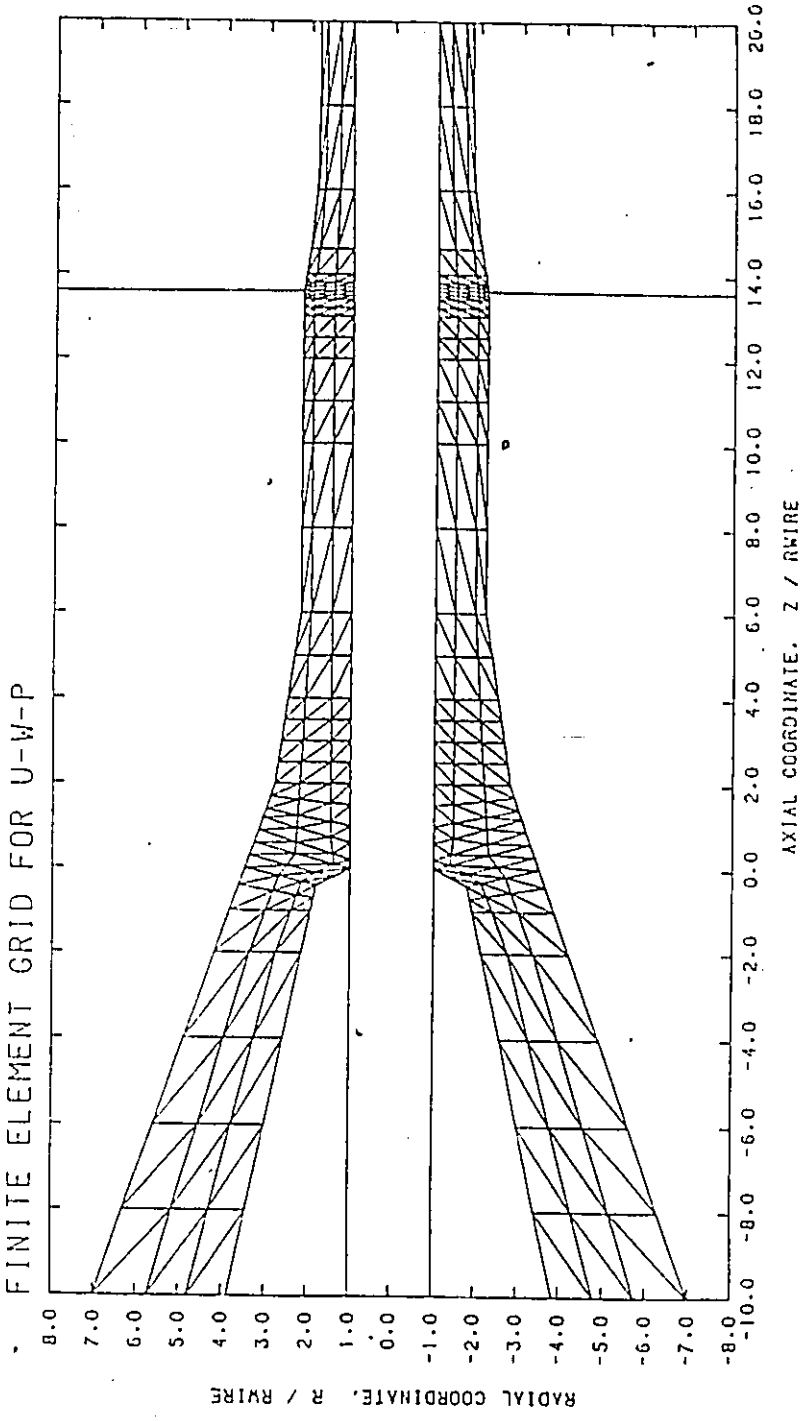

Figure 5.6: Finite Element Grid for Analysis of Caswell's Die.

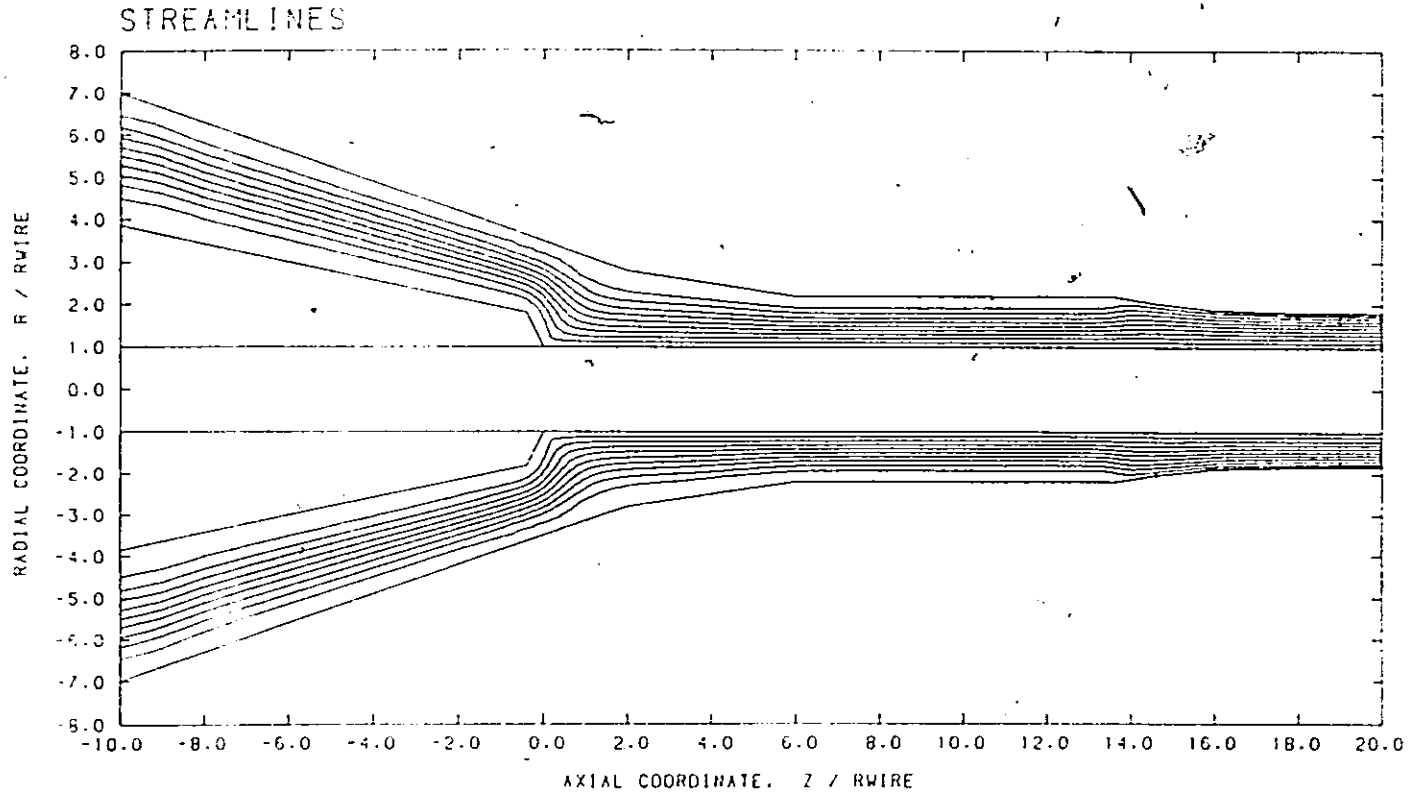

Figure 5.7: Streamline Pattern for a Newtonian Fluid in Caswell's Die.

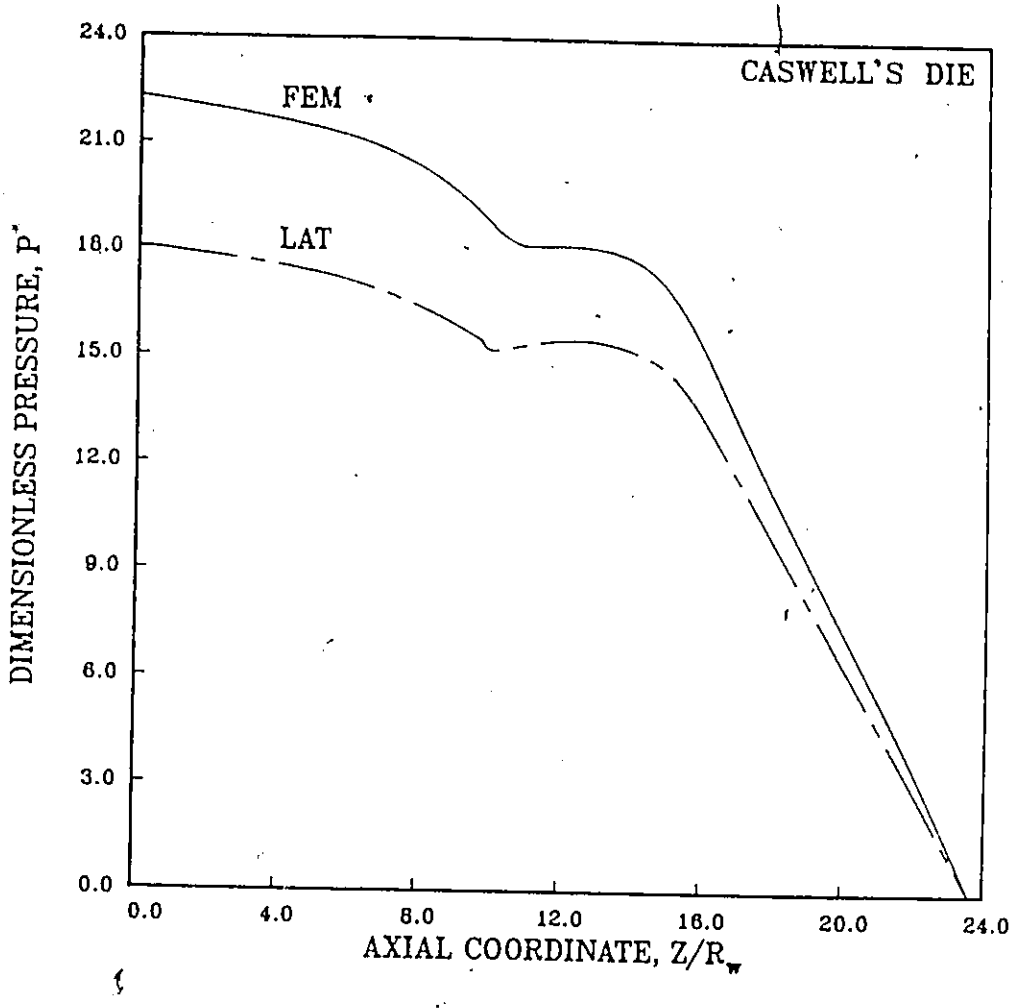

Figure 5.8: Dimensionless Pressure Distribution for a Newtonian Fluid in Caswell's Die.

melt temperature. Solution of the energy equation was required to account for the heating effect due to viscous dissipation in the melt.

Runs were performed with plasticized PVC using characteristic material properties found in Chapter 3, and described by the non-Newtonian model used by Carley et al. (1979). Wire speeds were set at 100 cm/s, 200 cm/s, 250 cm/s, 300 cm/s for each of three different operating temperatures at 170°C, 180°C, and 190°C. These conditions were assumed reasonable for actual wire-coating operations using PPVC.

When the thermal boundary conditions were set to 170°C, the results were found to be very unsatisfactory. The highly viscous melt led to a development of large amounts of viscous dissipation, subsequently resulting in unrealistically high temperature rises. In addition, excessive shear stresses were found to exist at the wire surface and die wall. This operating temperature was therefore deemed inappropriate. Thus all other runs were conducted at 180°C and 190°C, temperatures around which no appreciable degradation is believed to take place.

Flow recirculation has not been detected in this die under the isothermal assumption. However, the more realistic case of viscous heat generation has greater relevance with respect to actual process conditions. At a boundary temperature of 180°C with a speed of 250 cm/s, Figure 5.9 gives the resulting streamline pattern, with no recirculation found. The absence of recirculation under nonisothermal conditions was also true for all other runs performed. Therefore, neither the temperature-dependence of the fluid nor its shear-thinning behavior cause any secondary flow effects. The temperature development within the die can be easily and rapidly discerned by visual representation of the isotherms, as shown in Figure 5.10. In addition the temperature profiles can give important information regarding thermal effects in the melt. A presentation of these profiles in the die section (i.e. after melt impact) is made in Figure 5.11, with these trends basically similar in all other runs conducted. The temperature maxima again occur near the die wall, and the large increase in the temperature over the short distance towards the exit underlines potential problems involved when operating with PVC.

The maximum temperature distribution, as seen in Figure 5.12, shows a temperature rise of 16.5°C existing in this minute flow region resulting from the relatively intense conditions imposed on the viscous melt. Figure 5.13 shows the basic trend between temperature rises and different wire speeds

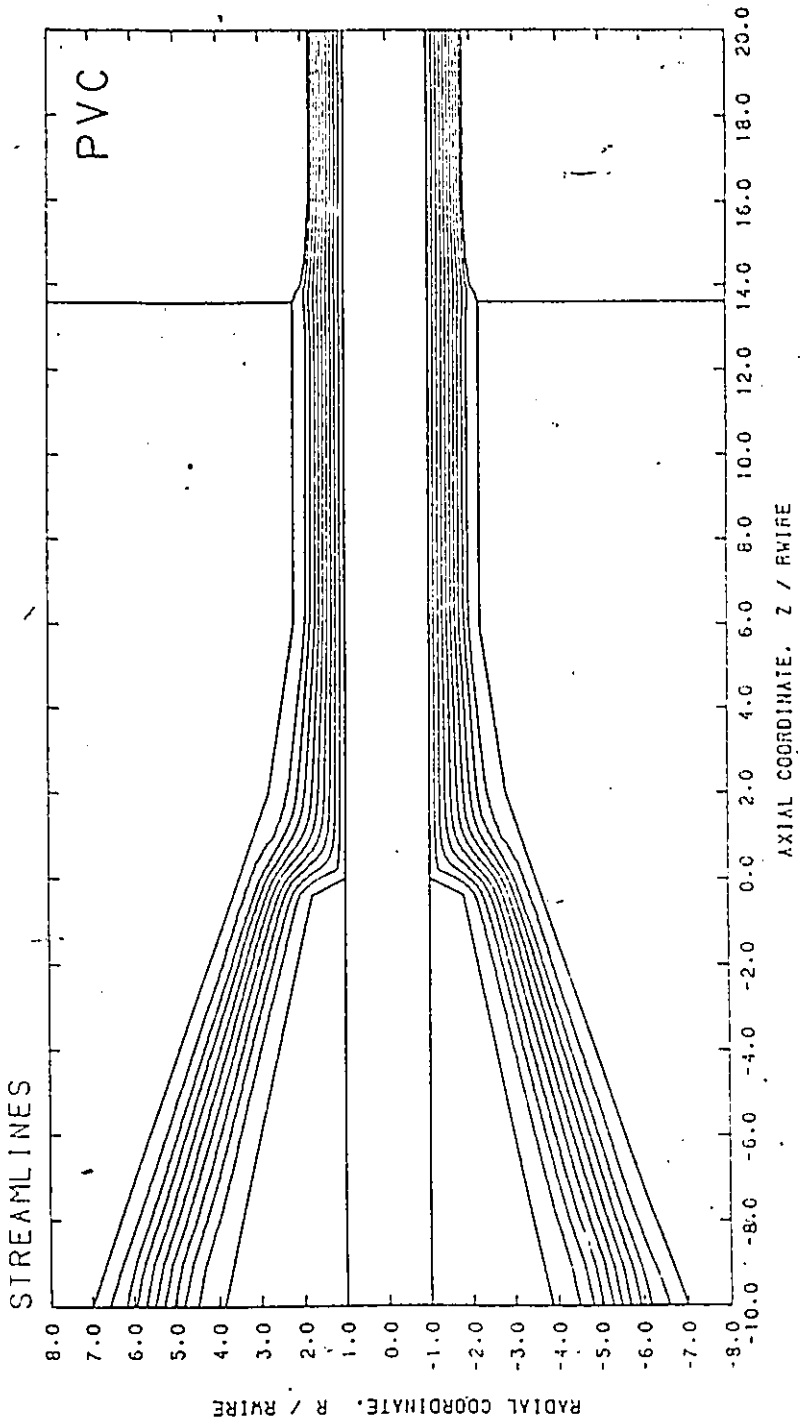

Figure 5.9: Streamline Pattern in Caswell's Die (V_w= 250 cm/s, T = 180°C).

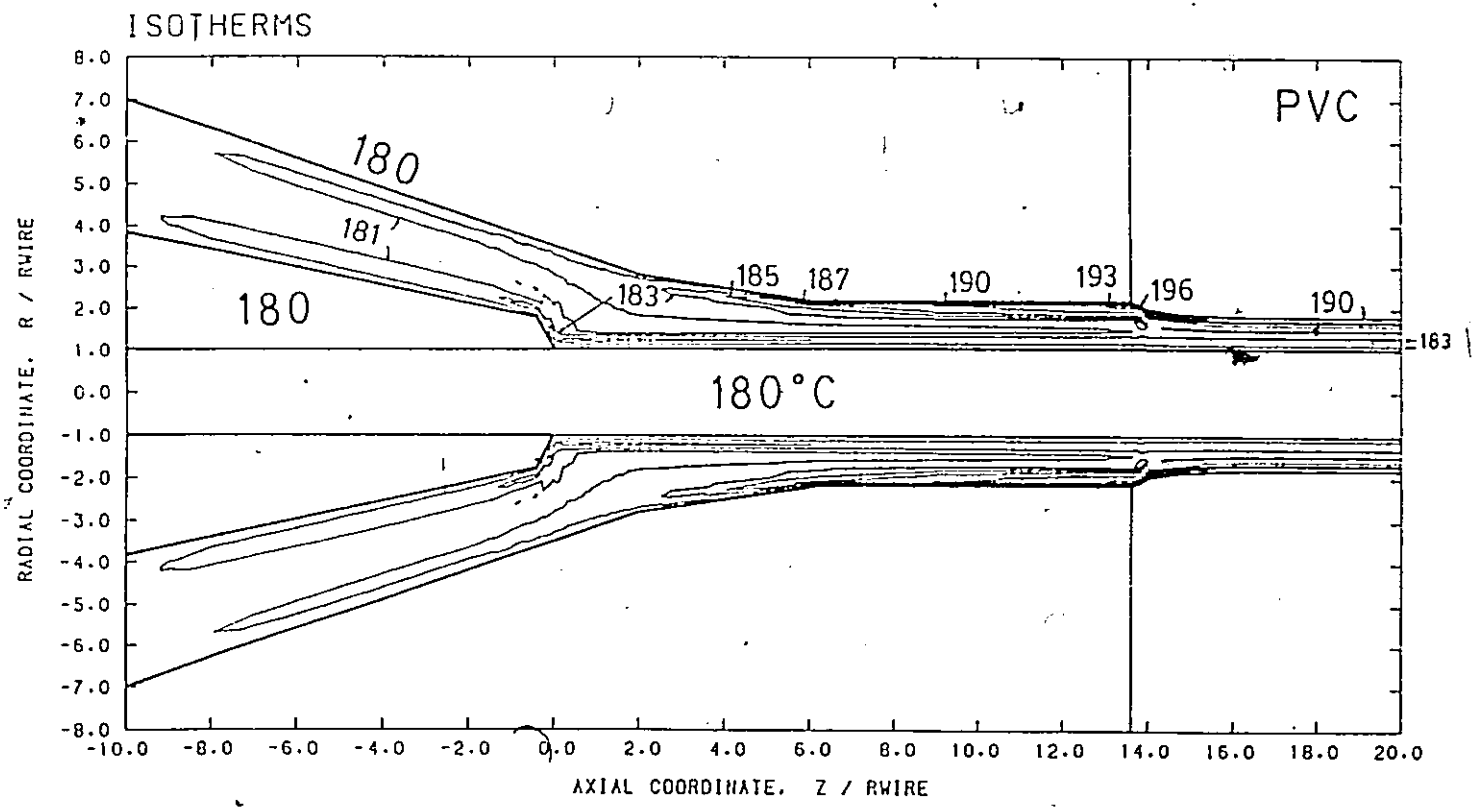

Figure 5.10: Temperature Pattern in Caswell's Die (V_w= 250 cm/s, T = 180°C).

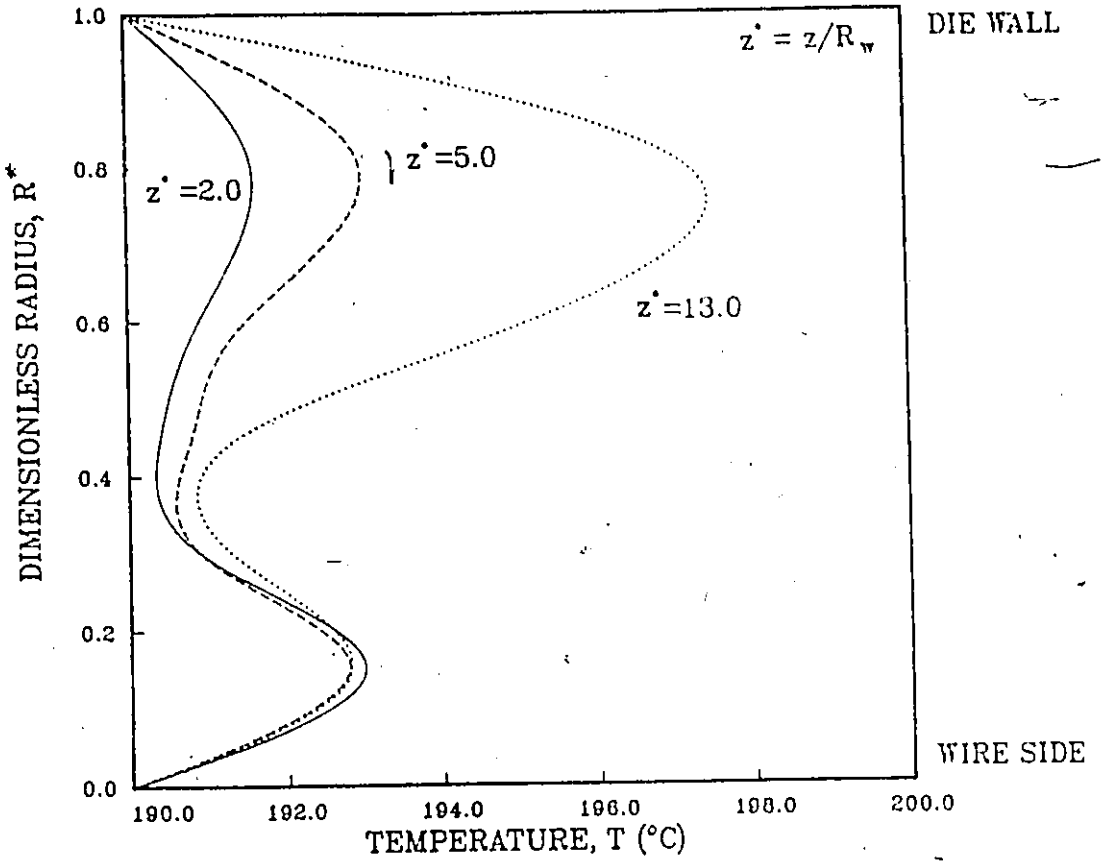

Figure 5.11: Temperature Profiles in Caswell's Die (V_w= 100 cm/s, T = 190°C).

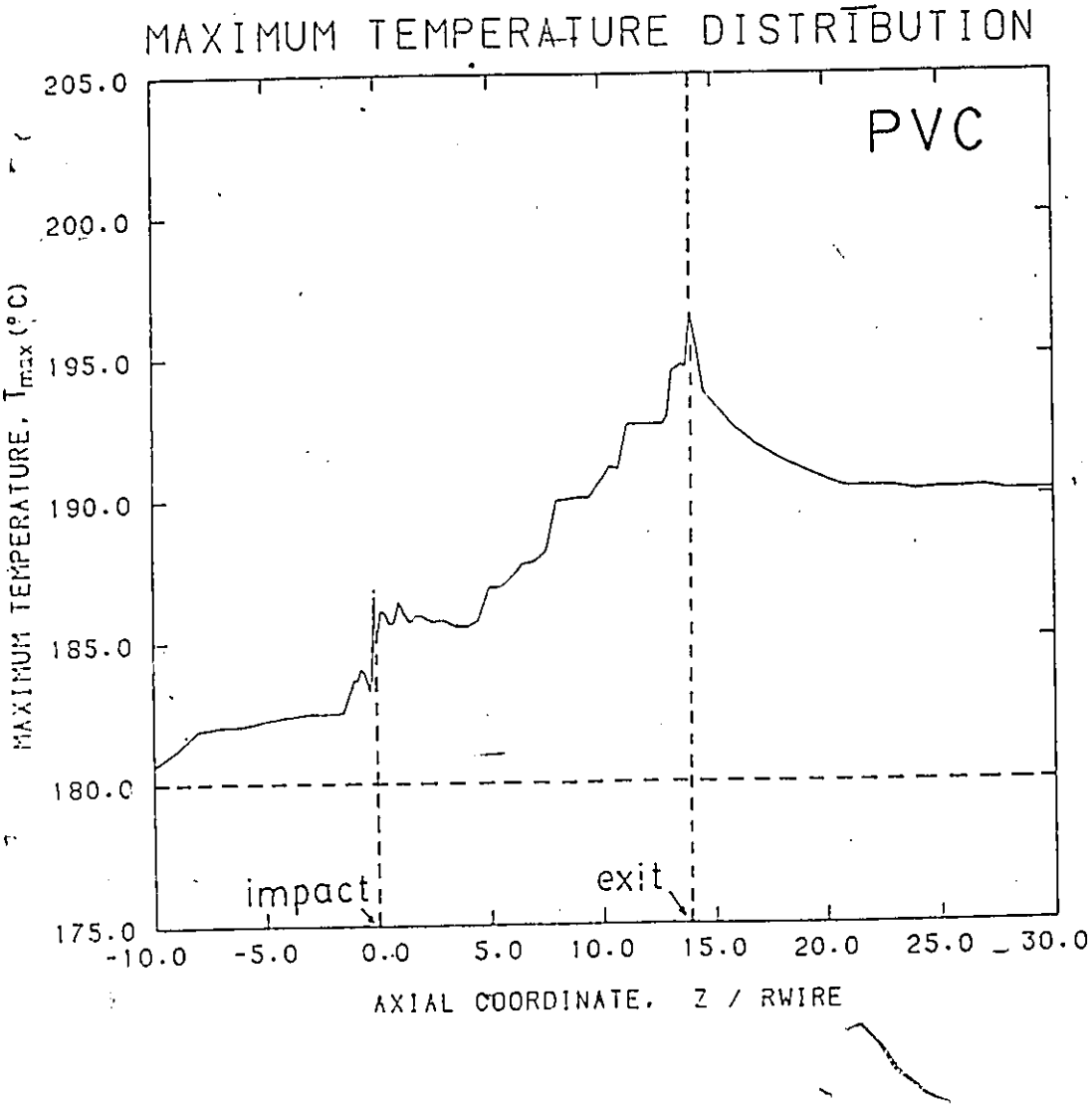

Figure 5.12: Axial Temperature Development in Caswell's Die (V_w= 250 cm/s, T = 180°C).

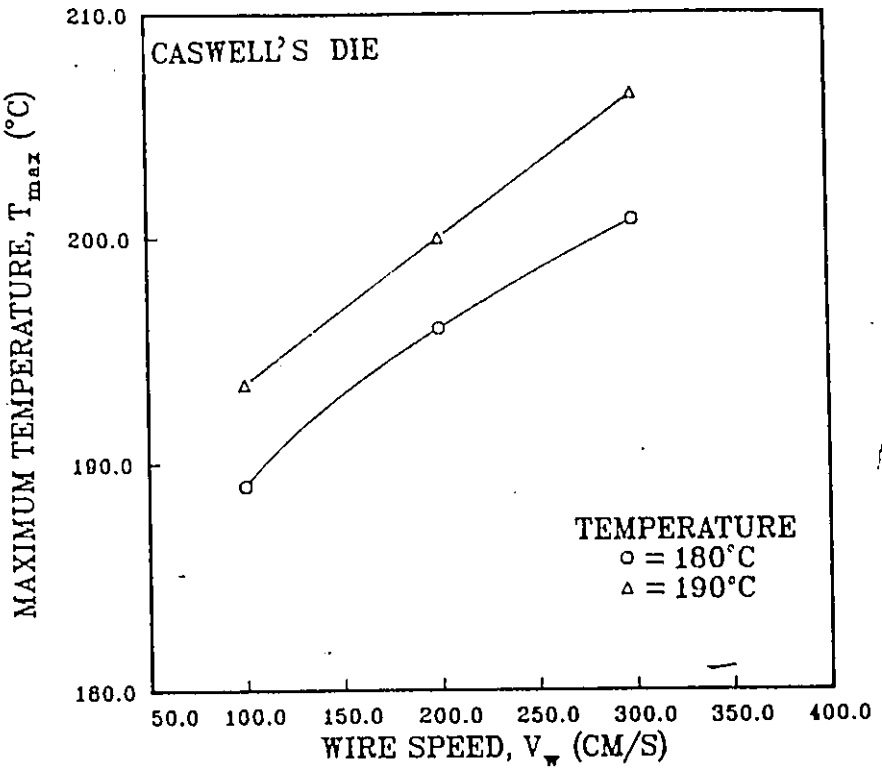

Figure 5.13: Maximum Temperature vs. Wire Speed in Caswell's Die (T = 180°C and 190°).

under nonisothermal conditions. It is evident that the more viscous melt at the lower temperature will experience greater viscous heating effects and thus lead to more dramatic temperature rises. It is also apparent that higher wire speeds could also lead to thermal degradation of the coating material. Problems in temperature simulation were encountered at high wire speeds, where oscillations in temperature values were observed. The cumulative effect of this is believed to be relatively minor with respect to overall results obtained. This point is discussed further and in more detail in the next chapter.

The axial pressure development is shown in Figure 5.14 . The almost linear pressure drop, particularly after the impact is generally the result of no taper in the die-land section, and further reflects the lack of any flow recirculation. Figure 5.15 gives the relationship between the entry pressure and wire speed in this die at two different die temperatures.

The velocity profile changes continually along the axial length, and the general pattern in the die section (i.e. beyond melt-wire impact) is shown in normalized form in Figure 5.16 for 200 cm/s and 180°C. The profile is initially rearranged due to the taper of the die wall, after which it is primarily influenced by viscous heating effects in the untapered section. The relatively short length of this final section prevents significant changes of the velocity profile.

Shear stress development in the die region along both the wire and die surfaces are given in Figure 5.17 . The maximum values were found to be 0.695 MPa at the wire impact, and 0.485 MPa at the die wall exit. The generation of viscous heat assists in reducing the severity of the stresses. Furthermore, Figure 5.18 illustrates the shear stress-wire speed relationship at 180°C and 190°C. It is interesting to note that shear stress maxima occur at the wire surface in this die design rather than the die wall as seen in the previous die. The short length of this die prevents shear stresses at the die wall from exceeding those initially formed at the wire surface. A 10°C increase, in general, reduces the viscosity by roughly one-half. The difference in shear stress magnitudes between the two temperatures is approximately proportional to the viscosity drop. This underlines the large influence of thermal effects within the polymer melts on the desired design variables. Upon close examination of given critical data, problems might be expected with respect to melt fracture when operating at 180°C. However, as discussed in the previous chapter, melt fracture can be avoided in a

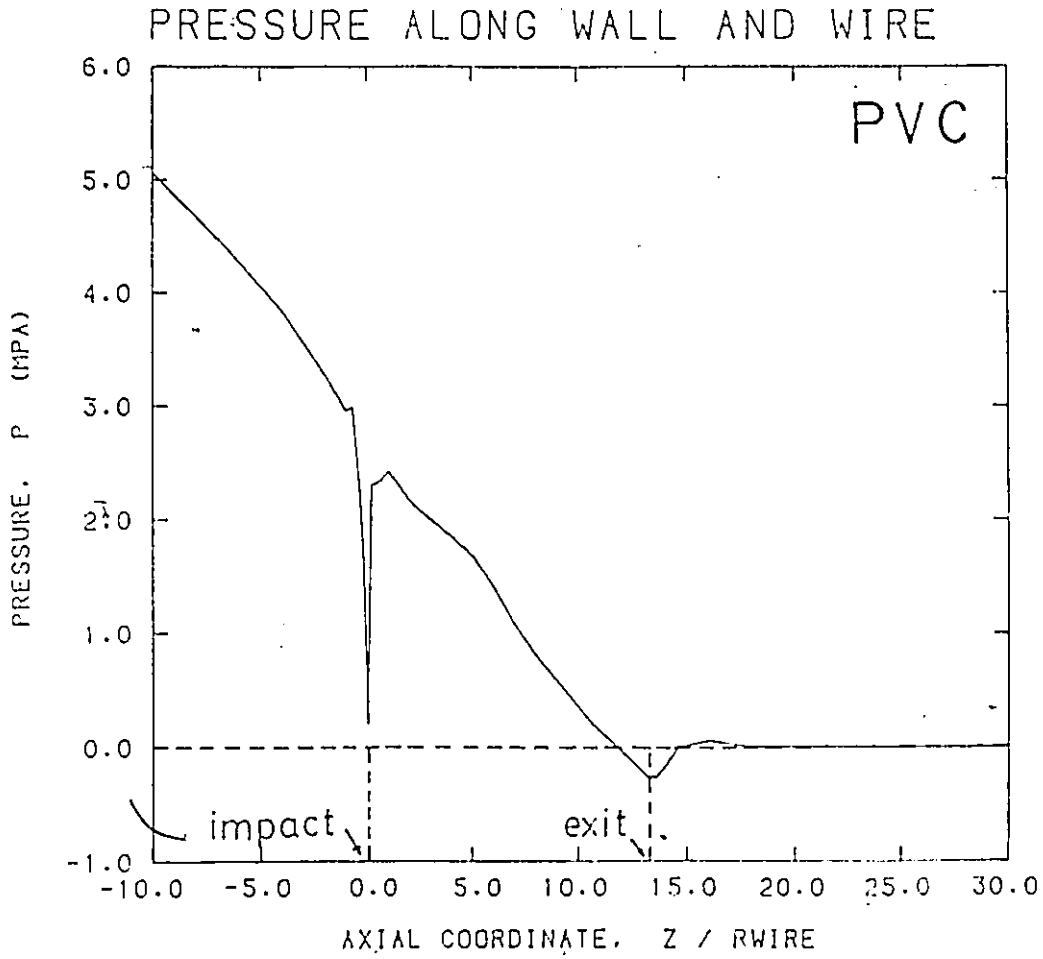

Figure 5.14: Axial Pressure Development in Caswell's Die (V_w= 250 cm/s, T = 180°C).

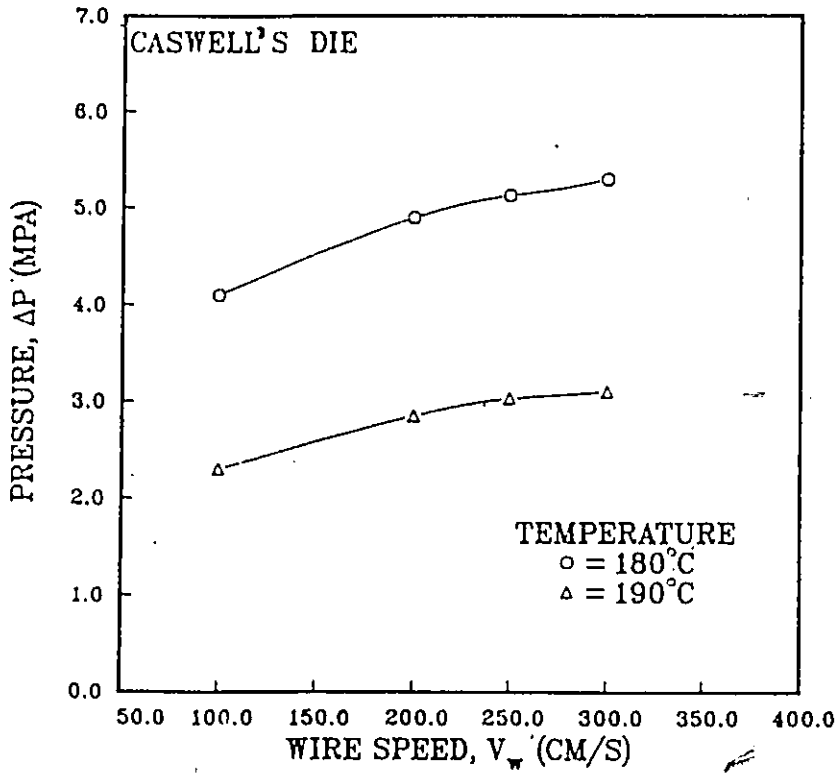

Figure 5.15: Pressure vs. Wire Speed in Caswell's Die (T = 180°C and 190°).

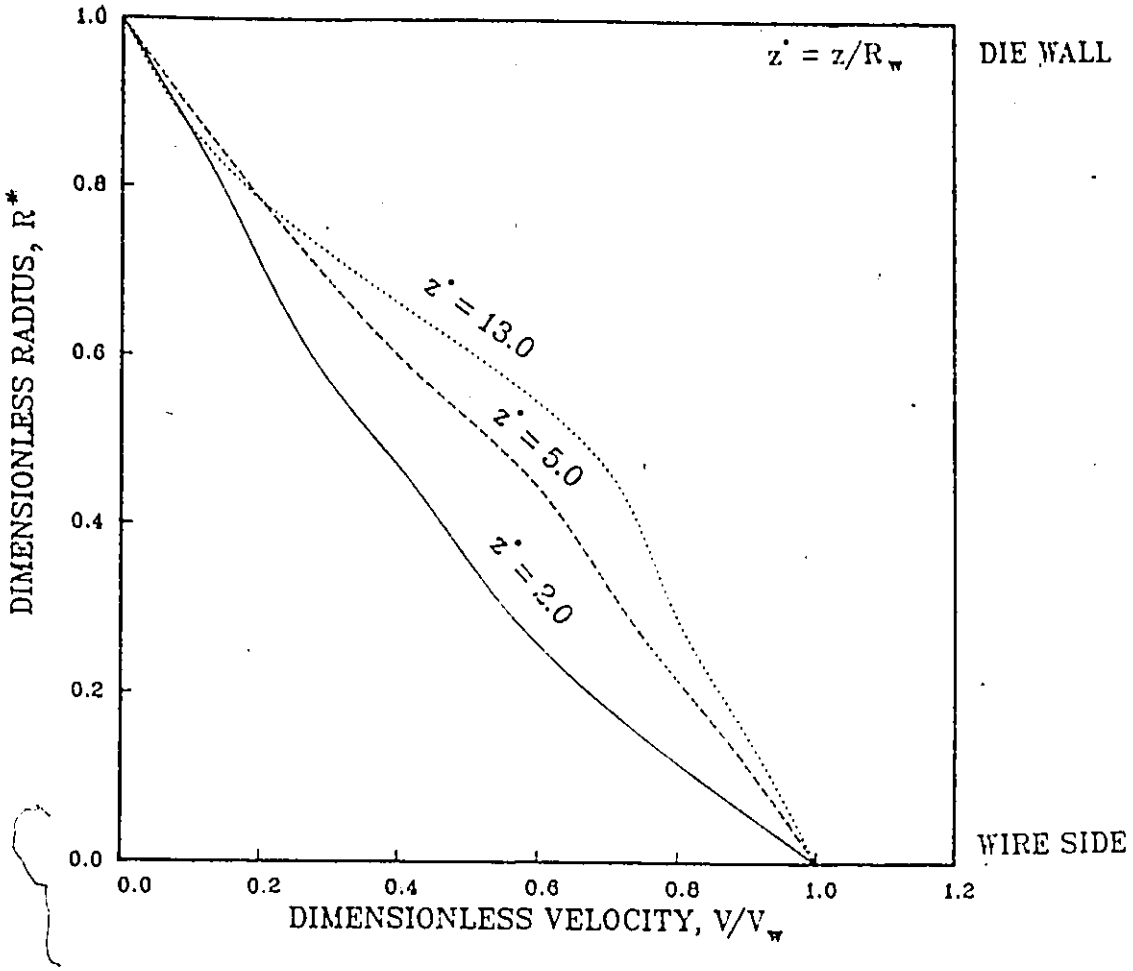

Figure 5.16: Dimensionless Velocity Profiles in the Die Section of Caswell's Die (V_w= 200 cm/s, T = 180°C).

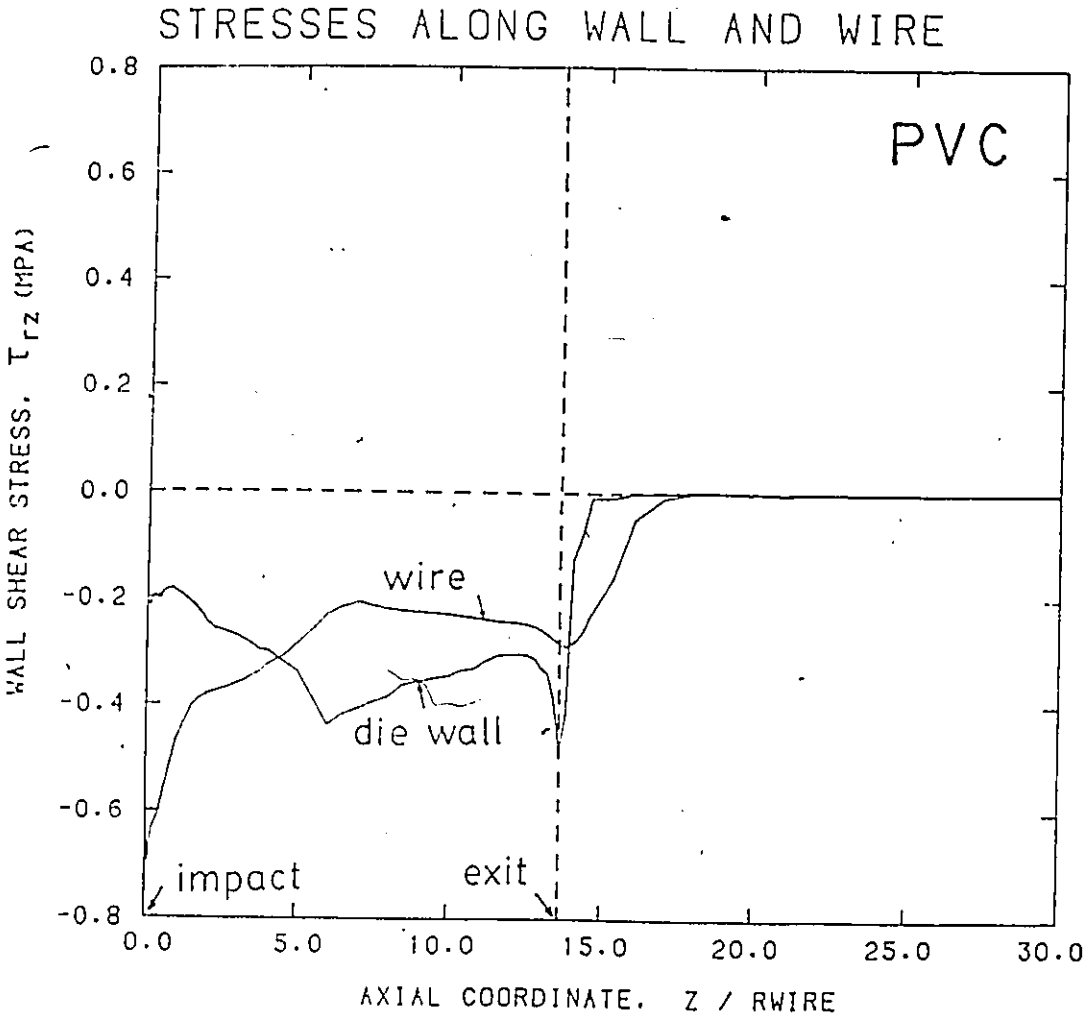

Figure 5.17: Shear Stress Development in Caswell's Die (V_w= 250 cm/s, T = 180°C).

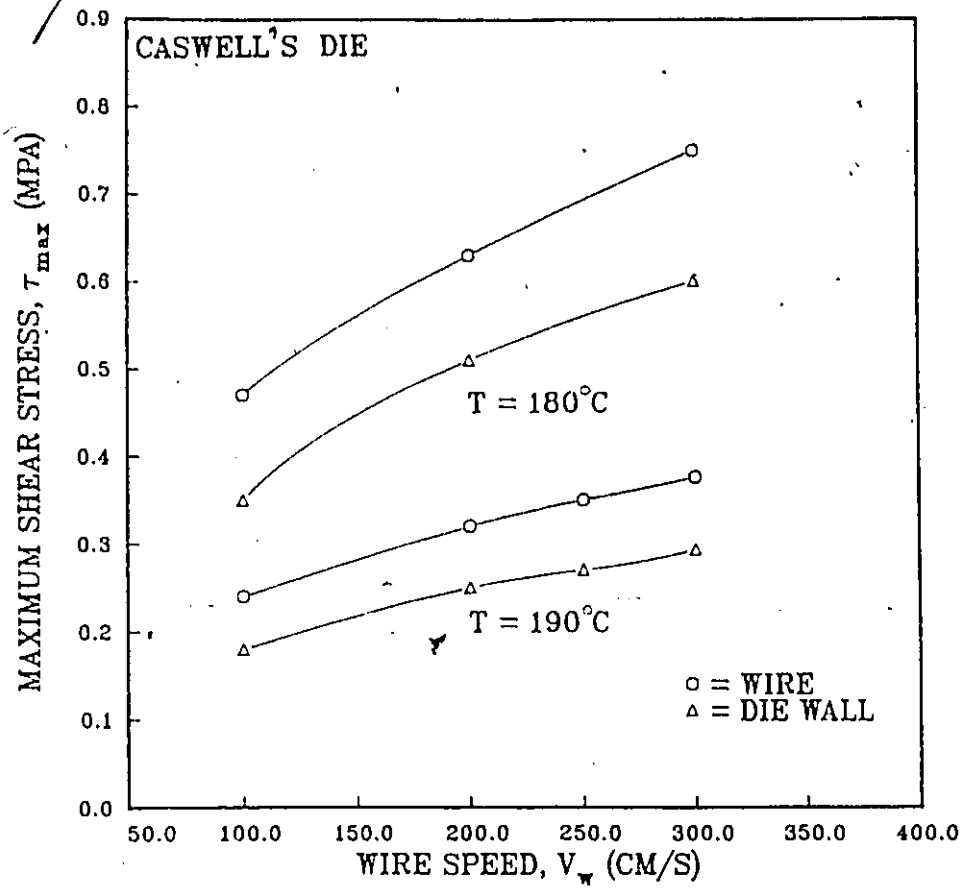

Figure 5.18: Maximum Shear Stress vs. Wire Speed in Caswell's Die (T = 180°C and 190°).

Table 5.1: Summary of Results for Caswell's Die.

	Case 1	Case 2	Case 3
Wire Speed (cm/s)	300	200	200
Temperature (°C)	190	190	200
Pressure Drop ΔP(MPa)	3.08	2.82	1.60
Maximum Temperature (°C)	206.2	200.0	205.3
Maximum Shear Stress at Die Wall $\tau_{d,max}$(MPa)	0.34	0.31	0.16
Maximum Shear Stress at Wire $\tau_{w,max}$(MPa)	0.25	0.24	0.13

properly designed die even if shear stresses exceed the critical values (Haas and Skewis, 1974). Table 5.1 summarizes results from some of the conditions previously examined to further illustrate their effect on the important die performance variables.

5.4 Concluding Remarks

The use of PVC as a wire-coating resin, unacceptable in the configuration of Fenner's die (Chapter 4), was tested in this particular die which was designed to avoid recirculation. The one-dimensional, isothermal LAT analysis gave quick estimations of expected pressure requirements, shear stresses, and wire tensions for assumed Newtonian and power-law fluids. In addition, it gave a preliminary indication that flow recirculation did not exist.

Extension of the FEM analysis to nonisothermal conditions using a characteristic temperature-dependent viscosity model gave results deemed to be more reasonable. The sensitivity of PVC to temperature puts constraints on several factors that contribute to viscous dissipation, such as wire speed and entry temperature. In addition, the minute length of the die illustrates

that die length is another requirement for successfully handling PVC. The fact that heat dissipation is so prevalent and that there is a significant effect on the overall results underlines the importance of considering nonisothermal conditions in the analysis.

Chapter 6

ANALYSIS OF HAAS AND SKEWIS'S DIE

A particular die design employed by Du Pont Co. is studied using both the LAT and FEM analysis. The LAT is applied for both Newtonian and power-law fluids assuming isothermal conditions. These findings are used to verify the results obtained by the FEM. The FEM is then extended to nonisothermal conditions for a comprehensive study using a commercially available wire-coating LDPE resin (Alathon 3535) for which experimental data is available. Finally a comparison between theory and experiments is made for a specific set of operating conditions.

6.1 Introduction

Haas and Skewis (1974) examined the relationship between wire-coating roughness and the design of the die and guider tip (torpedo) by two different approaches: an empirical approach and a rheological approach. In the guider tip-die configuration, the guider tip can be adjusted to enable the melt to meet the wire at a predetermined location along the die. The necessity to minimize entrance effects was cited as vital to avoid roughness, and thus yield smooth streamlined flow of the melt upon contact with the wire. This concept can be influenced by a design variable referred to as the "gum space". The gum space is defined as the closest axial distance between the guider tip and the die wall, and is illustrated in Figure 6.1. The authors discuss the existence of an optimum gum space, one which compromises

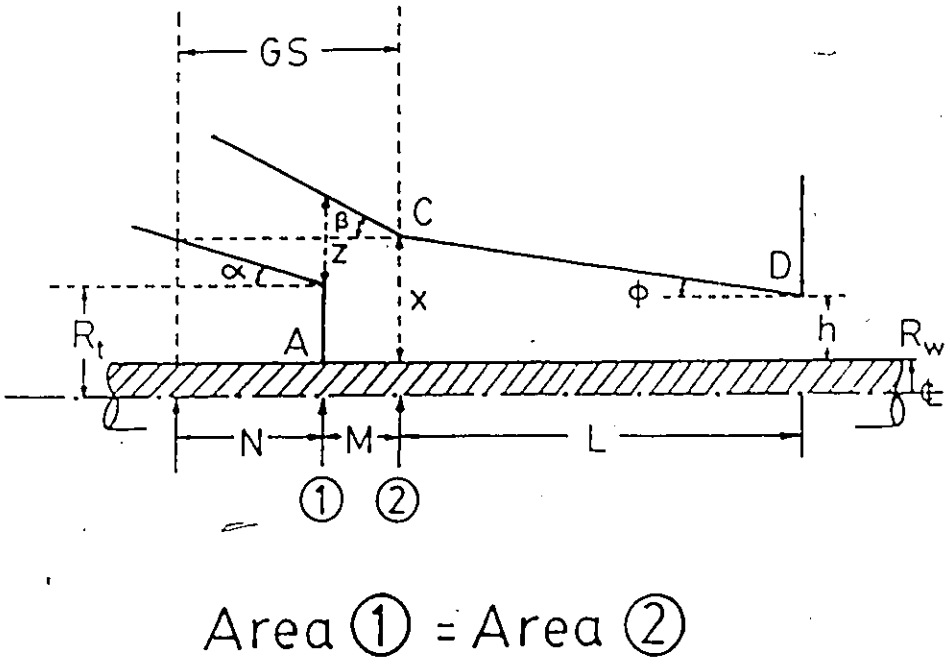

Figure 6.1: The "Gum Space" Concept and Relevant Notation.

between the large shear stresses developed in smaller gum spaces and the pronounced effect of the stress singularity at impact for larger gum spaces. The equation for this calculation is based on the assumption that the best gum space is found by equating the cross-sectional area at section 1, where the torpedo ends, and that at section 2, where the die wall changes slope (Figure 6.1). The optimum gum space, GS_{opt}, is given by

$$GS_{opt} = \frac{Z + N(\tan\beta - \tan\alpha)}{\tan\beta} \tag{6.1}$$

where Z is calculated from the equation

$$Z^2 + 2R_t Z = [(R_w + h) + L\tan\phi]^2 - R_w^2 \tag{6.2}$$

and N is found by

$$N = \frac{L\tan\phi + h + R_w + R_t}{\tan\alpha} \tag{6.3}$$

Haas and Skewis (1974) present several different designs along with corresponding GS_{opt} values for coating 10 mils (0.0254 cm) on a No. 22 AWG wire (R_w= 0.032 cm). In addition, data is presented which shows that the gum space plays an important role with respect to the quality of the coating of the final product.

A particular wire-coating die design used by Haas and Skewis (1974) (also referred to here as Haas's die) in their research at Du Pont Co. is shown in Figure 6.2. The guider-tip is characterized by a blunt nose and the die is tapered up to the exit. The wire used was a No. 22 AWG type wire, with a coating requirement of 80% of the radius (R_c = 0.0576 cm). Haas and Skewis (1974) give experimentally measured pressure drops for different wire speeds using a gum space of 100 mils (0.254 cm) in their design. A comparison between theory and these experimental results is a prime objective in this part of the research. It was apparent after preliminary runs that the LDPE resin used in the previous analysis (Fenner's die) was much less viscous than that used by Haas and Skewis (Alathon 3535). Therefore, information was needed and obtained from the authors on the rheological properties of this resin. Furthermore, a sample of the resin was received and fully characterized by Tzoganakis (1986) to give the viscosity curves of Figure 3.3 as explained in Chapter 3.

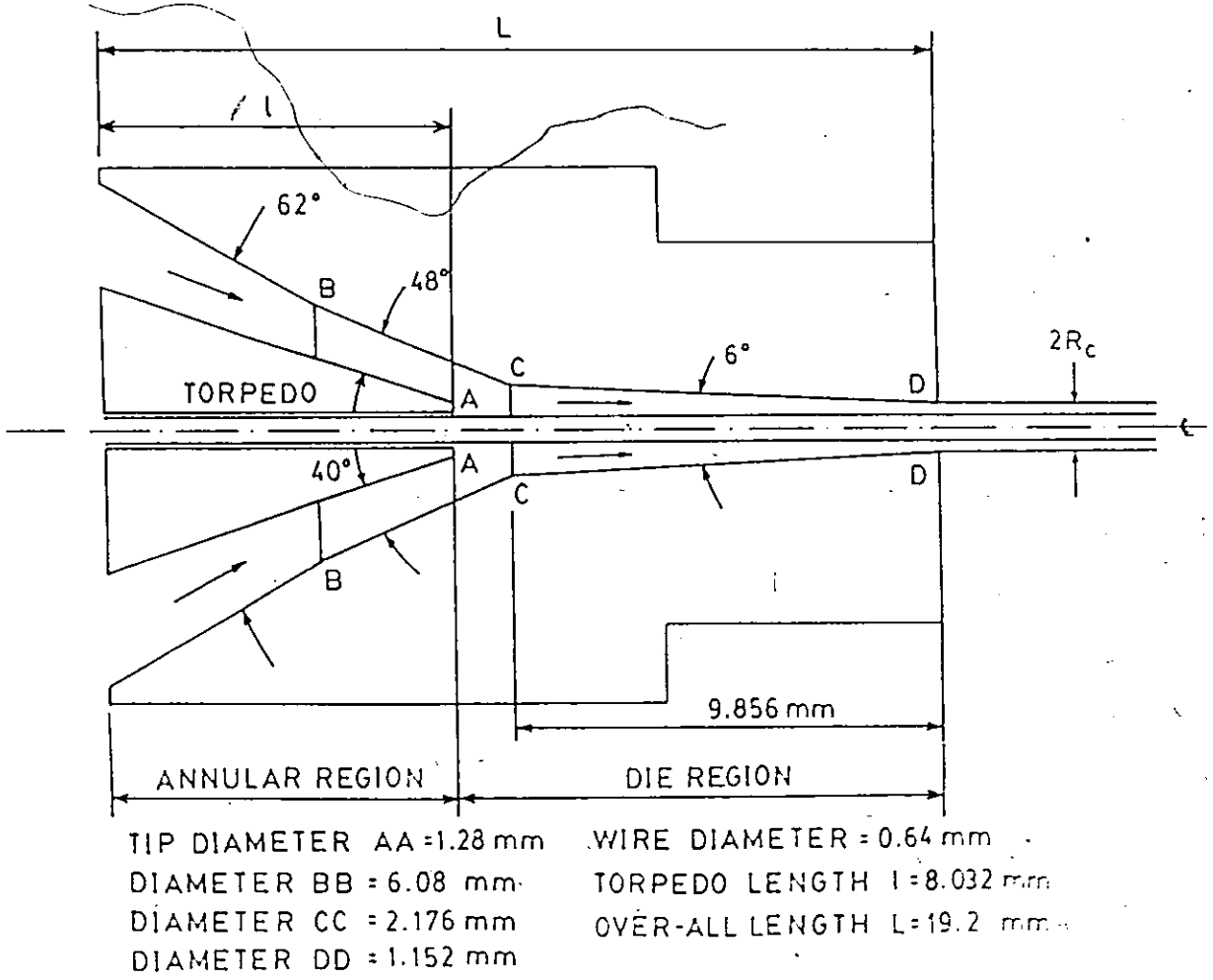

Figure 6.2: Die Design Employed by Haas and Skewis (1974) (Piece 22-1S).

6.2 Isothermal Analysis

This analysis assumes that the containing surfaces remain at a fixed temperature along the die and that the temperature of the LDPE melt stays unchanged. This assumption is carried through for both Newtonian and power-law fluids.

6.2.1 Lubrication Approximation Theory

Application of the LAT to the 100-mil gum space configuration (or GS = $7.9R_w$) of this die is done assuming that there is no density difference between the LDPE melt and the LDPE existing in the ambient state (h = $h_m = 0.8R_w$). Fluids of different power-law indices were examined (n = 0.25, 0.50, 0.75) along with the Newtonian case (n = 1.0). Figure 6.3 shows the pressure distribution in dimensionless form for each fluid, displaying the expected pattern of behavior. Recirculation, however, seems likely to exist in the case of the Newtonian fluid. It appears that the pressure build-up subsides when n is around 0.50. Shear stresses at the die wall and wire, and the wire tension are shown in Figures 6.4 and 6.5, respectively.

The previous results are independent of temperature (which affects m and n) and wire speed. To begin calculating the more significant dimensional values, an effective wire-coating temperature must be chosen. It is found that the greatest temperature rise occurs at the die wall exit. At high wire speeds (V_w > 1000 cm/s), convective heat transfer dominates, and temperature rise due to viscous dissipation occurs only in a very thin layer close to the walls while the remainder of the melt passes under almost isothermal conditions at die temperature. Therefore, it was decided to select the die temperature (232°C) as the effective operating temperature. From the data on Alathon 3535 in Chapter 3, an effective consistency index m = 9774 Pa·s^n and a power-law index n = 0.4406 are found.

Considering the temperature dependence of the density, it is found that at 232°C, the density of the melt, ρ_m, is 0.74 g/cm^3. Previously, the 80% coating requirement was specified when the wire emerged from the die. Requiring a cold coating thickness of $0.8R_w$, a mass balance reveals that the hot coating thickness must be $h_m = 0.94R_w$, assuming the ambient temperature is T_a = 23°C. Table 6.1 gives corresponding dimensionless parameters for the two cases, i.e. assuming no density differences (ρ_a/ρ_m

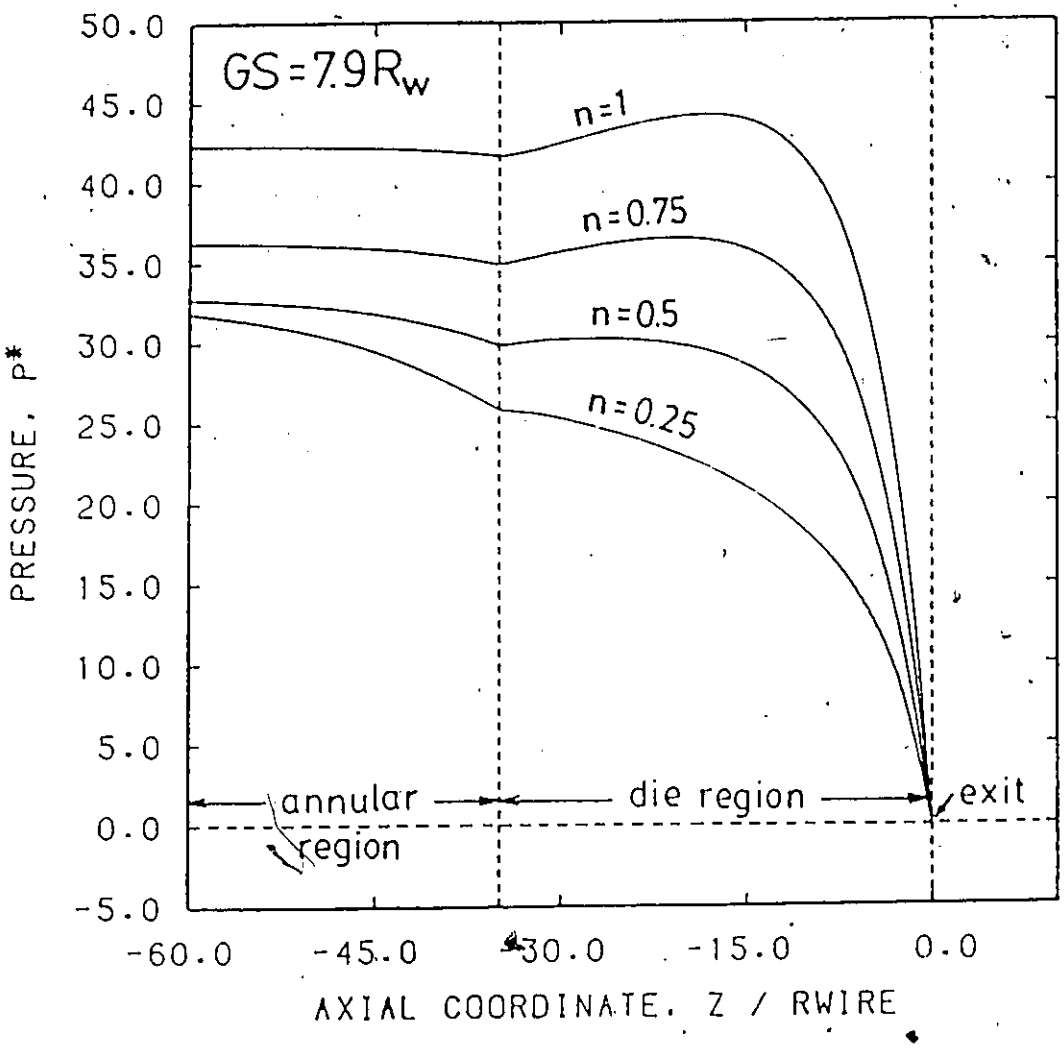

Figure 6.3: Dimensionless Pressure Distribution along Haas's Die for Power-law Fluids Using the LAT ($GS \cong 7.9R_w$).

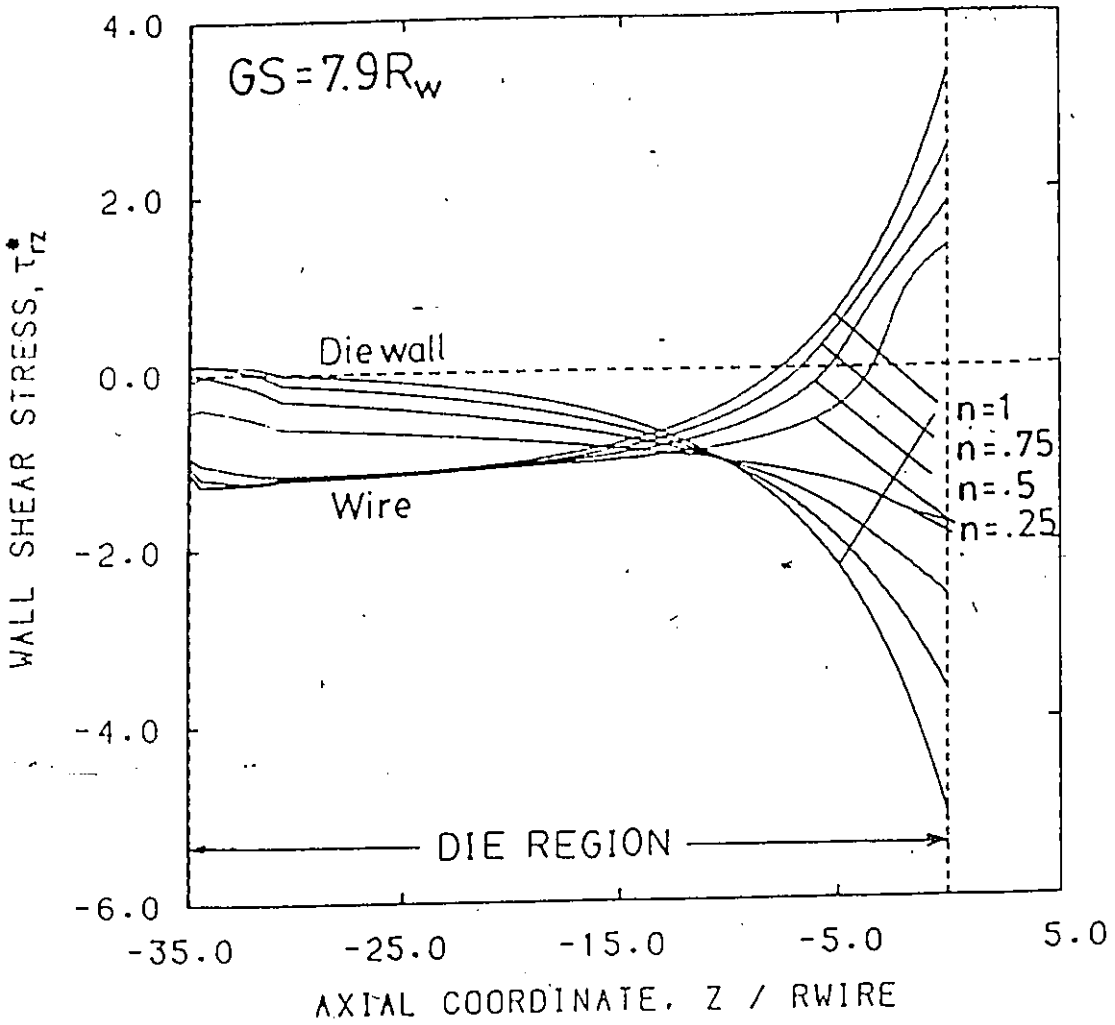

Figure 6.4: Dimensionless Shear Stress Distribution Along the Die Wall and Wire in Haas's Die for Power-law Fluids Using the LAT ($GS = 7.9R_w$)

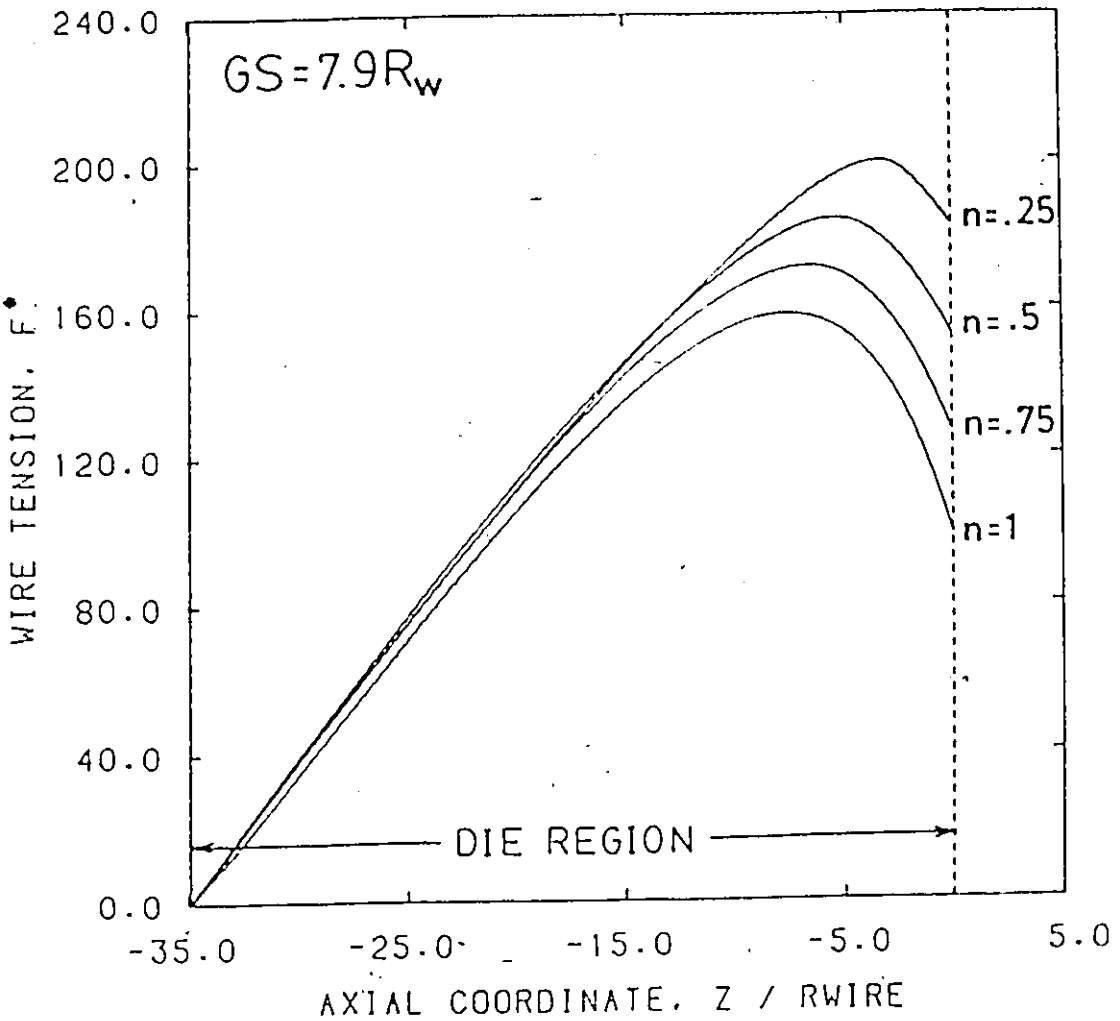

Figure 6.5: Dimensionless Wire Tension in Haas's Die for Power-law Fluids Using the LAT ($GS = 7.9R_w$).

Table 6.1: Dimensionless Quantities Obtained from LAT for Haas's Die (LDPE: $\tau = 9774\dot{\gamma}^{0.4406}$(Pa), T = 232°C, GS = $7.9R_w$).

Dimensionless Parameter	$h_m = h = 0.8R_w$		$h_m = 0.94R_w$	
$P_g^* = P/\bar{\tau}^\dagger$	32.29		45.41	
$F^* = F/\bar{\tau}R_w^2$	159.17		84.30	
$F^*_{max} = F_{max}/\bar{\tau}R_w^2$	187.50	at −5.12 ††	148.20	at -8.38
$\bar{\tau}^*_{w,max} = \bar{\tau}^*_{w,max}/\bar{\tau}$	1.70	at 0 (exit)	2.26	at 0 (exit)
$\bar{\tau}^*_{d,max} = \bar{\tau}^*_{d,max}/\bar{\tau}$	-2.41	at 0 (exit)	-2.71	at 0 (exit)

† $\bar{\tau} = m(V_w/R_w)^n$

†† Location defined as $z_o^* = z_o/R_w$ where the maximum occurs

= 1) and taking into account the temperature dependence ($\rho_a/\rho_m = 1.24$). From these dimensionless parameters, dimensional values can be calculated for different wire speeds.

The relationship between pressure drop and wire speed is detailed in Figure 6.6 for both density cases, along with the experimental data given by Haas and Skewis (1974). The agreement between experimental findings and those predicted with $h = 0.8R_w$ is good particularly up to 1000 cm/s, after which the LAT overestimates the experimental values. It is about this speed that Haas and Skewis (1974) note the onset of melt fracture, and this may have some significance in the new discrepancies. For the case of $h_m = 0.94R_w$, it is clear that the LAT overestimates the experimental values.

The results here can only be considered as a rough estimate since the analysis is constrained by assumptions that have been shown to have an effect on the computations. Thus a fully two-dimensional nonisothermal analysis is required, and this is accomplished by using the FEM.

6.2.2 Finite Element Method

The finite element grid employed in this analysis is shown in Figure 6.7. The grid contains a total of 216 elements for velocity-pressure computations and 511 nodes. A distance of 20 wire radii was incorporated after the exit to

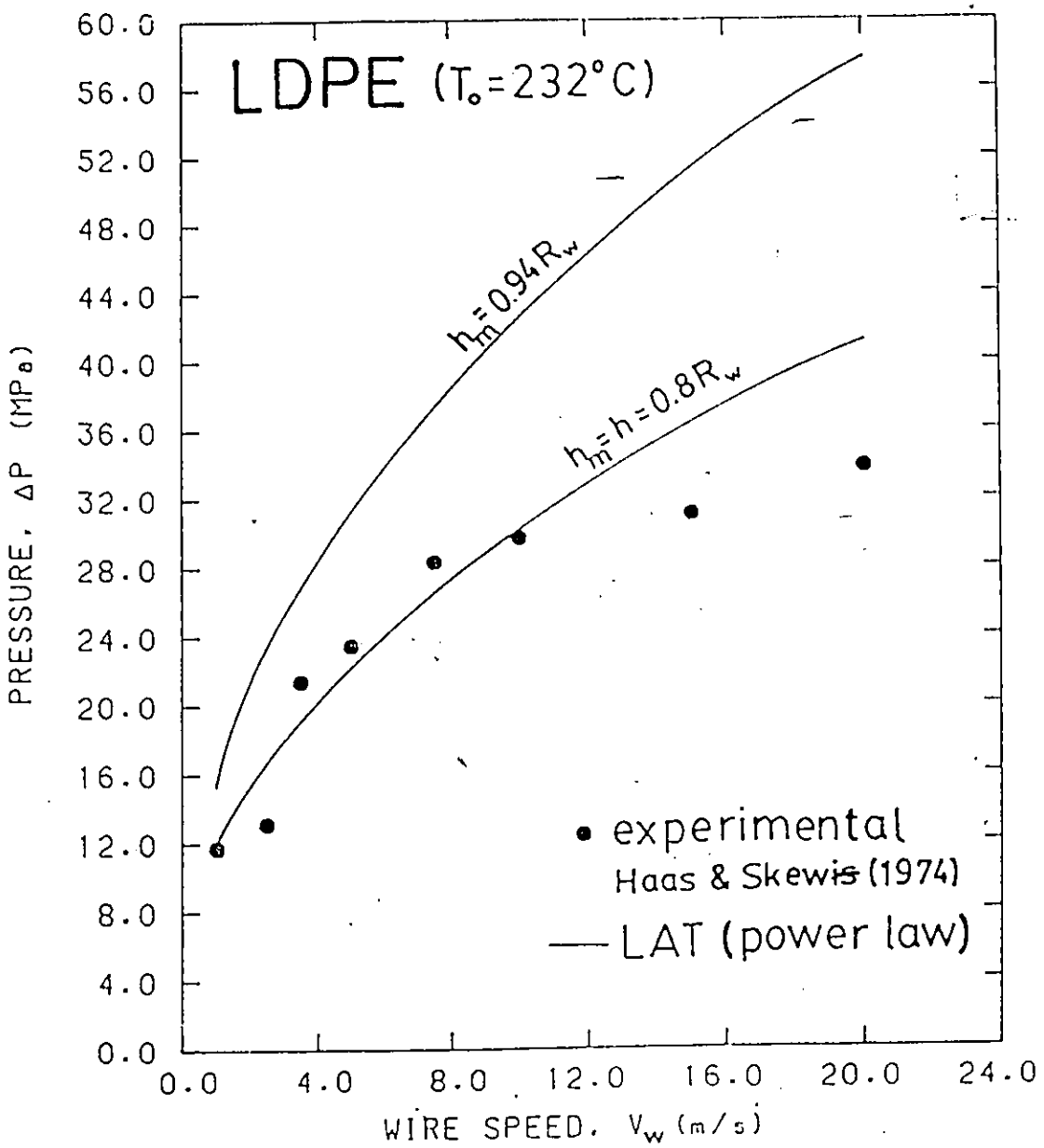

Figure 6.6: Pressure Drop vs. Wire Speed: Comparison of Experimental and LAT Results in Haas's Die (LDPE: $\tau = 9774\dot{\gamma}^{0.4400}$, T = 232°C).

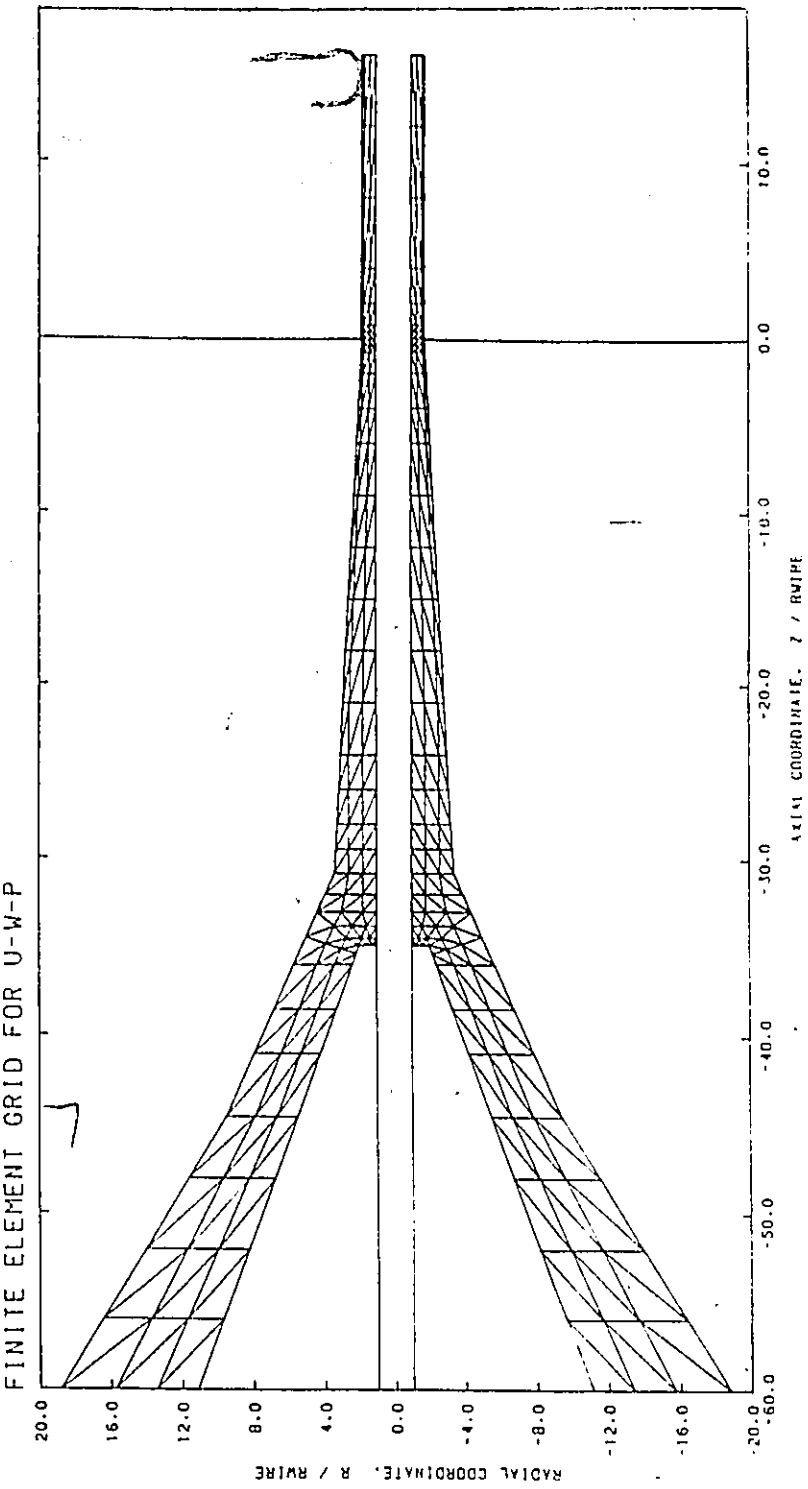

Figure 6.7: Finite Element Grid for Analysis of Haas's Die.

completely satisfy the natural boundary conditions far downstream. The density of the grid has been increased in regions where singularities are known to exist.

Initially, a run was made assuming a Newtonian fluid with n = 1 and having a coating requirement of $h = h_m = 0.8R_w$, these conditions also having been employed using the LAT. As seen in Figure 6.8, a small zone of recirculation of approximately 1% develops after the impact point. This recirculatory behavior is also predicted by the LAT. Adjusting the coating requirement to account for density changes (i.e. $h_m = 0.94R_w$) shows that recirculation is suppressed, this fact again supported by the LAT findings.

The pressure distribution for a Newtonian fluid (where $h = 0.8R_w$) is shown in Figure 6.9 in dimensionless form, and is compared with the distribution obtained using the LAT. The discrepancies can be attributed to the FEM grid used to model the impact region and the inability of the LAT to account for the radial flow that also exists in this region ($\frac{\partial p}{\partial r} \neq 0$).

The viscosity model describing Alathon 3535, the material used in actual experiments by Haas and Skewis (1974), is now employed (model is detailed in Chapter 3). A comparison between pressure drop-wire speed relationships obtained under isothermal conditions (T = 232°C) with both LAT and FEM analyses is shown in Figure 6.10. The lower values predicted by the FEM primarily result from the nature of the viscosity function, which shows a curvature at both low and high shear rates, unlike the power-law employed in the LAT.

6.3 Nonisothermal Analysis

Using the Alathon 3535 model, the analysis was extended to consider the effect of nonisothermal conditions on the overall results. A series of runs was performed for various wire speeds taking into account differences between the melt and ambient densities. Table 6.2 shows the results. Furthermore, Figure 6.11 compares the experimental results with those found by FEM under nonisothermal conditions, showing good agreement.

From the experimental values of pressure, and assuming Newtonian behavior, Haas and Skewis (1974) calculated shear rates and viscosities (hence shear stresses) for each wire speed. These computations along with results obtained from the nonisothermal FEM analysis (using Alathon 3535) are

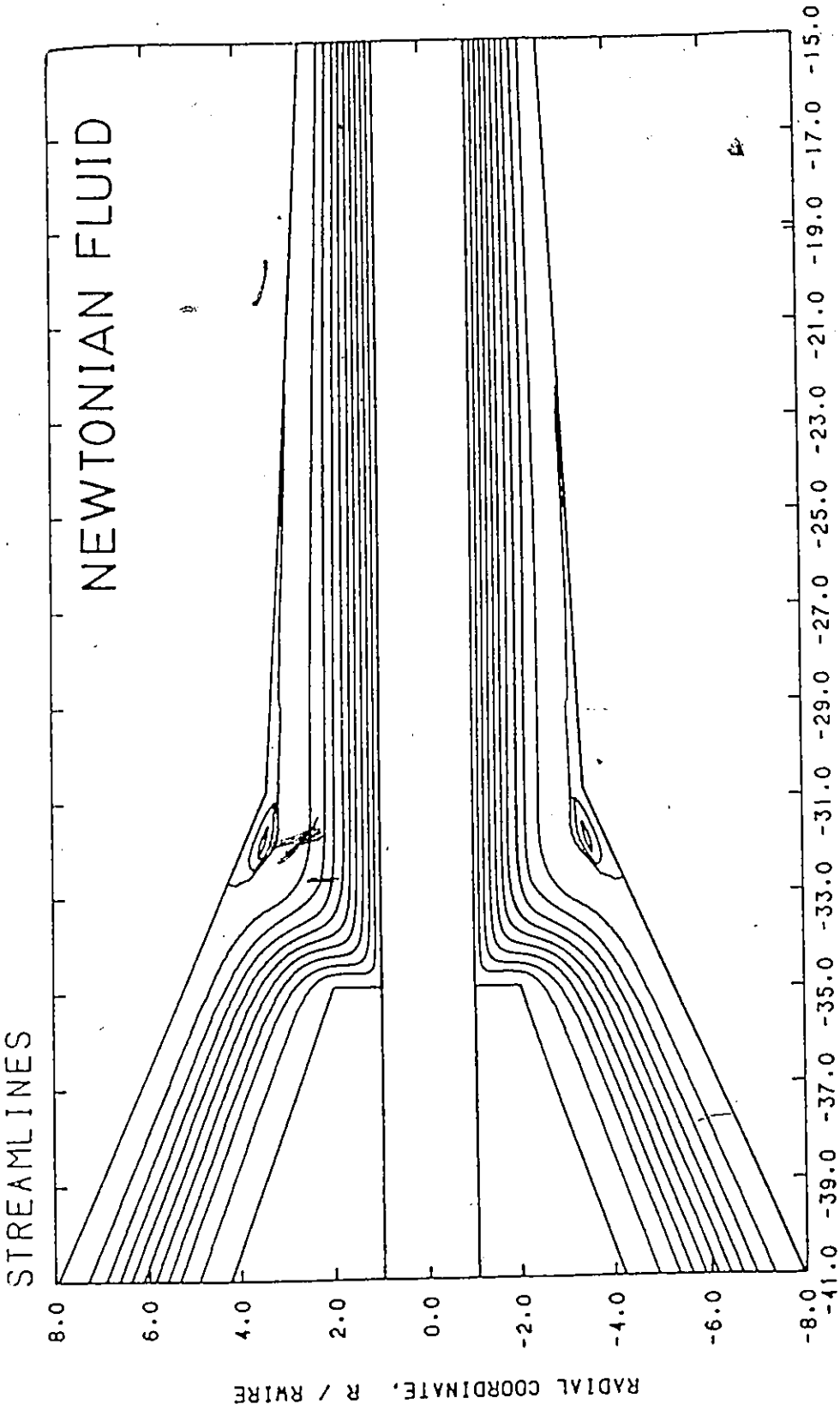

Figure 6.8: Streamline Pattern for a Newtonian Fluid near the Impact Region in Haas's Die (GS = $7.9R_w$, h = $0.8R_w$).

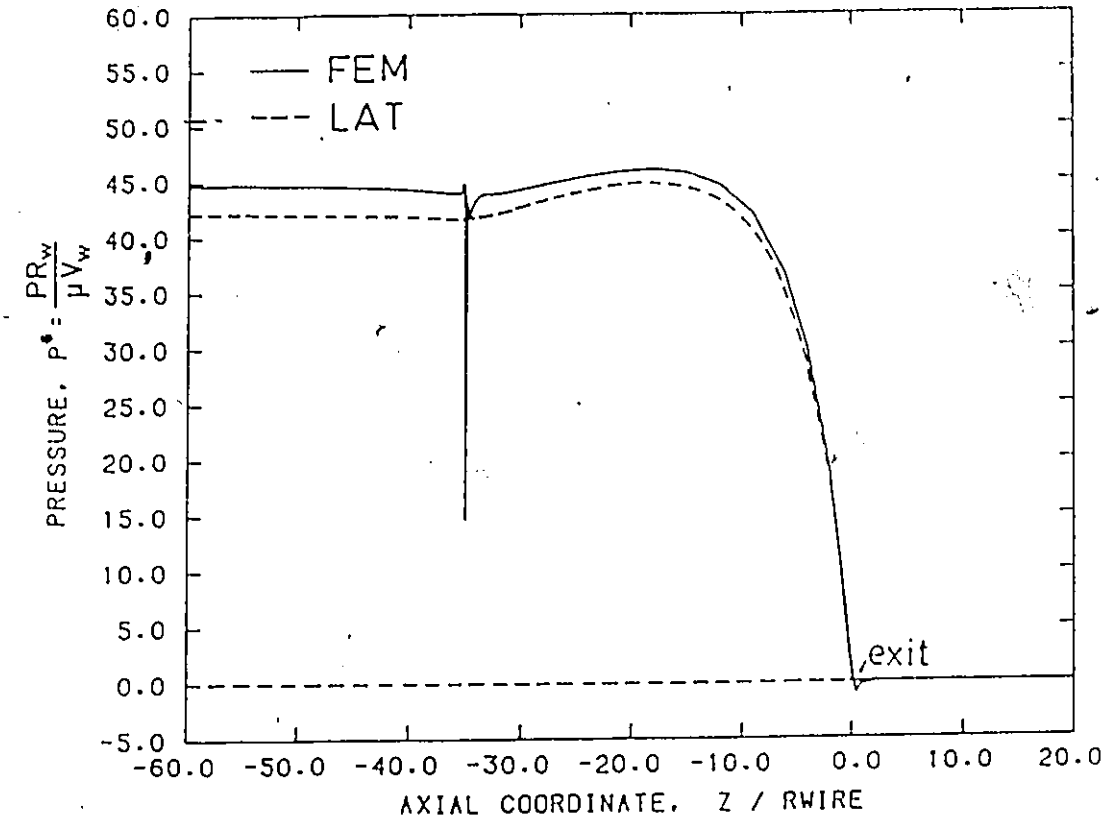

Figure 6.9: Dimensionless Pressure Distribution for a Newtonian Fluid in Haas's Die ($GS = 7.9R_w$, $h = 0.8R_w$).

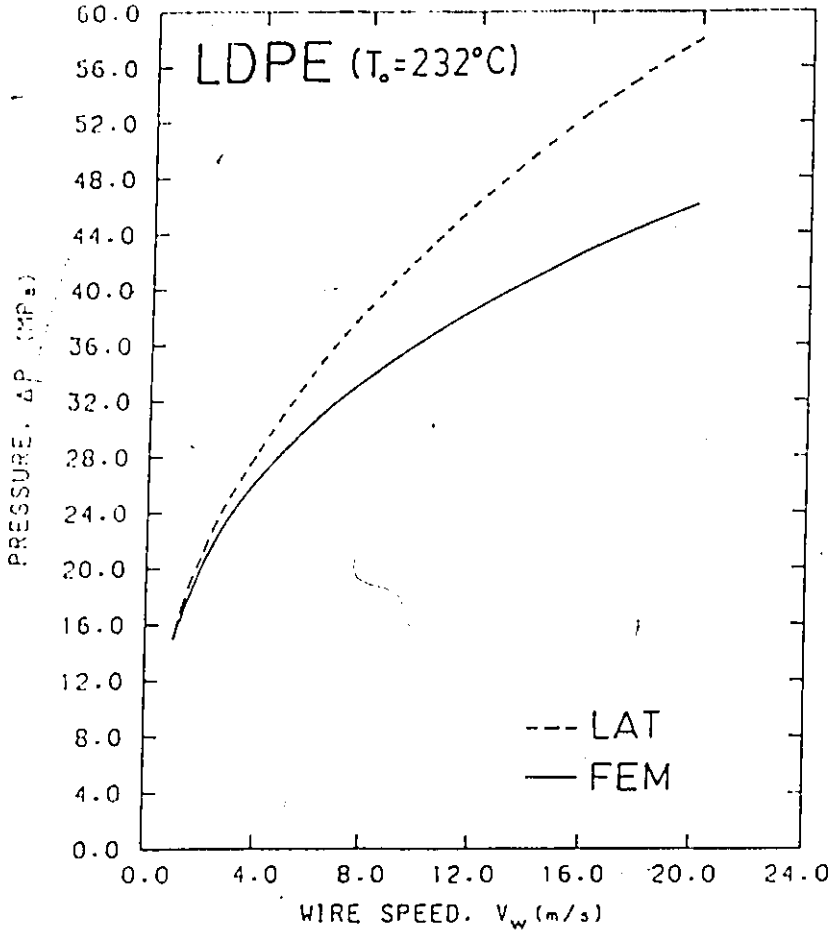

Figure 6.10: Pressure Drop vs. Wire Speed under Isothermal Conditions in Haas's Die (LAT and FEM, GS = $7.9R_w$, $h_m = 0.94R_w$).

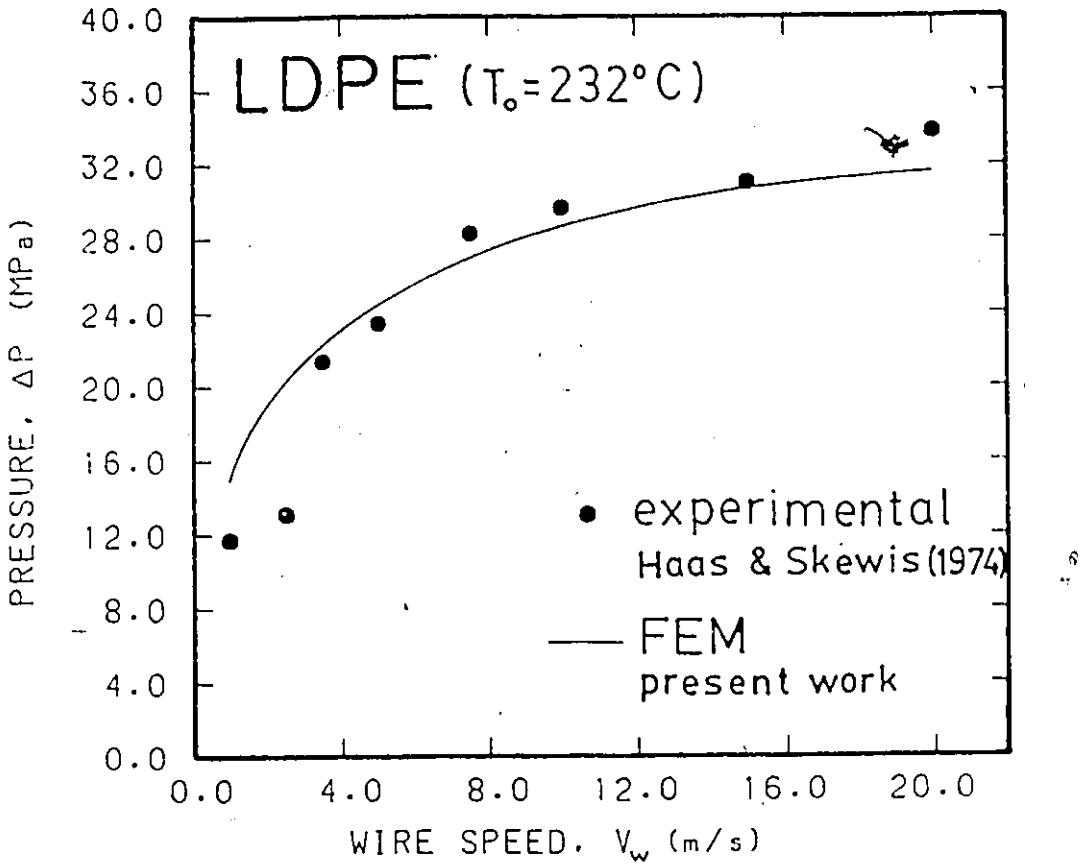

Figure 6.11: Comparison Between Experimental and Nonisothermal FEM Results in Haas's Die ($GS = 7.9R_w$, $h_m = 0.94R_w$).

Table 6.2: Overall Pressure Drop vs. Wire Speed for LDPE: Comparison between LAT, FEM and Experimental Results ($GS = 7.9R_w$, $h_m = 0.94R_w$).

Wire Speed V_w (cm/s)	LAT, Isothermal $\tau = 9774\dot{\gamma}^{0.4406}$(Pa)	FEM* Isothermal Alathon 3535	FEM* Nonisothermal Alathon 3535	Experimental Haas and Skewis (1974)
100	15.38	15.63	14.94	11.72
250	23.03	22.02	20.16	13.10
350	26.71	24.90	22.25	21.37
500	31.26	28.32	24.45	23.44
750	37.37	32.70	26.89	28.27
1000	42.42	36.16	28.57	29.65
1500	50.72	41.59	30.62	31.03
2000	57.58	45.87	31.79	33.78

* For FEM analysis, $T_m = 232°C$.

shown in Table 6.3. The discrepancies can be attributed mainly to the assumptions involved, such as Newtonian vs. non-Newtonian fluid, temperature dependence, etc. It is apparent that both the calculated shear stress values and those obtained by FEM are above the previously mentioned critical values for LDPE. However, it should be noted that the critical values are based on a flow into a sudden contraction rather than in a tapered flow domain (see Chapter 3). Furthermore, Haas and Skewis (1974) maintain that higher shear stress values are expected since three-taper dies appreciably diminish the entrance effects.

Figure 6.12 shows the pressure distribution curve at three wire speeds. The steady drop in the pressure throughout the die indicates that recirculation has been avoided. This is supported by the flow field representation in Figure 6.13 which also shows a streamlined flow.

The maximum temperature distribution is shown for the 500 cm/s case in Figure 6.14. The melt here experiences an overall rise of 72°C, which is in fact quite large. Shear stresses at the die wall and wire surface are presented in Figure 6.15. The maximum quantities were determined for each over the range of wire speeds considered and are found in Figure 6.16. It is evident that stresses at the die wall are higher than the corresponding

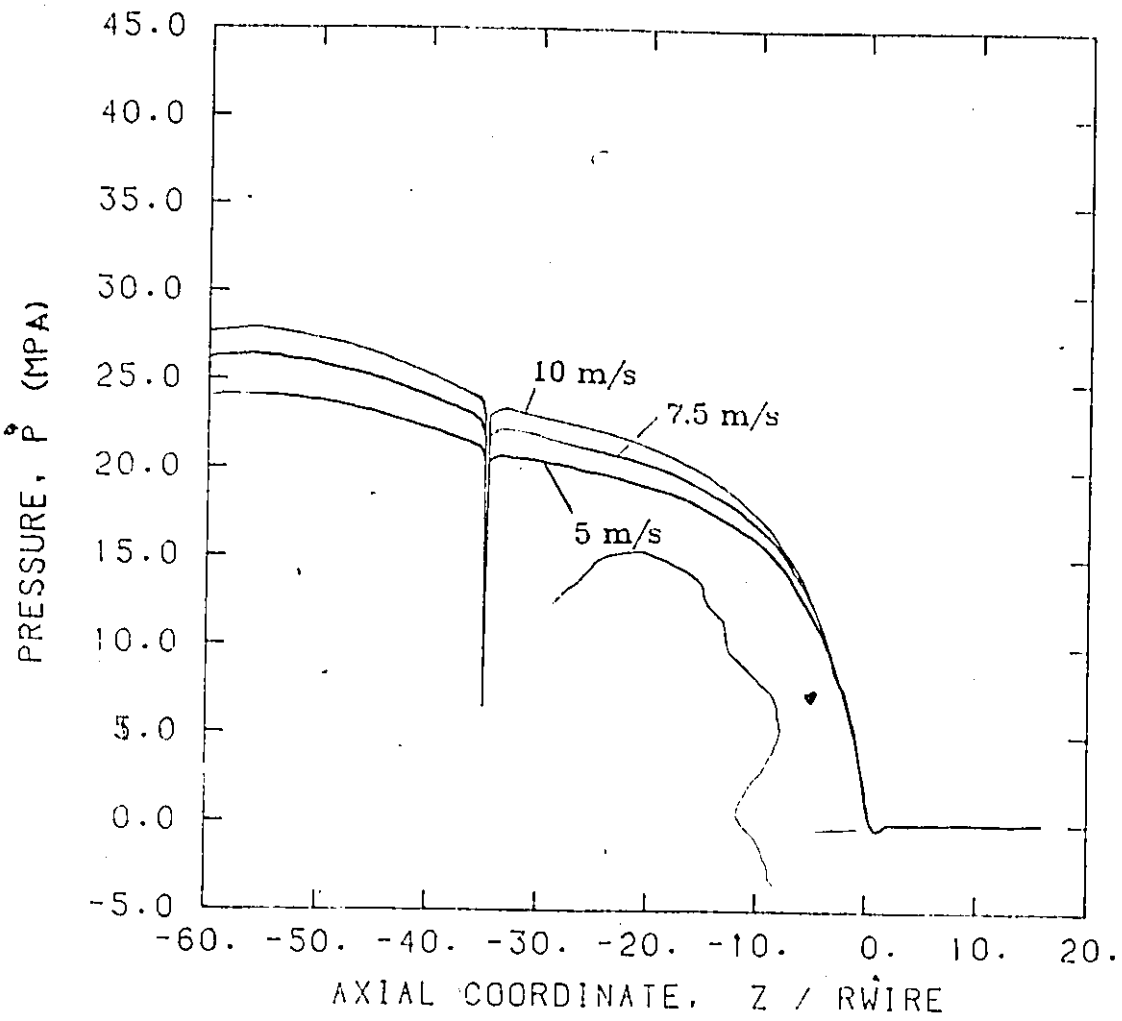

Figure 6.12: Pressure Distribution in Haas's Die under Nonisothermal Conditions (T = 232°C).

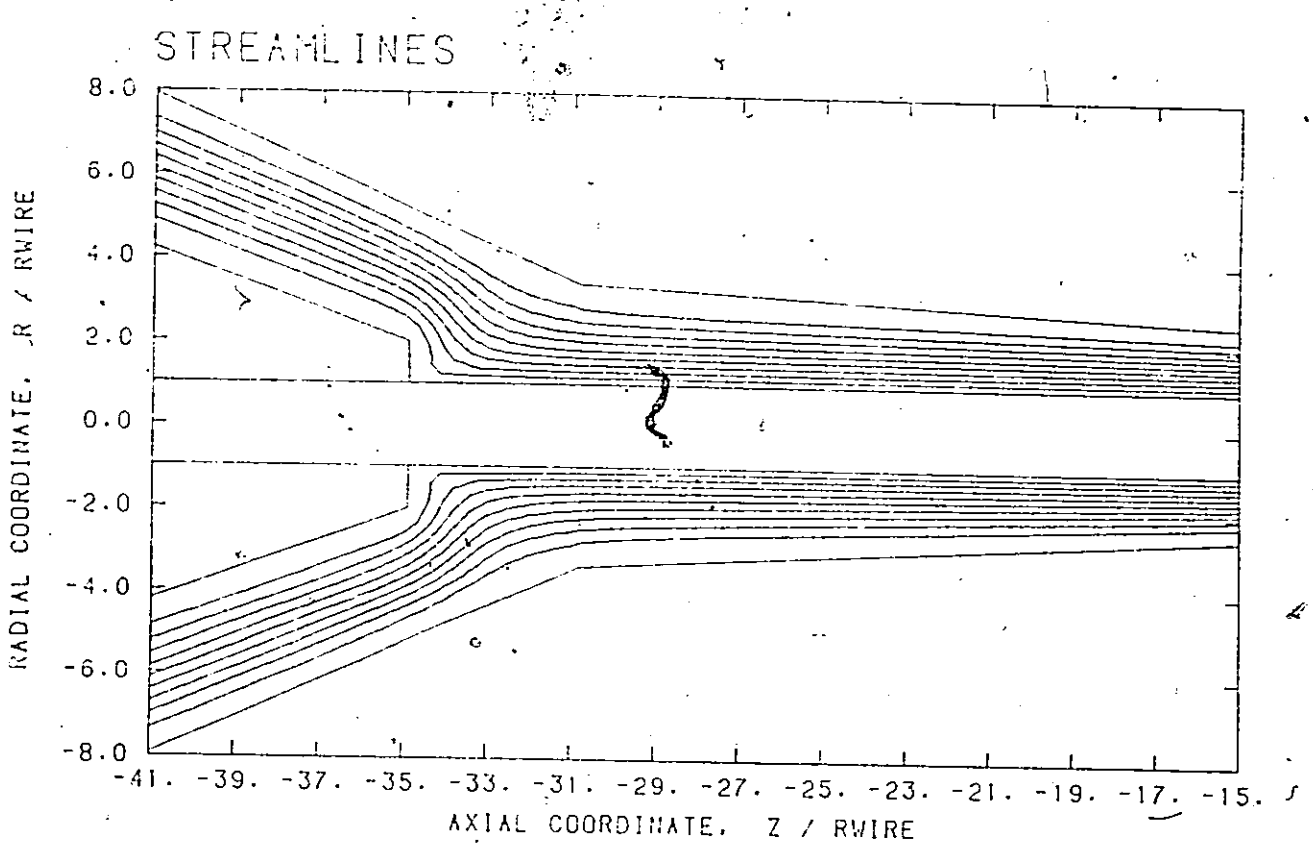

Figure 6.13: Streamline Pattern in Haas's Die under Nonisothermal Conditions (V_w= 1000 cm/s, T = 232°C).

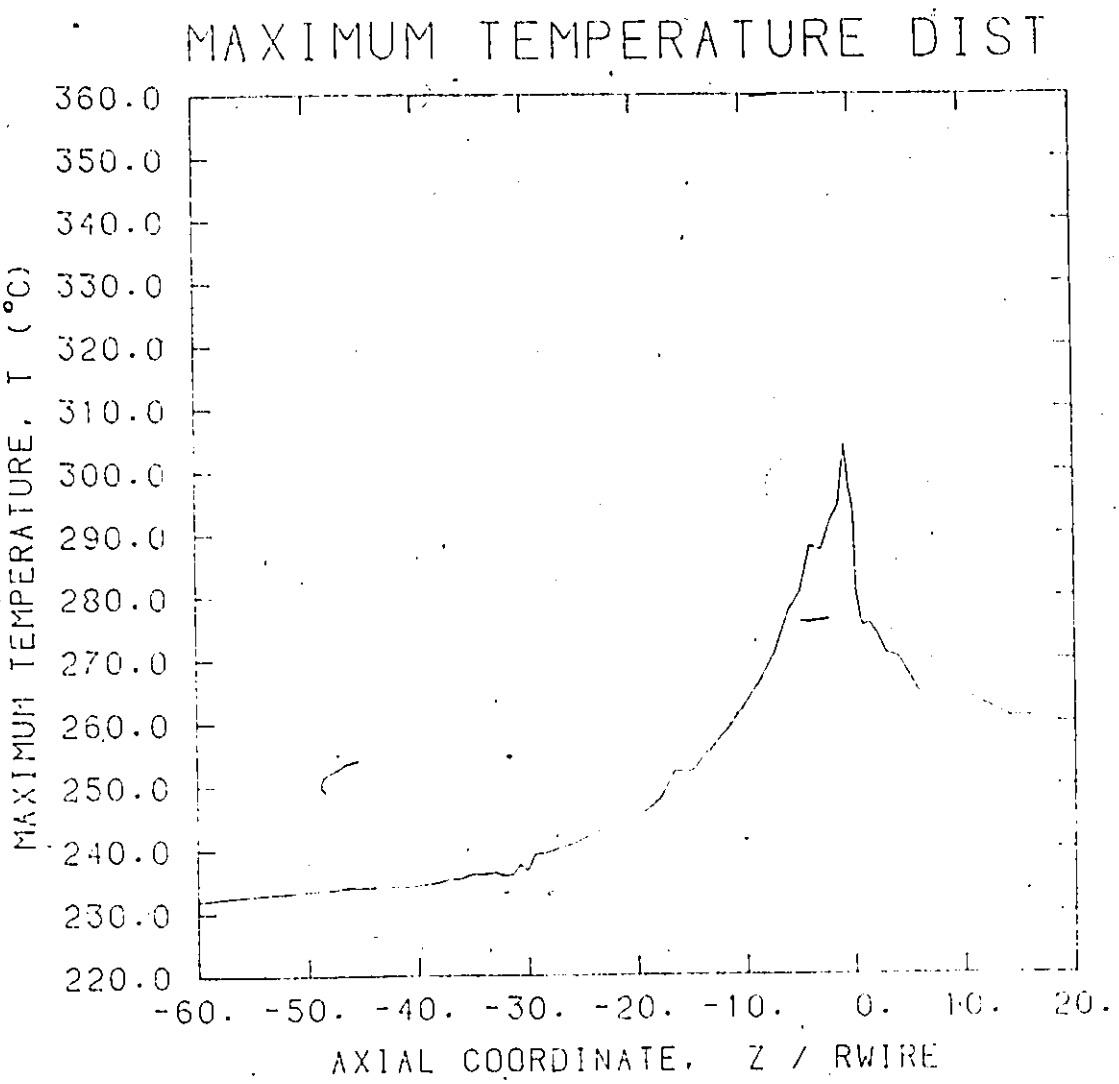

Figure 6.14: Temperature Distribution in Haas's Die under Nonisothermal Conditions (V_w= 500 cm/s, T = 232°C).

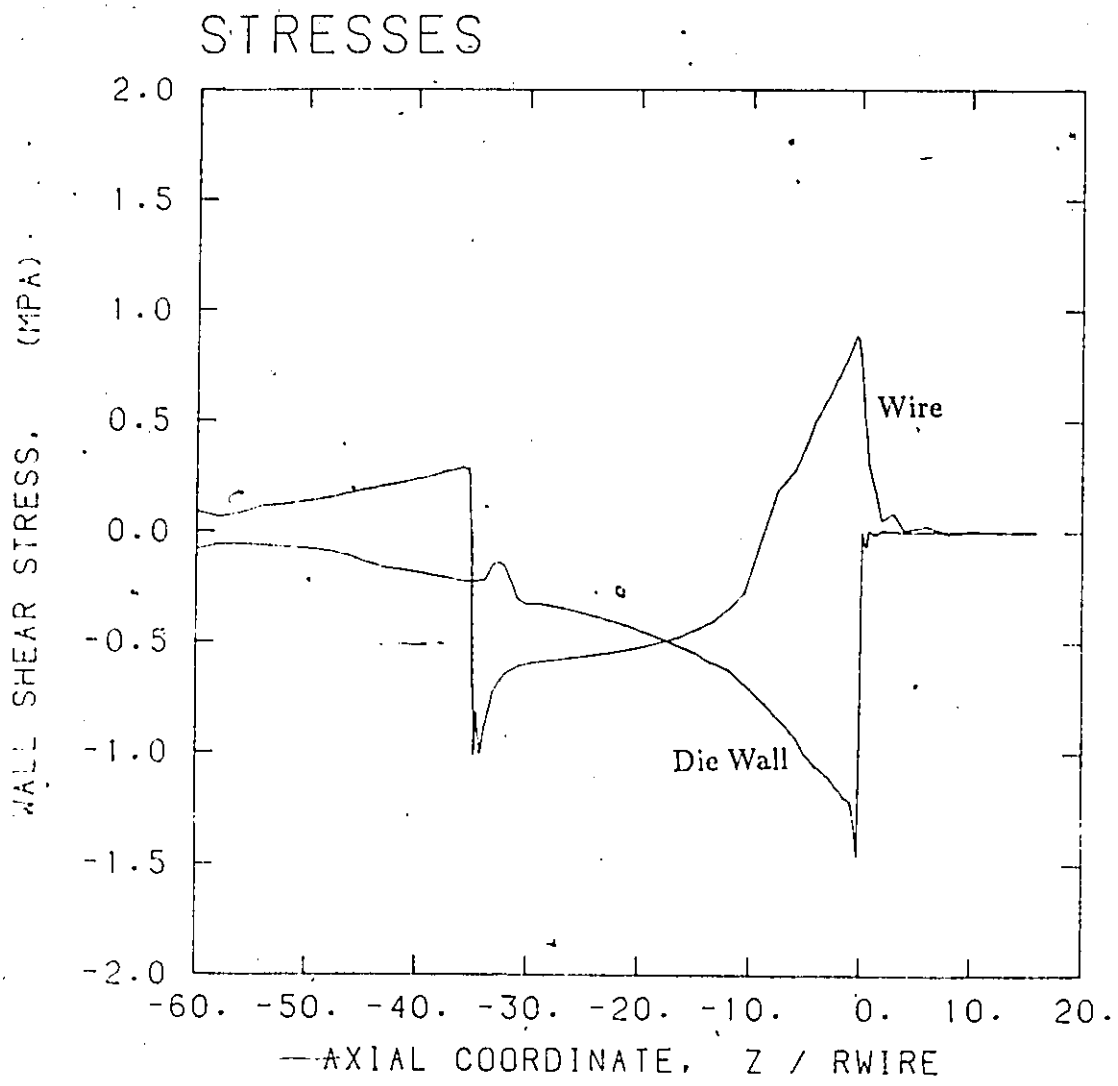

Figure 6.15: Shear Stress at the Die Wall and Wire in Haas's Die under Nonisothermal Conditions (V_w= 500 cm/s, T = 232°C).

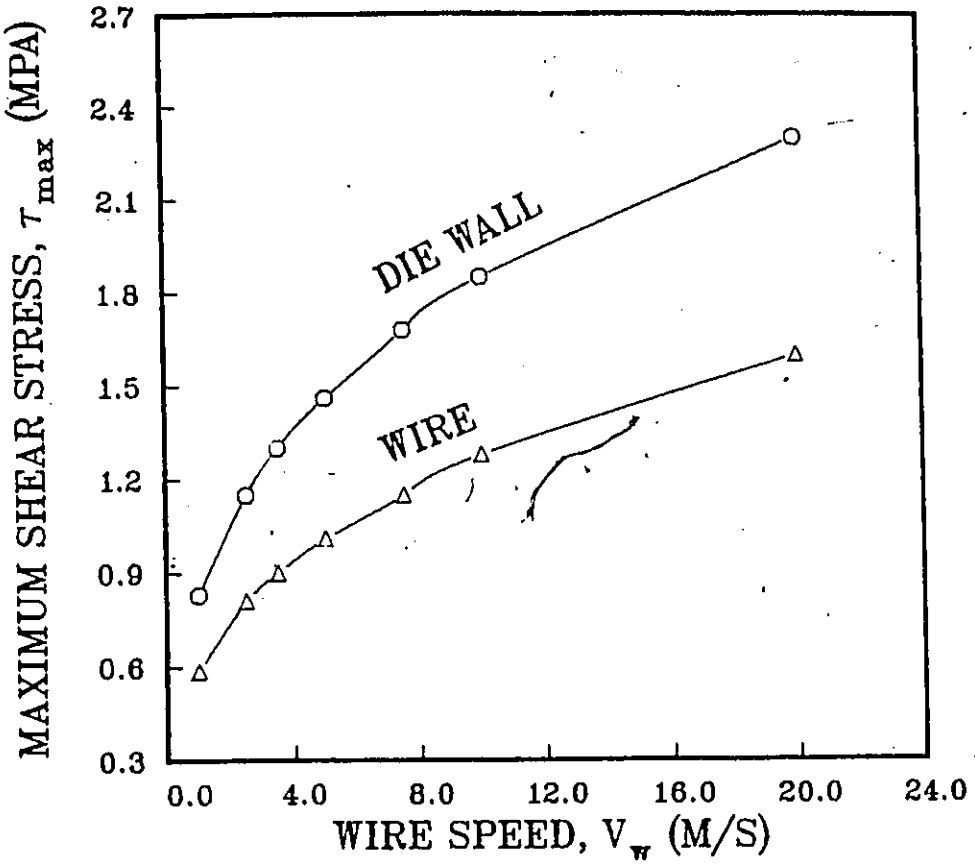

Figure 6.16: Shear Stress vs. Wire Speed in Haas's Die under Nonisothermal Conditions (T = 232°C).

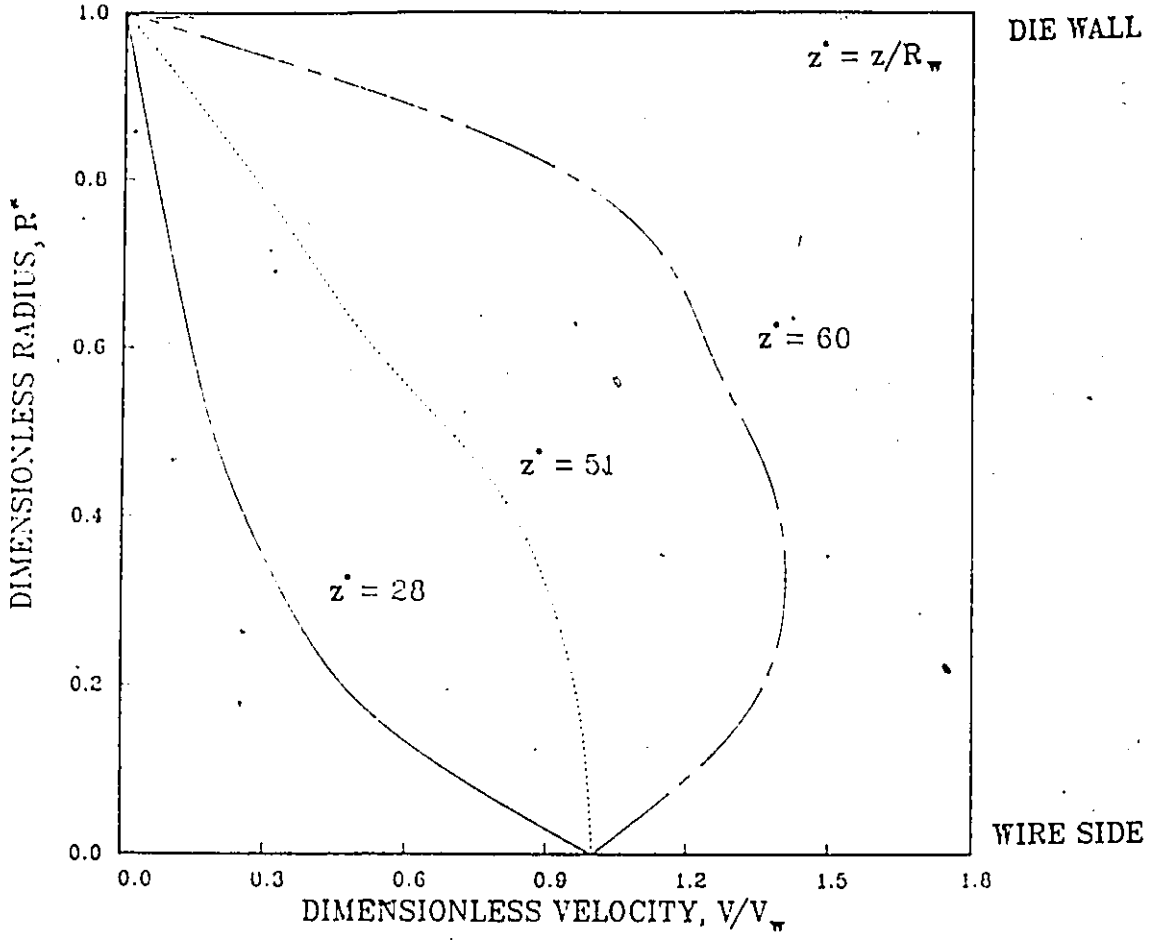

Figure 6.17: Velocity Profiles in Haas's Die at Various Axial Positions (T = 232°C).

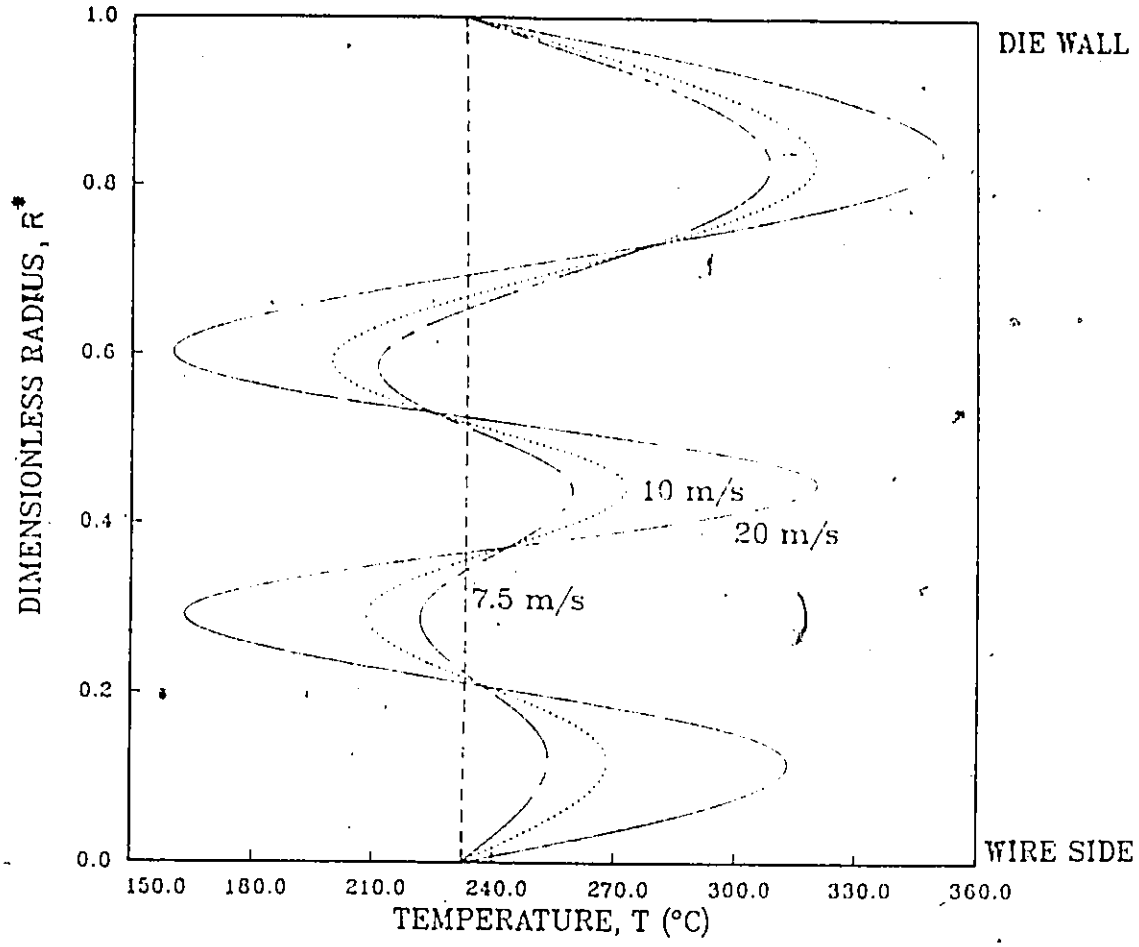

Figure 6.18: Temperature Oscillations at the Exit in Haas's Die for Various Wire Speeds (T = 232°C).

Table 6.3: Maximum Shear Rates and Shear Stresses at Die Wall in Haas's Die with 100-mil GS (T = 232°C, h = $0.8R_w$).

Wire Speed	Haas and Skewis		FEM Analysis, Nonisothermal	
V_w(cm/s)	$\dot{\gamma}_{d,max}s^{-1}$	$\tau_{d,max}$(MPa)	$\dot{\gamma}_{d,max}s^{-1}$	$\tau_{d,max}$(MPa)
100	16,000	0.18	46,600	0.83
250	40,000	0.20	121,000	1.15
350	56,000	0.32	172,300	1.29
500	80,000	0.35	251,600	1.46
750	120,000	0.43	387,200	1.68
1000	160,000	0.44	527,000	1.85
1500	240,000	0.46	816,000	2.12
2000	320,000	0.51	1,113,600	2.33

values at the wire and therefore require closer monitoring since they are more likely to cause melt fracture.

Related to this, velocity profiles, which depend to a large extent on the viscous nature of the fluid and the geometry involved, assume patterns shown in Figure 6.17 at different distances from the inlet ($z^* = z/R_w = 60$ is the exit). These profiles are very similar to those found using LDPE in the relatively long die employed by Fenner (1970), as shown in Chapter 4.

Finally, with regard to the temperature profiles, it was found that using the more viscous LDPE resin (Alathon 3535) at high speeds, oscillations occurred which were too significant to overlook. Figure 6.18 reveals the extent of oscillations found to exist under the more intense conditions examined. However, it is not believed that the oscillations of these nodal temperatures had a crucial net effect on the other field variables calculated, at least for speeds up to 1000 cm/s.

6.4 Concluding Remarks

The major objective of this chapter was to numerically simulate the experimental results available in the literature for a high-speed wire-coating industrial operation. Using the conditions under which the experimental runs were conducted, the LAT was first applied. Rough estimates of perfor-

mance variables were determined. In addition, the LAT predicted a small amount of recirculation for a Newtonian fluid. Further runs using various power-law fluids showed that flow recirculation and shear stresses were reduced as shear-thinning increased. Pressure drops obtained assuming a coating thickness of 80% of the wire radius ($0.8R_w$) at the melt temperature, gave results close to those found by experiment. However, when the coating requirement was altered to give a final 80% cold coating, that is $0.94R_w$ at melt temperature, the findings were no longer in good agreement. It is therefore clear that the density of the melt (i.e. mass flow requirements) will have an effect on the final results and has to be taken into account.

The effect of both viscosity and density were further illustrated by the nonisothermal FEM analysis. It was found that for better simulations, knowing the proper viscosity model for the resin used was a crucial matter. For example, assuming a power-law model under isothermal conditions (232°C), discrepancies were found from the experimental values, especially at higher speeds. The FEM analysis under nonisothermal conditions produced findings close to the experimental observations when the coating thickness was taken as that at the ambient temperature, which is also the actual case in wire-coating operations. Recirculation was not detected but maximum stresses were above critical values specified for the onset of melt fracture. However, as previously discussed, this does not necessarily indicate that melt fracture was occurring.

It has been previously noted that numerical problems existed in some computations resulting from the occurrence of oscillations in the temperature field. This was partially relieved by using a mathematical technique known as "upwinding". However, a need exists to improve the upwinding scheme employed in order to eliminate the temperature oscillations totally.

Chapter 7

CONCLUSIONS AND RECOMMENDATIONS

The wire-coating process was numerically analyzed by application of the Lubrication Approximation Theory (LAT) and the Finite Element Method (FEM) to three different die designs. The wire-coating die designs examined were taken from the following works:

- Fenner (1970)
- Caswell and Tanner (1978)
- Haas and Skewis (1974)

The polymer melts considered as coating materials were low-density polyethylene (LDPE) and plasticized polyvinyl-chloride (PPVC), both of which are commonly used coating resins. Material properties for both of these polymers are detailed in this research. The analyses assumed a steady, creeping, incompressible, inelastic flow, along with the appropriate velocity and temperature boundary conditions.

The results obtained from the two-dimensional FEM analysis were compared to predictions found by using the LAT for power-law fluids under isothermal conditions. This was done thoroughly in the examination of Fenner's die. Discrepancies between the computational methods were primarily due to the FEM modelling of the impact region and the one-dimensional nature of the LAT.

The LAT was found to be very valuable because of its simplicity and its ability to rapidly yield approximate results for certain performance variables such as pressure, shear stress at the die wall and wire, and wire tension. It was found that the pressure distribution curve generated by the LAT gave important information on the nature of flow conditions throughout the die, whether, for example, recirculatory flow was present. Recirculation was found to occur in cases where a positive pressure gradient had developed, as evidenced by a pressure build-up in the die section over and above the inlet pressure. Therefore, the LAT can be used to determine proper die design parameters to effectively avoid recirculation. Whenever an LAT analysis indicated that recirculation was likely to occur, the follow-up FEM analysis consistently supported this result.

When the process is assumed to operate under nonisothermal conditions, seemingly a more realistic situation, the FEM can be applied for a full two-dimensional analysis, taking into account the whole axisymmetric domain. Furthermore, the FEM allows determination of the free surface of the melt beyond the exit of the die. This gives important information on what form (i.e. thickness) the final coating will take.

The FEM analysis yielded a wealth of information on the overall performance of a wire-coating die. The flow and temperature fields were generated, along with distributions of pressure, maximum temperature and shear stress throughout the die. The visual presentation of the flow and temperature fields enabled quick and accurate determination of recirculation or hot-spots where the polymer is under severe heating, both of which would be detrimental to the final product.

Recirculatory flow was cited as a major problem in this process since subsequent surface irregularities damage the final wire product. Greater wire speeds and lower temperatures were both found to increase the intensity of recirculation, whereas it was seen that shear-thinning of the fluid had the effect of decreasing recirculation. Initial runs in Fenner's die using both LDPE and PPVC indicated flow recirculation. In the case of the LDPE resin, a wire having a greater radius was employed to eliminate excess space and ensure that the pressure build-up in the die region would not be too great. Runs that followed showed that most or all flow recirculation had been suppressed.

Thermal effects in the melt, resulting from viscous dissipation, were studied by the generation of temperature fields, maximum temperature

rises, and other thermally related data. Knowledge of the true temperature state is vital to the overall analysis. For example, the plasticized PVC melt was found to experience large temperature rises within very small distances when nonisothermal conditions were assumed. Since PPVC is prone to thermal degradation, it must be known whether the temperatures are too great, thereby leading to an unacceptable final product. The general trend showed that operating at high wire speeds and/or low die temperatures led to greater temperature rises in the melt. The temperature rises obtained were considered quite reasonable, thus further supporting the need for analyses under these conditions.

A comparison between the nonisothermal FEM analysis and the LAT showed that nonisothermal conditions had a significant effect on all performance quantities. For example, pressure predictions found with the LAT were now dramatically reduced. Other variables consistently experienced large changes. Since the temperature distribution influences the nature of the flow field, in turn affecting performance variables, it can be seen that isothermal analyses can give only rough approximations at best.

The shear stress distribution yields important information with respect to melt fracture, which occurs under excessively high shear stresses. Probably the most common cause of surface roughness is the onset of melt fracture. It was seen that in many cases the predicted shear stresses were greater than the critical shear stresses cited from previous research. However, it should be emphasized that these critical quantities are based on a 90-degree sudden contraction and thus ignore the effect of the tapered geometry in preventing melt fracture. Therefore it would appear that actual testing would be required to absolutely ensure the avoidance of melt fracture.

The effect of melt selection on wire-coating performance is illustrated by the unsatisfactory results obtained when PPVC was used in Fenner's die. This effectively showed that a die design must be made compatible with the polymer melt that it is supposed to handle. The examination of Caswell's die showed that it, unlike Fenner's die, was suitable for PPVC resins. Caswell's die is a much smaller die and has a relatively long parallel land length, both these adjustments allowing for better handling of PPVC. Nevertheless, the intense conditions generated in wire-coating operations made suitable performance only possible for wire speeds under 300 cm/s and for die temperatures less than 190°C. Temperatures greater than this

indicated the possibility of thermal degradation.

A prime objective of this research was the simulation of results obtained by experimental methods. Runs were therefore conducted using the LAT and FEM in Haas's die, for which experimental data were available as a basis of comparison.

The agreement between LAT-generated and experimental results was good when a commercially available LDPE resin (Alathon 3535) was used in Haas's die. This good agreement was found by assuming operation at die temperature and assuming no difference in density between the hot melt and cold coating. It was found that when a difference was considered in the latter, the pressure results were strongly affected. Therefore it is seen that the pressure is very sensitive to the assumed coating thickness.

The FEM was then employed under nonisothermal conditions, using experimental viscosity data for Alathon 3535. Good agreement was found with the experimental pressure results of Haas and Skewis (1974) after the density differences were taken into account, that is using $h_m = 0.94R_w$ in the computations. The discrepancies that do exist may be due to the thermal boundary conditions assumed (isothermal walls). It was also found that pressure values greatly depend on a good knowledge of the viscous behavior over the entire range of expected shear rates, particularly the magnitude of viscosity at high shear rates. The temperature dependence of the viscosity must also be accurately specified.

A problem experienced in this research was the occurrence of oscillations in temperature results under high Peclet number (i.e. high speeds). The remedy for such a problem lies in the development of a proper "upwinding" scheme. While there may be significant deviations in the point temperatures, the overall effect on performance-related variables, such as pressure, is likely to be small. However, to eliminate these fluctuations and ensure a better accuracy, an improvement in the "upwinding" procedure used in the nonisothermal analysis is essential.

The application of the FEM to the wire-coating shows great potential for the simulation of the process. Some of the recommendations for future work in this field include:

1. Further investigation of other industrially used die designs by application of the FEM and LAT, thus leading to an even better understanding of the process.

2. Use of polymer coating materials other than LDPE and PPVC to study the effect on overall die performance.

3. Extension of the wire-coating analysis to cover multi-layer coating of wires (coextrusion dies).

4. Improvement of the "upwinding" technique used in the FEM to effectively suppress oscillations in temperature that were observed in the nonisothermal analysis under high Peclet numbers.

5. Alteration of boundary conditions on temperature to reflect more realistic thermal conditions (i.e. based on heat flux) rather than assuming isothermal or adiabatic conditions.

6. Inclusion of a proper viscoelastic constitutive equation to account for elastic effects of the viscous flow. The consideration of melt compressibility can also be explored if a correct equation of state is known.

7. Determination of the extent of fluid slippage in actual operations to allow for incorporation of proper slip-at-the-wall boundary conditions in the FEM analysis.

8. A greater exploration of the significance of the wire tension in the process.

Experimental studies on actual wire-coating operations are few, and most of them with limited knowledge of melt properties. Thus there is a particular need for more experimental data. In addition, more information on the relationship between melt fracture and geometric configuration is needed if melt fracture is ever to be accurately predicted.

Finally, it can be said that the combination of the LAT and FEM analysis with good material property data and well defined and realistic boundary conditions is quite capable for the analysis of the wire-coating process. In general, improvements in predictions will be made with greater and more accurate information on the nature of polymer used.

Bibliography

[1] Agassant, J.F., *Le Calandrage des Matieres Thermoplastiques*, Doctoral Thesis, Univ. Pierre et Marie Curie, Paris 6 (1980).

[2] Agur, E.E., Vlachopoulos, J., "Numerical Simulation of a Single- Screw Plasticating Extruder", *Polym. Eng. Sci., 22*, 1084 (1982).

[3] Bagley, E.B., Storey, S.H., "Shear Rates and Velocities of Flow of Polymers in Wire Covering Dies", *Wire and Wire Products, 38*, 1104 (1963).

[4] Basu, S., "Theoretical Analysis of Non-Isothermal Flow in Wire Coating Co-Extrusion Dies", *Polym. Eng. Sci., 21* , 1128 (1981).

[5] Bird, R.B., Steward, W.F., Lightfoot, E.N., *Transport Phenomena* , J. Wiley, New York (1960).

[6] Bird, R.B., Armstrong, R.C., Hassager, O., *Dynamics of Polymeric Liquids*, Vol. 1, J. Wiley, New York (1977).

[7] Carley, J.F. in *Processing of Thermoplastic Materials, Chapt. 4*, E.C. Bernhardt, Ed., Reinhold, New York (1959).

[8] Carley, J.F., Endo, T., Krantz, W.B.,"Realistic Analysis of Flow in Wire Coating Dies", *Polym. Eng. Sci., 19* , 1178 (1979).

[9] Carley, J.F., "Die Design", *SPE Journal, 19* , 977 (1963).

[10] Caswell, B., Tanner, R.I., "Wirecoating Die Design Using Finite Elements", *Polym. Eng. Sci., 18* , 416 (1978).

[11] Chung, T.S., "Effect of Melt Compressibility on High Speed Wire Coating Process", *Polym. Eng. Sci. , 26*, 410 (1986).

[12] Cogswell, E.N., "Converging Flow of Polymer Melts in Extrusion Dies", *Polym. Eng. Sci., 12* , 64 (1972).

[13] Collins, E.A., Daniels, C.A., "PVC Melt Rheology III. Effect of Order and Molecular Weight on Shear Rate Dependence", *Polym. Eng. Sci., 14* , 357 (1974).

[14] Collins, E.A., "Relationship of Poly(Vinyl Chloride) Stability to Flow", *Polym. Eng. Sci., 18* , 1240 (1978).

[15] Dole, M., Hettinger, W.P., Larson, N.A., Wethington, J.A., " Specific Heat of Synthetic High Polymers. I. A Study of Polyethylene Including a Statistical Theory of Crystallite Length", *J. Chem. Phys., 20*, 781 (1952).

[16] Endo, T., *Numerical Analysis of Non-Isothermal Flow of Non-Newtonian Melts in Wire-Coating Dies* , M.Sc. Thesis, Dept. Chem. Eng., Univ. of Colorado (1976).

[17] Ettinger, R.J., "Polymer Requirements and Insulating Techniques for Obtaining the Maximum Benefits of High Density Polyethylene", *Wire and Wire Products, 36* , 1142 (1961).

[18] Fenner, R.T., *Extruder Screw Design, Chapter 11*, Iliffe, London (1970).

[19] Fenner, R.T., Williams, J.G., "Analytical Methods of Wire Coating Die Design", *Trans. Plast. Inst., 35* , 701 (1967).

[20] Ferrari A.G., "Extrusion Die Design to Reduce Melt Fracture", *Wire and Wire Products, 39* , 1036 (1964).

[21] Griff, A.L., *Plastics Extrusion Technology* , Reinhold, New York (1968).

[22] Haas, K.U., Skewis, F.H., "The Wire Coating Process: Die Design and Polymer Flow Characteristics", *SPE 32nd ANTEC, Tech. Papers, 20*, 8 (1974).

[23] Hammond, L.R., "The Design of Dies for High-Speed Wire Coating", *Wire and Wire Products, 35* , 725 (1960).

[24] Han, C.D., Rao, D., "Studies of Wire Coating Extrusion I. Rheology of Coating Extrusion", *Polym. Eng. Sci., 18* , 1019 (1978).

[25] Heng, F.L., *Wire-Coating Analysis Using the Lubrication Approximation*, Internal Report, Dept. Chem. Eng., Univ. of Ottawa (1986).

[26] Hood, P., "Frontal Solution Program for Unsymmetric Matrices", *Int. J. Num. Meth. Eng., 10*, 329 (1976).

[27] Hovey, V.W., "History of Extrusion Equipment for Rubber and Plastics" , *Wire and Wire Products, 36*, 192 (1961).

[28] Huebner, K.H., Thornton, E.A., *The Finite Element Method for Engineers*, Wiley, New York (1982).

[29] Kline C.H., *Plastics and Elastomers in Wire and Cable - USA 1986*, C.H. Kline and Co. Inc. (1986).

[30] Koleski, J.V., Wartmen, L.H., *Poly(vinyl) Chloride*, Gordon and Breach, New York (1969).

[31] McKelvey, J.M., *Polymer Processing* , Wiley, New York (1962).

[32] Middleman, S., *Fundamentals of Polymer Processing*, McGraw-Hill, New York (1977).

[33] Mitsoulis, E., Vlachopoulos, J., Mirza, F.A., *MACVIP - A Finite Element Program for Creeping Viscoelastic Flows*, Internal Report, Faculty of Eng., McMaster Univ. (1983).

[34] Mitsoulis, E., *Finite Element Analysis of Two-Dimensional Polymer Melt Flows*, Ph.D. Thesis, Dept. Chem. Eng., McMaster Univ. (1984).

[35] Mitsoulis, E., "Finite Element Analysis of Wire Coating", *Polym. Eng. Sci., 26* , 171 (1986).

[36] Owen, E.D., *Degradation and Stabilization of PVC* , J. Wiley, New York (1967).

[37] Parnaby, J., Worth, R.A., " Die Variator Mandrel Forces Encountered in Blow Moulding Parison Systems", *Proc. Inst. Mech. Eng., 25*, 357 (1974).

[38] Pearson, J.R.A., *Mechanics of Polymer Processing*, Elsevier, New York (1985).

[39] Raff, R.A.V., Allison, J.B., *Polyethylene* , Interscience, New York (1956).

[40] Rao, D.A., *A Study of Wire-Coating Extrusion*, Ph.D. Thesis, Dept. Chem. Eng., Polyt. Inst. of New York (1979).

[41] Stewart, W.E., McClelland, D., "Asymptotic Solutions of Three-Dimensional Flows with Viscous Dissipation", *AIChE J., 29*, 910 (1983).

[42] Tadmor, Z., Gogos, C.G., *Principles of Polymer Processing* , Wiley-Interscience, New York (1979).

[43] Taylor, C., Hughes, T.G., *Finite Element Programming of the Navier-Stokes Equations*, Pineridge Press, Swansea (1981).

[44] Tiu, C., "Wire Coating Extrusion - An Approximate Solution", *Polym. Eng. Sci., 26*, 957 (1986).

[45] Tzoganakis, C., *Priv. Commun.*, Dept. Chem. Eng., McMaster Univ. (1986).

[46] Vaughan, D.J., Spohn, W.W., "Properties and Processing of Ethylene Copolymers for Wire and Cable", *Wire and Wire Products, 35* , 1323 (1960).

[47] Vlachopoulos, J., Alam, M., "Critical Stress and Recoverable Shear for Polymer Melt Fracture", *Polym. Eng. Sci., 12* , 184 (1972).

[48] Vlachopoulos, J., Chan T.W., "A Comparison of Melt Fracture Initiation Conditions in Capillaries and Slits", *J. Appl. Polym. Sci., 21* , 1177 (1977).

[49] Winter H.H., "Temperature Fields in Extruder Dies with Circular, Annular, or Slit Cross-Section", *Polym. Eng. Sci., 15* , 84 (1975).

[50] Winter, H.H., "Viscous Dissipation in Shear Flows of Molten Polymers" , *Adv. Heat Trans., 13*, 205 (1977).

[51] Winter, H.H., "Thermal Capacitance and Cooling Length in the Wire-Coating Process", *SPE 36th ANTEC, Tech. Papers, 23*, 462 (1977).